UNIVERSITAT ROVIRA I VIRGILI

SIMULACIÓ DE L'EFECTE DE LES INCISIONS QUIRÚRGIQUES EN EL COMPORTAMENT DE LA PARET ABDOMINAL

Lluís Tuset Serra

ADVERTIMENT. L'accés als continguts d'aquesta tesi doctoral i la seva utilització ha de respectar els drets de la persona autora. Pot ser utilitzada per a consulta o estudi personal, així com en activitats o materials d'investigació i docència en els termes establerts a l'art. 32 del Text Refós de la Llei de Propietat Intel·lectual (RDL 1/1996). Per altres utilitzacions es requereix l'autorització prèvia i expressa de la persona autora. En qualsevol cas, en la utilització dels seus continguts caldrà indicar de forma clara el nom i cognoms de la persona autora i el títol de la tesi doctoral. No s'autoritza la seva reproducció o altres formes d'explotació efectuades amb finalitats de lucre ni la seva comunicació pública des d'un lloc aliè al servei TDX. Tampoc s'autoritza la presentació del seu contingut en una finestra o marc aliè a TDX (framing). Aquesta reserva de drets afecta tant als continguts de la tesi com als seus resums i índexs.

ADVERTENCIA. El acceso a los contenidos de esta tesis doctoral y su utilización debe respetar los derechos de la persona autora. Puede ser utilizada para consulta o estudio personal, así como en actividades o materiales de investigación y docencia en los términos establecidos en el art. 32 del Texto Refundido de la Ley de Propiedad Intelectual (RDL 1/1996). Para otros usos se requiere la autorización previa y expresa de la persona autora. En cualquier caso, en la utilización de sus contenidos se deberá indicar de forma clara el nombre y apellidos de la persona autora y el título de la tesis doctoral. No se autoriza su reproducción u otras formas de explotación efectuadas con fines lucrativos ni su comunicación pública desde un sitio ajeno al servicio TDR. Tampoco se autoriza la presentación de su contenido en una ventana o marco ajeno a TDR (framing). Esta reserva de derechos afecta tanto al contenido de la tesis como a sus resúmenes e índices.

WARNING. Access to the contents of this doctoral thesis and its use must respect the rights of the author. It can be used for reference or private study, as well as research and learning activities or materials in the terms established by the 32nd article of the Spanish Consolidated Copyright Act (RDL 1/1996). Express and previous authorization of the author is required for any other uses. In any case, when using its content, full name of the author and title of the thesis must be clearly indicated. Reproduction or other forms of for profit use or public communication from outside TDX service is not allowed. Presentation of its content in a window or frame external to TDX (framing) is not authorized either. These rights affect both the content of the thesis and its abstracts and indexes.

UNIVERSITAT ROVIRA i VIRGILI

Simulació de l'efecte de les incisions quirúrgiques en el comportament de la paret abdominal

LLUÍS TUSET SERRA

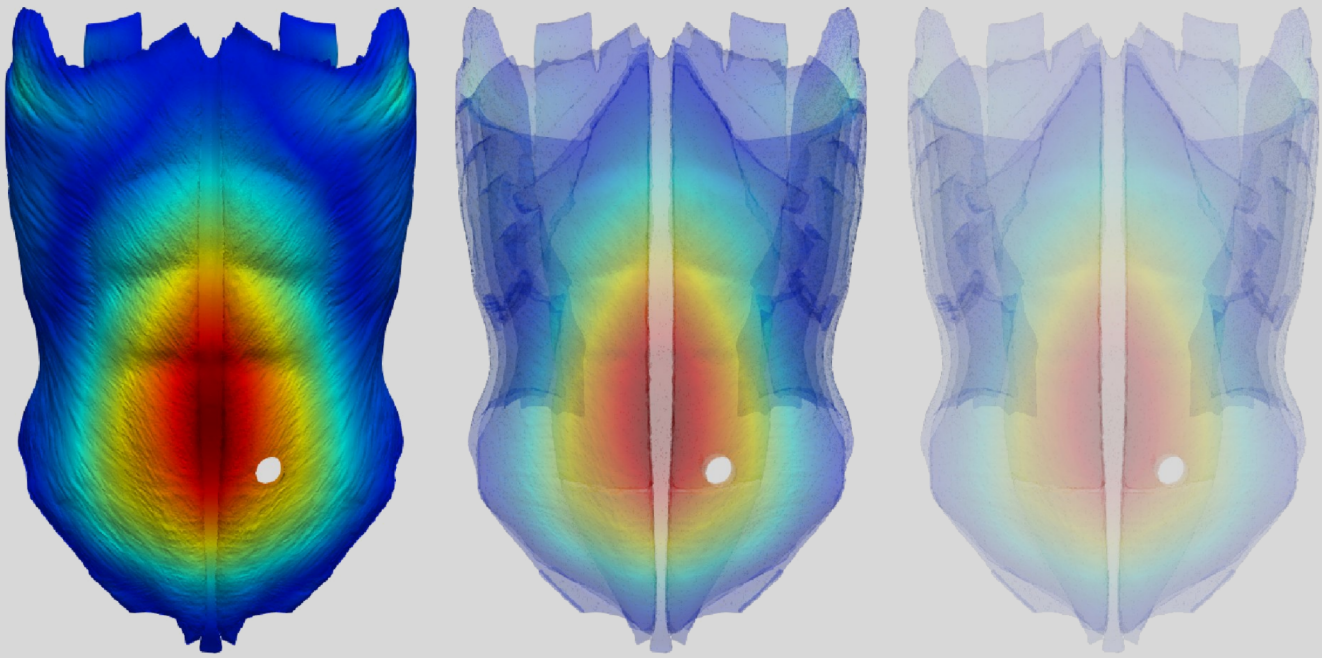

TESI DOCTORAL
2024

UNIVERSITAT ROVIRA I VIRGILI
SIMULACIÓ DE L'EFECTE DE LES INCISIONS QUIRÚRGIQUES EN EL COMPORTAMENT DE LA PARET ABDOMINAL
Lluís Tuset Serra

UNIVERSITAT ROVIRA I VIRGILI
SIMULACIÓ DE L'EFECTE DE LES INCISIONS QUIRÚRGIQUES EN EL COMPORTAMENT DE LA PARET ABDOMINAL
Lluís Tuset Serra

UNIVERSITAT ROVIRA I VIRGILI
SIMULACIÓ DE L'EFECTE DE LES INCISIONS QUIRÚRGIQUES EN EL COMPORTAMENT DE LA PARET ABDOMINAL
Lluís Tuset Serra

Lluís Tuset Serra

Simulació de l'efecte de les incisions quirúrgiques en el comportament de la paret abdominal

TESI DOCTORAL

Dirigida per la Dra. Dolors Puigjaner Riba
i pel Dr. Joan Herrero Sabartés

Departament d'Enginyeria Informàtica i Matemàtiques

UNIVERSITAT ROVIRA i VIRGILI

Tarragona, Catalunya
2024

UNIVERSITAT ROVIRA I VIRGILI
SIMULACIÓ DE L'EFECTE DE LES INCISIONS QUIRÚRGIQUES EN EL COMPORTAMENT DE LA PARET ABDOMINAL
Lluís Tuset Serra

UNIVERSITAT ROVIRA i VIRGILI

FEM CONSTAR que aquest treball, titulat “Simulació de l’efecte de les incisions quirúrgiques en el comportament de la paret abdominal”, que presenta Lluís Tuset Serra per a l’obtenció del títol de Doctor, ha estat realitzat sota la nostra direcció al Departament d’Enginyeria Informàtica i Matemàtiques d’aquesta universitat.

HACEMOS CONSTAR que el presente trabajo, titulado “Simulació de l’efecte de les incisions quirúrgiques en el comportament de la paret abdominal”, que presenta Lluís Tuset Serra para la obtención del título de Doctor, ha sido realizado bajo nuestra dirección en el Departamento de Ingeniería Informática y Matemàticas de esta universidad.

WE STATE that the present study, entitled “Simulació de l’efecte de les incisions quirúrgiques en el comportament de la paret abdominal”, presented by Lluís Tuset Serra for the award of the degree of Doctor, has been carried out under our supervision at the Department of Computer Engineering and Mathematics of this university.

Tarragona, 22/03/2024

Els directors de la tesi doctoral
Los directores de la tesis doctoral
Doctoral Thesis Supervisors

Firmado por Maria Dolores Puigjaner Riba - DNI 39867465R (TCAT) el día 21/02/2024 con un certificado emitido por EC-SectorPublic

Firmado por HERRERO SABARTES JUAN - ***5516** el día 21/02/2024 con un certificado emitido por AC FNMT Usuarios

Dra. Dolors Puigjaner Riba

Dr. Joan Herrero Sabartés

UNIVERSITAT ROVIRA I VIRGILI
SIMULACIÓ DE L'EFECTE DE LES INCISIONS QUIRÚRGIQUES EN EL COMPORTAMENT DE LA PARET ABDOMINAL
Lluís Tuset Serra

Agraïments

En primer lloc voldria agrair als membres del grup de recerca el seu suport des del primer dia, la seva dedicació i el seu acompanyament en tot moment. Ha estat un gran plaer poder treballar amb vosaltres i em sento molt orgullós d'haver format part del vostre equip durant tots aquests anys, m'heu fet sentir com un més.

Finalment, també voldria agrair al suport rebut per part de la família i de les amistats i molt especialment de tu, Anabel. Gràcies per la teva paciència i la teva calidesa. Gràcies per no deixar-me tirar la tovallola. Gràcies per ajudar-me tot i no dominar la matèria. Gràcies per estar al meu costat en tot moment.

Moltes gràcies a tots i a totes!

UNIVERSITAT ROVIRA I VIRGILI
SIMULACIÓ DE L'EFECTE DE LES INCISIONS QUIRÚRGIQUES EN EL COMPORTAMENT DE LA PARET ABDOMINAL
Lluís Tuset Serra

Resum

La simulació numèrica és una eina important per a la modelització del comportament mecànic de la paret abdominal. Gràcies a la modelització matemàtica és possible conèixer com responen els diferents teixits i músculs de la paret abdominal davant d'esforços, sense necessitat d'haver de recórrer a teixits reals, ja siguin humans o animals. Aquesta estratègia no invasiva fa possible estudiar diversos procediments quirúrgics i analitzar l'efecte d'un gran nombre de paràmetres. Aquest coneixement permet preveure la possible aparició d'hèrnies o la ruptura dels teixits, el que suposa un gran pas endavant tenint en compte la seva prevalença en l'actualitat.

De manera més concreta, s'estudia l'efecte de les incisions provocades per les ostomies i per les intervencions laparoscòpiques a partir d'un model geomètric de la paret abdominal que inclou els principals músculs d'aquesta capa que cobreix i protegeix els òrgans interns. Gràcies a les nombroses simulacions virtuals que s'han realitzat, s'ha pogut concloure que cal evitar la creació d'estomes al lateral dels músculs rectes així com sobre la línia alba. De la mateixa manera, s'ha conclòs que la resistència mecànica de les incisions laparoscòpiques es pot veure compromesa si aquestes se situen molt lateralment la qual cosa podria ser recomanable tancar les incisions laterals amb sutures o reforços protètics.

Tot i que en aquestes simulacions s'ha suposat un comportament elàstic lineal dels teixits de la paret abdominal, s'ha definit un nou model hiperelàstic transversalment isotròpic que considera el comportament com a no lineal en grans deformacions. Aquest model augmenta la precisió de les simulacions i proporciona una millor descripció de les propietats mecàniques a la vegada que millora l'eficiència d'altres models descrits en la literatura perquè es defineix exclusivament amb funcions polinòmiques. Per ajustar els paràmetres d'aquest nou model s'han utilitzat els resultats obtinguts en experiments in vivo presents en la literatura.

Finalment, convé subratllar que en tota aquesta investigació s'ha utilitzat exclusivament programari lliure de codi obert en la realització de totes les simulacions així com en l'anàlisi posterior dels resultats.

UNIVERSITAT ROVIRA I VIRGILI
SIMULACIÓ DE L'EFECTE DE LES INCISIONS QUIRÚRGIQUES EN EL COMPORTAMENT DE LA PARET ABDOMINAL
Lluís Tuset Serra

Abstract

Numerical simulation is an essential tool for modeling the mechanical behavior of the abdominal wall. The use of mathematical model makes it possible to comprehend the stress response of different tissues and muscles of the abdominal wall without having to rely on real human or animal tissues. This non-invasive approach facilitates the study of different surgical procedures and allows the analysis of the effect of numerous parameters. Therefore, it becomes feasible to predict the potential occurrence of hernias or tissue rupture which represents a noteworthy advancement given their current prevalence.

More specifically, the effects of incisions caused by ostomies and laparoscopic interventions are studied based on a geometric model of the abdominal wall that includes the main muscles of this layer which cover and protect the internal organs. Thanks to numerous virtual simulations, it was possible to conclude that it is necessary to avoid creating stomas located either laterally with respect to the rectus abdominis muscle or on the linea alba. Similarly, it was determined that the mechanical strength of laparoscopic incisions may be compromised if they are placed laterally. Therefore, it might be recommended to close these compromised incisions with sutures or even reinforce them with prosthetic materials.

Although a linear elastic behavior of the abdominal wall tissues was assumed in the simulations of the abdominal wall, a new non-linear transversely isotropic hyperelastic model was also developed. This model enhances the accuracy of the simulations and provides a more accurate description of the mechanical properties. Additionally, the model improves the efficiency of other reported models because it is characterized exclusively by polynomial functions. The parameters in the new model were adjusted using results obtained from in vivo experiments found in the literature.

Moreover, it is important to highlight that all the research was performed exclusively using free and open source software for numerical simulations as well as for the subsequent analysis of the results.

UNIVERSITAT ROVIRA I VIRGILI
SIMULACIÓ DE L'EFECTE DE LES INCISIONS QUIRÚRGIQUES EN EL COMPORTAMENT DE LA PARET ABDOMINAL
Lluís Tuset Serra

Resumen

La simulación numérica es una herramienta fundamental para modelar el comportamiento mecánico de la pared abdominal. Gracias a la modelización matemática, es posible comprender cómo responden los diferentes tejidos y músculos de la pared abdominal ante distintos esfuerzos, sin necesidad de utilizar tejidos reales, ya sean humanos o animales. Esta estrategia no invasiva permite estudiar diversos procedimientos quirúrgicos así como analizar el efecto de una amplia gama de parámetros. Con un conocimiento exhaustivo de estos efectos, es posible predecir la posible aparición de hernias o la ruptura de los tejidos, lo cual representa un gran avance considerando su prevalencia actual.

En particular, se estudia el efecto de las incisiones causadas por las ostomías y las intervenciones laparoscópicas utilizando un modelo geométrico de la pared abdominal que incluye los principales músculos de esta capa que cubre y protege los órganos internos. Gracias a las numerosas simulaciones virtuales realizadas, se ha llegado a la conclusión de que es necesario evitar la creación de estomas en los laterales de los músculos rectos y en la línea alba. Asimismo, se ha observado que la resistencia mecánica de las incisiones laparoscópicas puede verse comprometida si se colocan muy lateralmente, por lo que podría ser recomendable cerrar dichas incisiones con suturas o refuerzos protéticos.

Aunque en estas simulaciones se ha supuesto un comportamiento elástico lineal de los tejidos de la pared abdominal, se ha desarrollado también un nuevo modelo hiperelástico transversalmente isotrópico que considera el comportamiento no lineal y las grandes deformaciones. Este modelo mejora la precisión de las simulaciones y proporciona una descripción más precisa de las propiedades mecánicas, al mismo tiempo que optimiza la eficiencia de otros modelos previamente descritos debido a que se basa únicamente en funciones polinómicas. Para ajustar los parámetros de este nuevo modelo, se han utilizado los resultados obtenidos en experimentos in vivo presentes en la literatura.

Por último, es importante destacar que en toda esta investigación se ha empleado exclusivamente software libre de código abierto en la realización de todas las simulaciones así como en el análisis posterior de los resultados.

UNIVERSITAT ROVIRA I VIRGILI
SIMULACIÓ DE L'EFECTE DE LES INCISIONS QUIRÚRGIQUES EN EL COMPORTAMENT DE LA PARET ABDOMINAL
Lluís Tuset Serra

Índex

UNIVERSITAT ROVIRA I VIRGILI
SIMULACIÓ DE L'EFECTE DE LES INCISIONS QUIRÚRGIQUES EN EL COMPORTAMENT DE LA PARET ABDOMINAL
Lluís Tuset Serra

1. Introducció

En aquest capítol es detalla la justificació per dur a terme aquesta investigació i quins són els objectius que es volen assolir. A la Secció 1.1 s'explica la motivació principal que ha portat a realitzar aquest estudi. A la Secció 1.2 s'especifiquen els principals objectius que pretén assolir aquest treball i a la Secció 1.3 quina serà la metodologia emprada. Finalment, a la Secció 1.4 es descriu com s'ha estructurat la resta del document.

1.1 Motivació

Una hèrnia és una afecció que es produeix quan part d'un teixit surt de la seva posició habitual a través d'una obertura degut al debilitament de l'estructura que l'envolta. Les hèrnies més habituals són les abdominals [1] i consisteixen en una una protrusió del sac peritoneal a través del conjunt muscular i aponeuròtic[1]. Es quantifica en 20 milions el nombre de reparacions anuals d'hèrnies arreu del món [2]. La prevalença de les hèrnies i les complicacions que poden aparèixer en la seva reparació [3], fa que l'estudi dels motius d'aparició d'aquestes protuberàncies sigui d'especial interès. La majoria de les hèrnies es produeixen a causa d'una combinació entre la debilitat estructural i la pressió interna.

La cavitat abdominal no està protegida per cap estructura rígida i el seu suport el proporciona la paret abdominal. Aleshores, la integritat d'aquesta paret és essencial per al correcte funcionament fisiològic de la cavitat abdominal, és a dir, per tal de mantenir situacions dinàmiques i per suportar altes pressions [4]. Cal destacar que una hèrnia abdominal pot afectar totes les capes musculars de la paret o tan sols una d'elles [5].

En ocasions algunes obertures de la paret abdominal són realitzades de forma artificial com a part del procediment per a tractar determinades malalties relacionades amb l'aparell digestiu o urinari. Aquest tipus de procediment s'anomena ostomia i l'obertura artificial creada estoma. Aquestes intervencions es duen a terme per permetre la sortida de productes de rebuig del cos [6] en diverses situacions com en el cas de malalties inflamatòries de l'intestí, càncer o lesions traumàtiques. Els estomes poden ser temporals o permanents i les tipologies més freqüents són la ileostomia (obertura per treure l'intestí prim) i la colostomia (obertura per treure el colon o intestí gros) [7]. Tot i que la realització d'un

[1] Estructura plana i fibrosa similar a un tendó composta principalment de fibres de col·lagen.

estoma és una pràctica relativament senzilla, les seves conseqüències poden ser complexes i potencialment mortals [8].

Una de les complicacions més freqüents de les ostomies és l'aparició de les hèrnies paraestomals [9] amb una incidència que gairebé arriba al 50% en determinats casos [10]. Les hèrnies paraestomals són difícils de tractar i disminueixen significativament la qualitat de vida dels pacients a la vegada que influeixen negativament en la seva pròpia imatge corporal [11]. Hi ha diversos factors de risc pel que fa a la seva aparició entre els quals destaquen la localització i la mida de l'estoma [12]. Donat que no hi ha suficients dades clíniques que permetin determinar la millor ubicació de l'estoma, una alternativa menys invasiva és la modelització tridimensional de la paret abdominal per tal de determinar el seu comportament mecànic davant de variacions anatòmiques com són els estomes [13].

El comportament de la paret abdominal es pot estudiar mitjançant tècniques experimentals, *in vivo*, que acostumen a ser difícils de desenvolupar a més de ser invasives, o bé a través de tècniques numèriques, *in silico*, que utilitzen simulacions computacionals basades en el mètode d'anàlisi per elements finits [14] per a modelitzar el comportament de la paret abdominal de manera no invasiva. Aquesta estratègia és d'especial interès ja que permet analitzar un gran nombre de paràmetres així com l'efecte dels procediments quirúrgics o les propietats mecàniques dels teixits de la paret abdominal [15].

L'hèrnia incisional (o eventració) és un altre tipus d'hèrnia de l'abdomen que consisteix en una protuberància en la zona on s'ha realitzat una incisió degut al debilitament del teixit. La seva incidència després de determinades cirurgies abdominals és d'entre el 2% i el 18% [16], [17]. Un d'aquests procediments és la laparoscòpia que en els darrers anys ha passat de ser una eina diagnòstica a ser una tècnica quirúrgica [18]. Aquesta tècnica, en comparació amb les cirurgies obertes, té molts beneficis ja que el fet de no haver de fer grans incisions fa que la pèrdua de sang sigui menor, que la recuperació sigui més ràpida i que els pacients pateixin menys dolor postoperatori [19]. Tot i això, aquesta pràctica, com qualsevol altre procediment quirúrgic, pot provocar certes complicacions com per exemple les infeccions, el sagnat, les lesions en òrgans i les hèrnies incisionals [18], [20]. Precisament el desenvolupament d'una hèrnia incisional és la complicació més habitual [21] i es creu que té una prevalença d'entre el 0.8% i el 2.9% [22].

El risc d'aparició d'una hèrnia incisional depèn de diversos factors com la localització de la incisió, el material de sutura utilitzat i la tècnica de tancament de la incisió realitzada [23]. De nou, la modelització del comportament de l'abdomen a través de les simulacions numèriques pot ajudar a comprendre com les ferides provocades per aquestes incisions quirúrgiques alteren el comportament biomecànic de la paret abdominal.

La paret abdominal està formada per teixits tous que s'encarreguen de connectar i envoltar altres estructures i òrgans del cos. Aquests teixits inclouen els músculs, els tendons, el

greix, els vasos sanguinis, etc., i estan formats per proteïnes entre les quals destaca el col·lagen que és qui en determina les seves propietats mecàniques [24].

Ja que els teixits tous tenen un comportament elàstic molt elevat i són capaços de suportar grans deformacions sense trencar-se o perdre les seves propietats mecàniques, s'acostumen a modelitzar matemàticament com a materials hiperelàstics [25]. A diferència dels materials elàstics, que es caracteritzen per una relació tensió-deformació lineal, els materials hiperelàstics tenen una resposta no lineal quan se'ls aplica una càrrega externa. El fet de considerar la hiperelasticitat enriqueix la precisió de les simulacions numèriques i ofereix una millor descripció de les propietats mecàniques dels teixits ja que descriu de manera més precisa el seu comportament quan s'aplica poca tensió i s'obtenen grans deformacions [26].

La motivació d'aquesta tesi radica en el desig d'aprofundir en el coneixement de com influeixen les hèrnies incisionals en el comportament mecànic de la paret abdominal a través de simulacions virtuals eficients que modelitzin de forma precisa aquest comportament. A més, es vol contribuir de manera significativa en aquest camp acadèmic aportant eines que generin oportunitats als professionals de la cirurgia abdominal.

1.2 Objectius

L'objectiu principal d'aquest treball és modelitzar adequadament el comportament biomecànic de la paret abdominal per tal de poder realitzar simulacions numèriques que permetin ampliar el coneixement actual que es té sobre aquesta matèria. El fonament principal d'aquest estudi és aprofitar el potencial computacional actual per tal d'ajudar als professionals de la cirurgia a prendre decisions a l'hora de realitzar determinats procediments quirúrgics amb l'objectiu de reduir la probabilitat d'aparició de determinades complicacions postoperatòries.

Es vol dissenyar i implementar un nou model hiperelàstic a través d'una funció d'energia que sigui computacionalment senzilla i eficient i que permeti millorar el rendiment de les simulacions numèriques. Aquest model es caracteritza per l'ús exclusiu de funcions polinòmiques.

Per altra banda, es vol estudiar com afecten certes incisions que es practiquen sobre la paret abdominal en el comportament mecànic d'aquesta i determinar quines característiques han de tenir aquestes incisions per tal de reduir el risc d'aparició d'hèrnies incisionals. Aquest se centra en dos aspectes de les incisions: la seva localització i les seves característiques físiques.

Es consideren dos tipus d'incisions:

- Els estomes que es realitzen en les ostomies per tractar certes malalties relacionades amb l'aparell digestiu o urinari.
- Les incisions laparoscòpiques (incisions mínimament invasives) realitzades en la paret abdominal quan es realitzen cirurgies laparoscòpiques.

Es pretén determinar la regió idònia on practicar cadascuna d'aquestes incisions tenint en compte variables com el camp de tensió-deformació dels principals músculs implicats, la deformació de la ferida i paràmetres com l'estat físic de la ferida (elasticitat) i la mida de la incisió.

Finalment, el darrer objectiu d'aquesta tesi és utilitzar exclusivament programari lliure de codi obert i gratuït.

1.3 Mètodes

La metodologia emprada en aquesta tesi està formada per diverses etapes relacionades entre elles amb l'objectiu final d'obtenir un model matemàtic que descrigui el més acuradament possible el comportament real de la paret abdominal. El punt de partida és la definició d'un model geomètric que inclou els principals músculs que formen la paret abdominal i les seves característiques físiques i mecàniques. Seguidament es dissenya un model matemàtic constitutiu del comportament biomecànic de la paret abdominal. A partir d'aquests dos elements inicials i tenint en compte unes condicions de contorn prèviament establertes, es realitza una simulació numèrica d'aquest comportament a través d'eines computacionals.

Aquesta darrera etapa permet obtenir uns resultats i dades que són difícils o impossibles d'obtenir experimentalment. Havent obtingut aquests resultats, se'n fa una interpretació crítica i detallada per tal de comprendre millor el comportament de la paret abdominal i també per avaluar l'adequació del model proposat. La interpretació dels resultats comprén l'anàlisi visual i l'anàlisi quantitatiu dels valors numèrics obtinguts. Finalment, per tal de validar i millorar el model desenvolupat, es comparen els resultats obtinguts amb les dades experimentals o numèriques disponibles en la bibliografia actual. Això permet contrastar la precisió i la fiabilitat del model i, si és necessari, ajustar-lo per tal d'aproximar-se més a la realitat (Fig. 1.1).

Aquesta metodologia integrada té com a principal objectiu millorar la comprensió i el coneixement del comportament de la paret abdominal així com de les incisions que s'hi practiquen proporcionant aportacions que s'espera que siguin d'utilitat en aplicacions pràctiques reals.

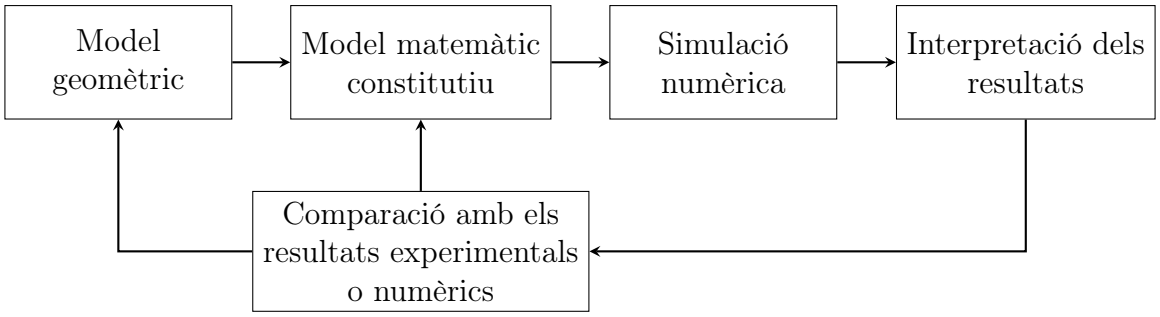

Figura 1.1: Diagrama esquemàtic de la metodologia emprada en aquesta investigació.

1.3.1 Model geomètric

El model geomètric utilitzat s'ha obtingut de la base de dades BodyParts3D [27]. A partir de les malles disponibles en aquesta base de dades s'ha fet un treball de millora d'aquestes i s'ha construït una malla volumètrica que serà el model geomètric amb el qual es duran a terme totes les simulacions. Aquest model consta de quatre parells de músculs superposats: els dos músculs oblics externs, els dos músculs oblics interns, els dos músculs rectes abdominals, els dos músculs transversos de l'abdomen i la línia alba (Fig. 1.2).

L'aponeurosi dels transversos i dels oblics interns i externs formen l'anomenada beina del recte [28], [29]. Ja que el teixit de la beina del recte és més fibrós que el teixit muscular normal, s'han definit tres regions per als oblics interns, els oblics externs i els transversos: la part corresponent al múscul regular (que és la més allunyada del recte), la beina dels músculs que està en contacte directe amb el recte i una regió fina de transició intermèdia entre les dues regions anteriors (Fig. 1.3).

Pel que fa a les incisions, els estomes s'han modelitzat com a orificis cilíndrics circulars de 2 cm de diàmetre considerats en 17 posicions diferents (Fig. 1.4a). Pel que fa a les incisions laparoscòpiques, s'han modelitzat les ferides de les sutures com a cilindres el·líptics ortogonals a la superfície de la paret abdominal i s'han considerat dos patrons diferents per aquestes ferides: el model A amb 6 incisions (Fig. 1.4b) i el model B amb només 5 (Fig. 1.4c) d'entre 5 i 12 mm de la longitud. Cal destacar que, a diferència dels estomes (estudi 2, Secció 2.2) que són orificis sobre la paret abdominal, les ferides de la laparoscòpia (estudi 3, Secció 2.3) es consideren com a ferides un cop suturades, no com a orificis.

1.3.2 Model constitutiu

Ja que la paret abdominal està formada per diversos músculs amb diferents propietats mecàniques que contribueixen al seu comportament mecànic [30], s'ha desenvolupat un nou model constitutiu (estudi 1, Secció 2.1) que permeti simular el comportament mecànic de la paret abdominal d'una manera computacionalment robusta i eficient.

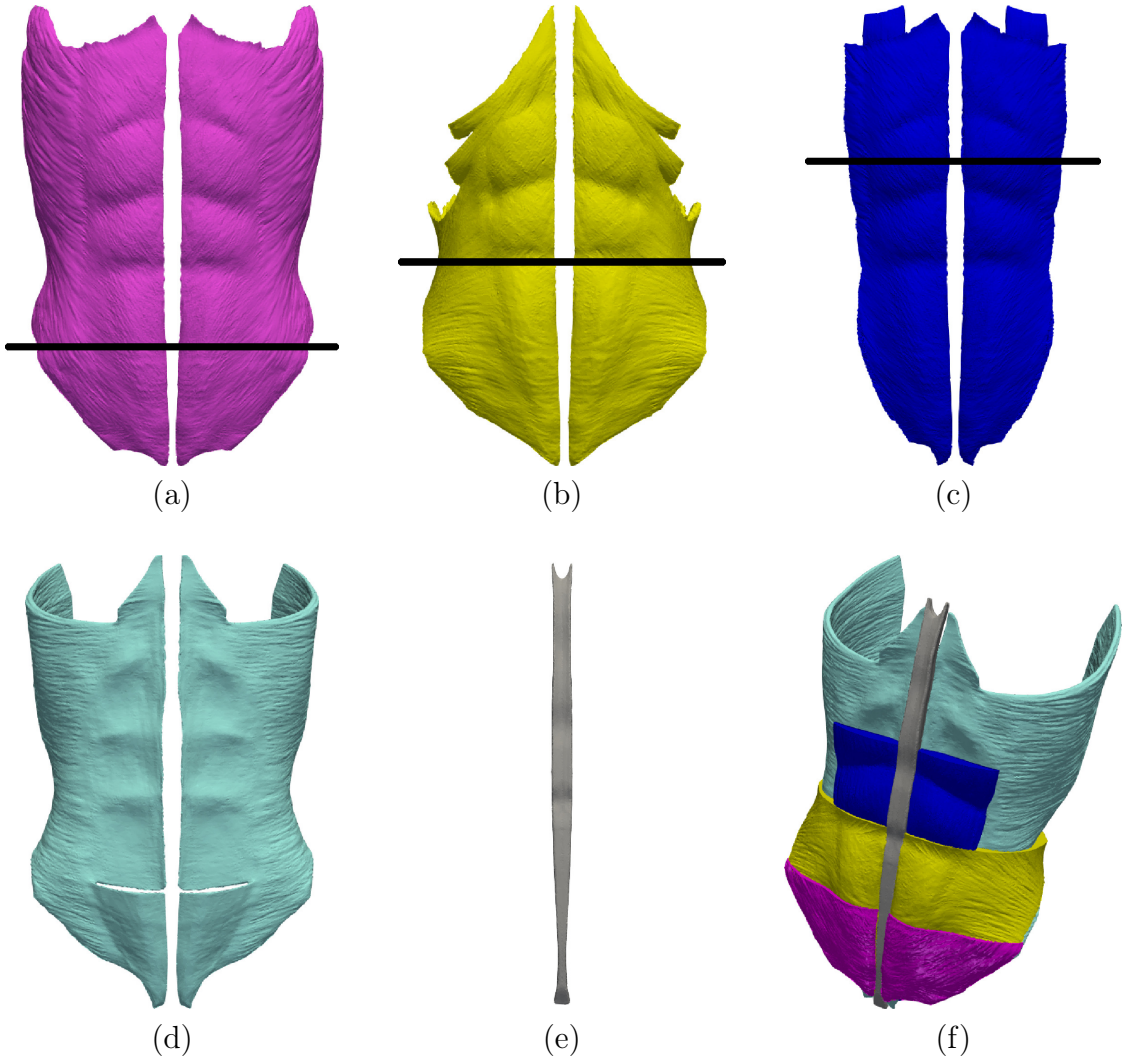

Figura 1.2: Model geomètric de la paret abdominal. Els elements inclosos són: músculs oblics externs (a), músculs oblics interns (b), músculs rectes abdominals (c), músculs transversos de l'abdomen (d) i línia alba (e). Ja que els músculs implicats estan superposats, en la figura de tot el model geomètric (f) només es mostra la part de cada múscul per sota de la línia negra.

A diferència dels models elàstics lineals, la relació tensió-deformació del model hiperelàstic es descriu a través d'una funció d'energia de deformació[2], Ψ, que depèn del gradient de deformació, F [32]. Existeixen diverses formulacions amb propietats i característiques diferents que les fan apropiades per a caracteritzar els materials hiperelàstics [33]. Un model que té en compte l'anisotropia[3] del teixit [34] i un comportament no lineal en grans deformacions [24] és el model hiperelàstic transversalment isotròpic.

La funció d'energia del nou model constitutiu que s'ha desenvolupat es descompon en una part volumètrica $U(J)$ i una altra d'isocora $\Psi_{ich}(J, C)$ ja que se suposa que el teixit és

[2]Funció matemàtica que representa l'energia potencial emmagatzemada dins d'un material que ha estat sotmès a una deformació [31].

[3]Característica dels teixits tous per la qual presenten propietats amb diferents valors quan es mesuren en diferents direccions.

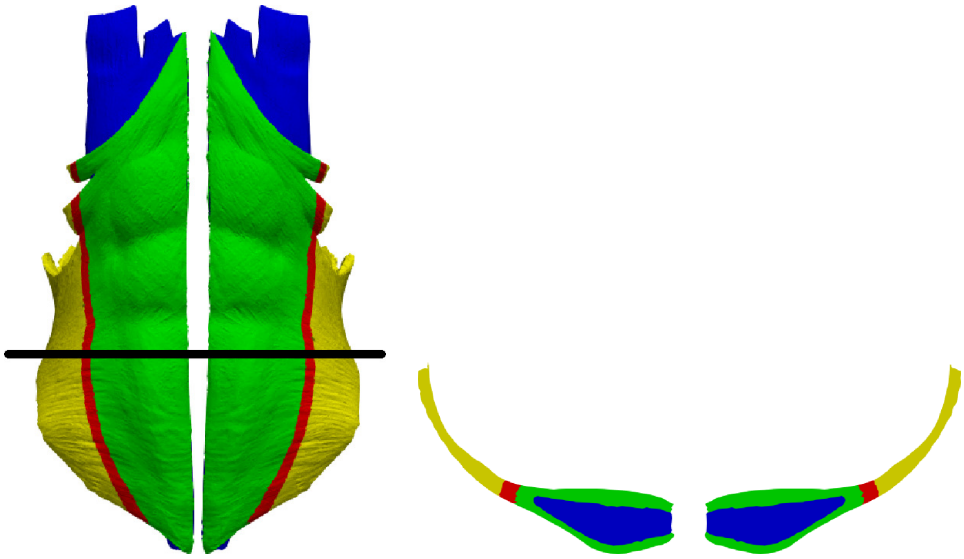

(a) (b)

Figura 1.3: Exemple de transició entre el teixit del múscul regular i la seva aponeurosi en el cas de l'oblic intern: múscul regular (groc), zona de transició (vermell) i la beina que està en contacte amb el recte (verd). La línia negra de la figura (a) indica la zona on s'ha realitzat el tall (b).

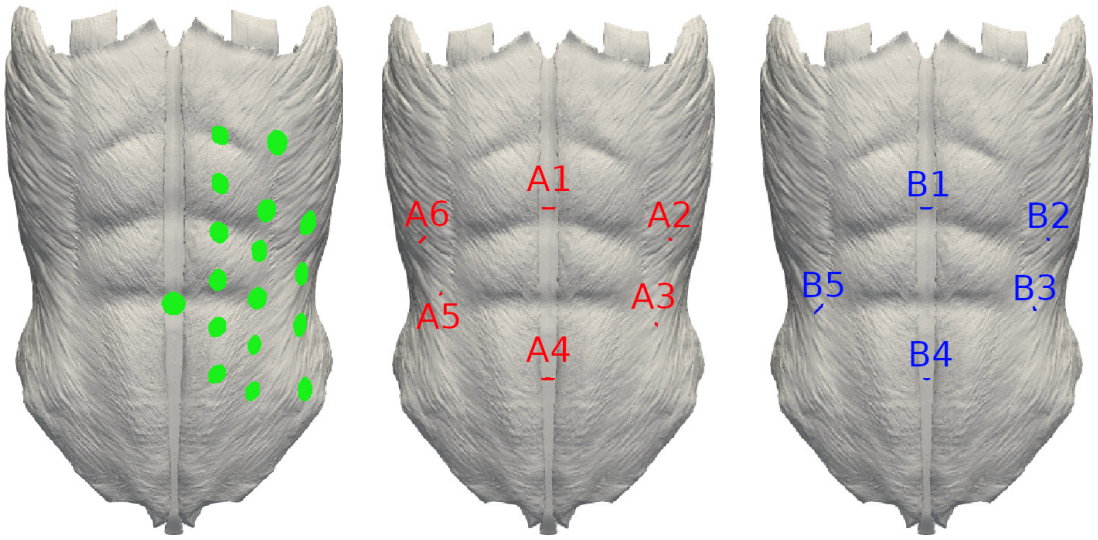

(a) (b) (c)

Figura 1.4: Les 17 localitzacions diferents de l'estoma que s'han considerat (a). Patrons de distribució de les ferides laparoscòpiques: patró A (b) i patró B (c).

lleugerament compressible:

$$\Psi(J, C) = U(J) + \Psi_{ich}(J, C) \tag{1.1}$$

essent J el determinant del gradient F i C el tensor dret de deformació de Cauchy-Green definit per $C = F^T F$. La part volumètrica, $U(J)$, es defineix com a:

$$U(J) = \frac{1}{2}K\left(J^2 - 1 - 2\ln J\right) \tag{1.2}$$

essent K el mòdul de compressibilitat. Pel que fa a la part isocora, $\Psi_{ich}(J, C)$, ja que se suposa que el teixit tou és un compost format per un material isotròpic i un conjunt de fibres que tenen una direcció preferent a_0, també es descompon en:

$$\overline{\Psi}(\overline{C}, a_0) = \overline{\Psi}_{iso}(\overline{C}) + \overline{\Psi}_{fib}(\overline{C}, a_0) \tag{1.3}$$

essent $\overline{C} = J^{-2/3}C$ el tensor dret de deformació de Cauchy-Green modificat. El model proposat està format exclusivament per funcions polinòmiques i es va comprovar inicialment que ajustava a les dades experimentals:

$$\overline{\Psi}_{iso} = C_1(\overline{I}_1 - 3) + C_2(\overline{I}_1 - 3)^2 \tag{1.4}$$

$$\overline{\Psi}_{fib} = C_3(\overline{I}_4 - 1)^2 + C_4(\overline{I}_4 - 1)^4 \tag{1.5}$$

essent $\overline{I}_1$ i $\overline{I}_4$ els pseudoinvariants de $\overline{C}$. L'objectiu d'aquesta investigació és obtenir el valor del mòdul de compressibilitat K i dels paràmetres C_1, C_2, C_3 i C_4 per a cadascun dels músculs del model geomètric. Per fer-ho es comparen els resultats teòrics obtinguts en les simulacions numèriques amb les dades experimentals disponibles en la literatura les quals s'obtenen majoritàriament gràcies a assajos de tracció amb teixits reals.

Aquest nou model constitutiu ha de permetre implementar el problema numèric de forma eficient realitzant un gran nombre d'execucions amb una quantitat limitada de recursos computacionals.

Tot i que l'objectiu final és fer simulacions de tota la paret abdominal amb aquest nou model, per començar i per tal de poder veure si hi ha canvis significatius en els resultats, les simulacions de les incisions practicades sobre la paret (estudis 2 i 3, seccions 2.2 i 2.3 respectivament) s'han fet considerant un model elàstic lineal:

$$\sigma = E \cdot \varepsilon \tag{1.6}$$

σ el tensor tensió, ε el tensor deformació i E el mòdul elàstic o mòdul de Young, que és una propietat intrínseca del material que indica la seva rigidesa i resiliència.

1.3.3 Simulació numèrica

La simulació numèrica és una tècnica computacional que a través d'algorismes i mètodes numèrics permet modelar i estudiar el comportament de sistemes complexos. A partir d'un model que representa el sistema real i aplicant tècniques de mètodes numèrics, permet simular el seu comportament i obtenir uns resultats aproximats. És una eina valuosa per tal d'analitzar escenaris hipotètics, predir resultats, optimitzar dissenys i prendre decisions. En general, és una alternativa més eficient i econòmica respecte l'experimentació real.

En aquest treball s'ha aplicat el mètode d'anàlisi per elements finits per a realitzar les simulacions. Aquest mètode és àmpliament utilitzat per analitzar el comportament mecànic dels teixits biològics ja que permet fer simulacions repetitives canviant múltiples paràmetres, fet que no és possible amb experiments amb teixits reals [35]. La simulació numèrica es basa en discretitzar el model geomètric en una malla d'elements finits en els quals s'obtenen les seves propietats mecàniques a través de la resolució de sistemes d'equacions associats al problema.

1.3.4 Eines

Aquesta recerca s'ha desenvolupat exclusivament amb programari lliure de codi obert partint de la premissa que aquests programes es caracteritzen per una major flexibilitat respecte el programari privatiu. Les principals eines utilitzades es detallen a continuació:

- **Gmsh**: generador de malles tridimensionals d'elements finits tridimensionals amb un motor CAD integrat i un postprocessador [36]. En aquesta investigació s'ha utilitzat per a generar les malles volumètriques del model de la paret abdominal per ser utilitzades posteriorment amb Code_Aster.

- **Code_Aster**: programa de simulació numèrica. Principalment és un motor de processament (*solver*) basat en la teoria dels medis continus[4] que utilitza el mètode dels elements finits per a resoldre diferents problemes mecànics [37]. Aquest programari s'ha utilitzat en cadascuna de les simulacions numèriques que s'han realitzat.

- **Salome-Meca**: plataforma de simulació numèrica i anàlisi que utilitza, com a motor de càlcul, Code_Aster. Proporciona una interfície gràfica per a l'ús de Code_Aster i, a més, facilita la preparació dels models, la gestió de les propietats materials, l'aplicació de càrregues i condicions de contorn i l'anàlisi dels resultats. S'ha utilitzat per al preprocessament (geometria de la paret abdominal, condicions de contorn,

[4]La mecànica dels medis continus és una eina que permet estudiar el comportament mecànic d'un material considerant-lo com un sistema continu. És especialment efectiva en l'estudi de materials deformables com són els teixits tous.

pressió aplicada i mallat); i en el postprocessament (anàlisi dels resultats obtinguts en les simulacions).

- **MFront**: és un generador de codi que permet definir models de simulació numèrica amb diverses propietats materials i comportaments mecànics [38]. El principal avantatge de MFront és que el seu llenguatge computacional té punts en comú amb el llenguatge matemàtic emprat a través d'instruccions simples. Aquesta eina s'ha utilitzat per definir el nou model hiperelàstic transversalment isotròpic i incorporar-lo a Code_Aster.

1.4 Estructura del document

Aquest document està estructurat com a compendi dels articles que es reprodueixen al Capítol 2. En l'estudi 1 (Secció 2.1) es proposa i s'implementa un nou model constitutiu del comportament dels músculs de la paret abdominal basat en els models hiperelàstics transversalment isotròpics. En l'estudi 2 (Secció 2.2) es fa una simulació numèrica extensa sobre l'efecte que tenen les posicions dels estomes sobre el comportament mecànic de la paret abdominal. Finalment, en l'estudi 3 (Secció 2.3) es fa de nou una simulació virtual, com en l'estudi anterior, però en aquest cas s'estudia quin és l'efecte de les cicatrius d'una laparoscòpia.

El Capítol 3 resumeix les principals conclusions d'aquesta tesi així com les principals propostes de continuació i treball futur d'aquesta investigació.

2. Contribucions de la tesi

Seguidament s'inclouen els tres articles publicats durant el desenvolupament d'aquesta tesi doctoral els quals representen el resultat i discussió del treball realitzat. El candidat a doctor és l'autor principal de cadascun d'aquests articles que estan indexats a la base de dades internacional ISI-JCR.

Articles publicats

UNIVERSITAT ROVIRA I VIRGILI
SIMULACIÓ DE L'EFECTE DE LES INCISIONS QUIRÚRGIQUES EN EL COMPORTAMENT DE LA PARET ABDOMINAL
Lluís Tuset Serra

2.1 Estudi 1 - Nou model constitutiu

Implementation of a new constitutive model for abdominal muscles

Lluís Tuset, Gerard Fortuny, Joan Herrero, Dolors Puigjaner i Josep M. López. *Computer Methods and Programs in Biomedicine, 179, 104988, 2019.*
DOI: 10.1016/j.cmpb.2019.104988

Computer Methods and Programs in Biomedicine 179 (2019) 104988

Contents lists available at ScienceDirect

Computer Methods and Programs in Biomedicine

journal homepage: www.elsevier.com/locate/cmpb

Implementation of a new constitutive model for abdominal muscles

Lluís Tuset[a,*], Gerard Fortuny[a], Joan Herrero[b], Dolors Puigjaner[a], Josep M. López[a]

[a] Departament d'Enginyeria Informàtica i Matemàtiques, Universitat Rovira i Virgili, Av Països Catalans 26, Tarragona, Catalunya, Spain
[b] Departament d'Enginyeria Química, Universitat Rovira i Virgili, Av Països Catalans 26, Tarragona, Catalunya, Spain

ARTICLE INFO

Article history:
Received 7 June 2019
Revised 2 July 2019
Accepted 15 July 2019

Keywords:
Abdominal wall
Open-source software
Strain energy functions
Hyperelasticity
Finite element method

ABSTRACT

Background and objective: Abdominal hernia repair is one of the most often performed surgical procedures worldwide. Numerical simulations of the abdominal wall mechanics can be a valuable tool to devise actions aimed at preventing hernia formation. A first step towards this goal is the development of consistent constitutive models for the tissues that form the human abdominal wall. In this study we propose, for each of the tissues involved, a new formulation of the so–called transversely isotropic hyperelastic model (TIHM).
Methods: We propose a new TIHM for the human abdominal wall tissues and we present a systemic view of the methodology that we have implemented in the present study. First we consider the mathematical background of the TIHM. The novelty of our formulation is that both the isotropic and the fiber contributions to the strain energy function are characterized exclusively by polynomial convex functions of certain invariant quantities. Then, we provide a detailed description on how the constitutive model is implemented into an open source finite element (FE) software. In our approach we use the specific interface provided by the `MFront` software to incorporate our TIHM formulation into the `Code Aster` FE solver. For each of the tissues considered, the values of the TIHM constants are adjusted by means of a numerical simulation of previous experimental data from tensile tests.
Results: We studied the following abdominal wall tissues: linea alba, rectus sheath, external oblique muscle, internal oblique muscle, transversus abdominis muscle and rectus abdominis muscle. Our formulation closely reproduces tensile test data for each tissue in the corresponding FE numerical simulation.
Conclusions: The new TIHM formulation is suitable for a future numerical investigation of the abdominal wall, which will in turn help us to assess the best zone to practice a colostomy. The methodology implemented in the present study can be easily extended in the future to develop and implement a TIHM for active muscles and/or a different type of constitutive model which might be suitable to characterize other tissues of biomedical interest.

© 2019 Elsevier B.V. All rights reserved.

1. Introduction

The study of the mechanical behavior of the abdominal wall is fundamental for the knowledge of the genesis of abdominal hernias. An abdominal hernia is a protrusion of the peritoneal sac through the muscular and aponeurotic set. Abdominal hernia repair is a quite common surgical operation. Actually, it is estimated that more than 20 million hernias are repaired throughout the world every year [1,2]. In particular, more than 300 000 ventral hernia repairs and 700 000 inguinal hernia repairs were performed in 2003 in the USA [3]. Moreover, ventral hernia repairs are increasing at an estimated rate of 3% per year [3]. All these figures lead to a significant burden on the costs of healthcare systems. Therefore any action aimed at preventing hernia formation or improving hernia surgical interventions will be highly helpful.

The origin and recurrence of abdominal hernias are mostly still unknown today. Notwithstanding, it is known that a most common long–term complication following a colostomy is the creation of a hernia [4]. Therefore numerical simulations of the abdominal wall mechanics are a valuable tool to shed some light on this health problem. The abdominal wall is a composite of several muscles with different mechanical properties that contribute to its mechanical behavior [5]. Constitutive models of the different muscle tissues that form the abdominal wall play a key role in the simulations of its mechanics. The purpose of the current study is the development and implementation of a methodology that allows the simulation of the mechanical behavior of each type of muscle tissue and, moreover, to do so in a computationally robust, transparent and efficient way.

* Corresponding author.
E-mail addresses: ltuset@xtec.cat (L. Tuset), gerard.fortuny@urv.cat (G. Fortuny), joan.herrero@urv.cat (J. Herrero), dolors.puigjaner@urv.cat (D. Puigjaner), josep.m.lopez@urv.cat (J.M. López).

https://doi.org/10.1016/j.cmpb.2019.104988
0169-2607/© 2019 Elsevier B.V. All rights reserved.

UNIVERSITAT ROVIRA I VIRGILI
SIMULACIÓ DE L'EFECTE DE LES INCISIONS QUIRÚRGIQUES EN EL COMPORTAMENT DE LA PARET ABDOMINAL
Lluís Tuset Serra

A common physical model of the abdominal wall, which we assume in the present study, comprises the linea alba (LA), the two external oblique muscles (EO), the two internal oblique muscles (IO), the two transversus abdominis muscles (TR) and the two rectus abdominis muscle (RA). The model also considers the rectus-sheath (RS), which is a connective tissue made of collagen that encloses the RA. Soft tissues are usually modelled as hyperelastic materials [6], i.e., materials for which a strain energy function (SEF), also known as Helmholtz free-energy function, Ψ, is defined. If, in addition, the tissue is assumed to be slightly compressible then the SEF is decoupled into a volumetric and an isochoric part,

$$\Psi(J,\mathbf{C}) = U(J) + \Psi_{ich}(J,\mathbf{C}) \tag{1}$$

and the second Piola–Kirchoff stress tensor, $\mathbf{S}$, is consequently decoupled as,

$$\mathbf{S} = \mathbf{S}_{vol}(J) + \mathbf{S}_{ich}(J,\mathbf{C}) \tag{2}$$

where the volumetric and isochoric parts are defined as:

$$\mathbf{S}_{vol}(J) = 2\left(\frac{\partial U(J)}{\partial \mathbf{C}}\right) = 2U(J)_{,\mathbf{C}} \tag{3}$$

$$\mathbf{S}_{ich}(J,\mathbf{C}) = 2\left(\frac{\partial \Psi_{ich}(J,\mathbf{C})}{\partial \mathbf{C}}\right) = 2\Psi_{ich}(J,\mathbf{C})_{,\mathbf{C}} \tag{4}$$

In Eqs. (1)–(4) $\mathbf{C}$ denotes the right Cauchy–Green symmetric tensor, defined as $\mathbf{C} = \mathbf{F}^T\mathbf{F}$, where $\mathbf{F}$ is the deformation gradient and J is the determinant of $\mathbf{F}$. In Eqs. (3) and (4) the compact $()_{,\mathbf{C}}$ notation for the partial derivative of a tensor–valued function is introduced. At this point it is worth noting that the second Piola–Kirchoff strain tensor is the dual of the Green–Lagrange strain tensor and that the use of the right Cauchy–Green tensor $\mathbf{C}$ ensures objectivity (frame–independence).

To simulate the behavior of soft tissues such as those found in the abdominal wall it is necessary to consider anisotropy [7,8], as fibers tend to have preferred directions and a non-linear behavior at large strains [9]. The so–called transversely isotropic hyperelastic model (TIHM) fulfills both theoretical requirements [6] and has been therefore frequently used to model soft tissue behavior. It is worth noting that the TIHM, as is the case with any purely elastic constitutive model, is not suited to predict short–term memory effects such as the rate–induced hardening of pig skin reported by Zhou et al. [10]. One approach to model such effects consists in the addition of a viscous SEF into the r.h.s. of Eq. (1) [11]. Recently published proposals of the so–called transversely isotropic viscous–hyperelastic constitutive model may be found in Refs. [12–14].

In the TIHM the soft tissue is assumed to be a composite formed by a ground isotropic material and one family of fibers which have a preferred direction, $\mathbf{a}_0$. It is customary to implement the constitutive Eq. (4) in terms of the modified SEF, $\overline{\Psi} = \overline{\Psi}(\overline{\mathbf{C}}, \mathbf{a}_0)$, where $\overline{\mathbf{C}} = J^{-2/3}\mathbf{C}$ is the modified right Cauchy–Green tensor:

$$\begin{aligned}\mathbf{S}_{ich}(J,\mathbf{C},\mathbf{a}_0) &= 2\Psi_{ich}(J,\mathbf{C},\mathbf{a}_0)_{,\mathbf{C}} = 2\overline{\Psi}(\overline{\mathbf{C}},\mathbf{a}_0)_{,\mathbf{C}} \\ &= 2\overline{\Psi}(\overline{\mathbf{C}},\mathbf{a}_0)_{,\overline{\mathbf{C}}} : \overline{\mathbf{C}}_{,\mathbf{C}} = \overline{\mathbf{S}} : \mathbb{P}\end{aligned} \tag{5}$$

The tensor quantities $\overline{\mathbf{S}}$ and $\mathbb{P}$ introduced in Eq. (5) are defined as [6]:

$$\overline{\mathbf{S}}(\overline{\mathbf{C}},\mathbf{a}_0) = 2\overline{\Psi}(\overline{\mathbf{C}},\mathbf{a}_0)_{,\overline{\mathbf{C}}} \tag{6}$$

$$\mathbb{P}(J,\mathbf{C}) = \overline{\mathbf{C}}_{,\mathbf{C}} = J^{-2/3}\left(\mathbb{I} - \frac{1}{3}\mathbf{C}\otimes\mathbf{C}^{-1}\right) \tag{7}$$

In Eq. (7) $\mathbb{I}$ denotes the fourth–order unit tensor. In practice, the rather expensive evaluation of the $\overline{\mathbf{S}} : \mathbb{P}$ double contraction in Eq. (5) can be circumvented using the following identity [15]:

$$\overline{\mathbf{S}} : \mathbb{P} = J^{-2/3}\left(\overline{\mathbf{S}} - \frac{1}{3}(\overline{\mathbf{S}} : \mathbf{C})\mathbf{C}^{-1}\right) \tag{8}$$

In the TIHM formulation a fibrous tissue is modeled by decomposing the modified SEF, $\overline{\Psi}$, into a ground isotropic contribution, $\overline{\Psi}_{iso}$, plus a fiber contribution, $\overline{\Psi}_{fib}$:

$$\overline{\Psi}(\overline{\mathbf{C}},\mathbf{a}_0) = \overline{\Psi}_{iso}(\overline{\mathbf{C}}) + \overline{\Psi}_{fib}(\overline{\mathbf{C}},\mathbf{a}_0) \tag{9}$$

Since the SEF must be independent of the coordinate system $\overline{\Psi}_{iso}$ and $\overline{\Psi}_{fib}$ are expressed as functions of invariants and pseudo–invariants of $\overline{\mathbf{C}}$ and $\mathbf{a}_0\otimes\mathbf{a}_0$ [6]

$$\overline{\Psi}_{iso} = \overline{\Psi}_{iso}\left(\bar{I}_1(\overline{\mathbf{C}}), \bar{I}_2(\overline{\mathbf{C}})\right) \tag{10}$$

$$\overline{\Psi}_{fib} = \overline{\Psi}_{fib}\left(\bar{I}_4(\overline{\mathbf{C}},\mathbf{a}_0), \bar{I}_5(\overline{\mathbf{C}},\mathbf{a}_0)\right) \tag{11}$$

where

$$\bar{I}_1(\overline{\mathbf{C}}) = \mathrm{tr}(\overline{\mathbf{C}}) \tag{12}$$

$$\bar{I}_2(\overline{\mathbf{C}}) = \frac{1}{2}\left[\left(\mathrm{tr}(\overline{\mathbf{C}})\right)^2 - \mathrm{tr}\left(\overline{\mathbf{C}}^2\right)\right] \tag{13}$$

$$\bar{I}_4(\overline{\mathbf{C}},\mathbf{a}_0) = \overline{\mathbf{C}} : (\mathbf{a}_0\otimes\mathbf{a}_0) = \mathbf{a}_0^T\cdot\overline{\mathbf{C}}\cdot\mathbf{a}_0 = \lambda^2 \tag{14}$$

$$\bar{I}_5(\overline{\mathbf{C}},\mathbf{a}_0) = \overline{\mathbf{C}}^2 : (\mathbf{a}_0\otimes\mathbf{a}_0) = \mathbf{a}_0^T\cdot\overline{\mathbf{C}}^2\cdot\mathbf{a}_0 \tag{15}$$

Note that the $\bar{I}_4$ pseudo–invariant has a direct physical interpretation as in Eq. (14) λ denotes the fiber stretching factor. As discussed in Section 2.2 the convexity of a SEF is a valuable property to ensure the stability of the model. Let us recall that if a SEF depends on certain variables (invariants) and it is twice differentiable then its convexity is guaranteed if and only if its Hessian matrix is positive semidefinite.

In previous studies where a TIHM is proposed exponential functions of the invariants ($\bar{I}_1, \bar{I}_2, \bar{I}_4, \bar{I}_5$) are commonly used in the SEF formulation (see, for example, the review by Chagnon et al. [16]). In general, such exponential functions are found to describe well strong slope changes in the stress-strain curves. Notwithstanding, exponential functions have also been reported [17] to not always fit well experimental data for some strain ranges because of the exponential nature of the curves.

Narrowing the focus to abdominal wall tissues, Calvo et al. [18] adapted a TIHM previously formulated for the plantar fascia [19] to characterize the LA, RA, IO and EO of New Zealand White rabbits. Calvo et al.'s formulation was subseqently used by Grasa et al. [20] to simulate the passive response of the RA, EO and a multi-layered sample formed by EO, IO and TA. Calvo et al.'s model assumes a linear function of $\bar{I}_1$ for the isotropic part of SEF, Eq. (10), and a exponential function of $\bar{I}_4$ for the fiber contribution, Eq. (11). Pachera et al. [21] adapted a previous TIHM for arterial walls [22] to characterize the whole set of human abdominal tissues (LA, RS, RA, TR, IO and EO). In particular, Pachera et al.'s model uses a linear function of $\bar{I}_1$ in Eq. (10) and, depending on the particular tissue, either an exponential (LA, RS, RA and IO) or quadratic (EO and TR) function of $\bar{I}_4$ in Eq. (11).

The aim of the present study is the development of a new TIHM for the human abdominal wall tissues (LA, RS, RA, TR, IO and EO). In our model, the isotropic ($\overline{\Psi}_{iso}$) and fiber ($\overline{\Psi}_{fib}$) contributions to the SEF are characterized exclusively by polynomial functions of the invariants of $\overline{\mathbf{C}}$ and $\mathbf{a}_0\otimes\mathbf{a}_0$. Linear and exponential functions of the invariants do not provide, in some cases, a good enough fit to data because of too slow (linear) or too sudden (exponential) changes in the slope. Another good reason for adopting polynomial functions in the present study was the observation that in almost every available experimental studies the reported stress-strain curves of the tissues involved have a markedly polynomial

UNIVERSITAT ROVIRA I VIRGILI
SIMULACIÓ DE L'EFECTE DE LES INCISIONS QUIRÚRGIQUES EN EL COMPORTAMENT DE LA PARET ABDOMINAL
Lluís Tuset Serra

look in the range of interest (typically $1 \leq \xi \leq 1.8$, where ξ denotes the stretch factor applied to the tissue sample).

From a methodological standpoint, we will perform numerical simulations of previously reported tensile tests [7,23,24] in order to determine the optimal values of the constitutive model parameters for each tissue. An additional objective of the present study is therefore an efficient implementation of the numerical problem that will allow us to perform a large number of runs with a limited amount of computational resources. In particular, we will pay attention to a both flexible and concise deployment of the constitutive model into the framework of a finite element (FE) software. Moreover, we will show that these methodological objectives can be achieved using free and open source software (FOSS). The FOSS packages available to tackle the present problem are not just inexpensive but powerful as well.

2. Material and methods

2.1. Constitutive model

Following the trend often observed in the literature [16] we first neglected the $\bar{I}_2$ and $\bar{I}_5$ invariants in Eqs. (10) and (11), respectively. After some preliminary numerical tests, we set the target on polynomial functions of the form:

$$\overline{\Psi}_{iso} = C_1\left(\bar{I}_1 - 3\right) + C_2\left(\bar{I}_1 - 3\right)^2 \tag{16}$$

$$\overline{\Psi}_{fib} = C_3\left(\bar{I}_4 - 1\right)^2 + C_4\left(\bar{I}_4 - 1\right)^4 \tag{17}$$

where C_i are positive constants. The quadratic form (16) was previously used by Raghavan and Vorp [25] as these authors found it to fit well data from uniaxially loaded tests on the wall of abdominal aortic aneurysms. The quartic function (17) was previously proposed by Peng et al. [26] as the fiber part of a SEF model for the human annulus fibrosus tissue. Note that the $\overline{\Psi}_{iso}$ and $\overline{\Psi}_{fib}$ functions defined in Eqs. (16) and (17) are strictly convex functions of I_1 and I_4, respectively.

For the volumetric contribution to $\mathbf{S}$ in Eq. (3) we used the following formulation:

$$U(J) = \frac{1}{2}K(J^2 - 1 - 2\ln J) \tag{18}$$

$$\mathbf{S}_{vol} = 2U(J)_{,\mathbf{C}} = U'J\mathbf{C}^{-1} = K\left(J^2 - 1\right)\mathbf{C}^{-1} \tag{19}$$

where $U' = \dfrac{dU}{dJ}$ and K is the bulk modulus. The particular form (18) for the volumetric function $U(J)$, proposed by Simo and Miehe's [27] as a refinement of Ogden's [28] model, relies on solid theoretical grounds and has become popular in the literature [29]. The isochoric–volumetric decoupling (2) is specially convenient when the constitutive model is implemented into a finite element (FE) nonlinear solver [16,29] in order to avoid volumetric locking [30]. From a numerical standpoint, the volumetric contribution $\mathbf{S}_{vol}$ can be understood as a penalty function: the larger the value of K the smaller the volumetric strain $(J-1)$ will be.

Taking into account the identities [6],

$$\bar{I}_{1,\bar{\mathbf{C}}} = \mathbf{I} \quad ; \quad \bar{I}_{4,\bar{\mathbf{C}}} = \mathbf{a}_0 \otimes \mathbf{a}_0 \tag{20}$$

then for the SEF formulation (16)–(17) proposed in this study the particular form of $\bar{\mathbf{S}}$ (see Eqs. (6) and (9)) is given by:

$$\bar{\mathbf{S}} = \overline{\gamma}_1\mathbf{I} + \overline{\gamma}_4\mathbf{a}_0 \otimes \mathbf{a}_0 \tag{21}$$

$$\overline{\gamma}_1\left(\bar{I}_1\right) = 2\left(\frac{\partial\overline{\Psi}_{iso}}{\partial\bar{I}_1}\right) = 2C_1 + 4C_2(\bar{I}_1 - 3) \tag{22}$$

$$\overline{\gamma}_4\left(\bar{I}_4\right) = 2\left(\frac{\partial\overline{\Psi}_{fib}}{\partial\bar{I}_4}\right) = 4C_3(\bar{I}_4 - 1) + 8C_4(\bar{I}_4 - 1)^3 \tag{23}$$

2.2. Ellipticity of the governing equations

Some authors [18–20,26] imposed the additional constraint that the fibers do not contribute to the SEF when they are under contraction:

$$\overline{\Psi}_{fib} = 0 \qquad \forall \bar{I}_4 < 1 \tag{24}$$

The $\overline{\Psi}_{fib}$ formulation (17) automatically fulfills the conditions

$$\overline{\Psi}_{fib}(1) = 0, \quad \left(\frac{\partial\overline{\Psi}_{fib}}{\partial\bar{I}_4}\right)(1) = 0, \quad \left(\frac{\partial^2\overline{\Psi}_{fib}}{\partial\bar{I}_4{}^2}\right)(1) \geq 0 \tag{25}$$

It is easy to show that the use of Eq. (17) also implies the additional conditions,

$$\frac{\partial\overline{\Psi}_{fib}}{\partial\bar{I}_4} > 0 (< 0) \quad \text{for} \quad \bar{I}_4 > 1 (< 1) \tag{26}$$

that is, some positive (negative) stress is actually to be exerted by a stretched (compressed) fiber. Note that the constraint (24) is incompatible with Eq. (26).

It is known that fibers tend to suffer failure mechanisms, such as fiber kinking or fiber splitting, when compressed. Merodio and Ogden [31] and Holzapfel et al. [22] analyzed the relation between the onset of such failure mechanisms and the loss of ellipticity of the governing equations in transversely isotropic elastic solids reinforced with a fiber contribution. These authors showed that, whenever a strictly convex function of $(\bar{I}_4 - 1)$ is prescribed, a necessary condition for the breakdown of ellipticity is that $\partial\overline{\Psi}_{fib}/\partial\bar{I}_4 < 0$, which means that the loss of ellipticity is to be expected under fiber compression $(\bar{I}_4 < 1)$.

Thus, it follows on account of (26) that whenever $\overline{\Psi}_{fib}$ is a strictly convex function of $\bar{I}_4$, as is the case of Eq. (17), the strong ellipticity of the governing equations is not guaranteed. This is probably the reason why several authors assume the constraint (24). In the present study we will apply Eq. (17) with no additional constraint. Note that Eq. (17) will be used, in the worst case scenario, with $\bar{I}_4$ values slightly below one. That is, when considering a tensile loading along a direction normal to the main fiber orientation the fibers will be somewhat compressed because of the (nearly) incompressibility of the material. In this situation ($\bar{I}_4$ slightly below one) the stability of the overall SEF model (9) may well be maintained even when the fiber contribution part alone would become unstable [31].

2.3. Tensile testing simulation

Tensile tests [7,23,24] are typically performed on a thin rectangular tissue sample, as sketched in Fig. 1. The tissue sample, having initially a length L_0, a width W_0 and a thickness H_0 (not shown in the sketch), is fixed on one lateral edge and is pulled on the opposite one. For every particular value of the external load applied (f), the stretch of the sample, ΔL, is measured.

2.3.1. Finite element simulation

The `Code Aster` open source FE software [32] was used in the present simulations. In the geometrical model the tissue sample was defined as a cuboid of dimensions $L_0 = 35$ mm, $W_0 = 10$ mm and $H_0 = 1$ mm. The computational meshes were created by first meshing the surfaces of the cuboid using isosceles and equilateral triangles and then generating the corresponding three-dimensional (3D) mesh of tetrahedra. Conditions of zero displacement and homogeneous stress level were imposed at the left and

UNIVERSITAT ROVIRA I VIRGILI
SIMULACIÓ DE L'EFECTE DE LES INCISIONS QUIRÚRGIQUES EN EL COMPORTAMENT DE LA PARET ABDOMINAL
Lluís Tuset Serra

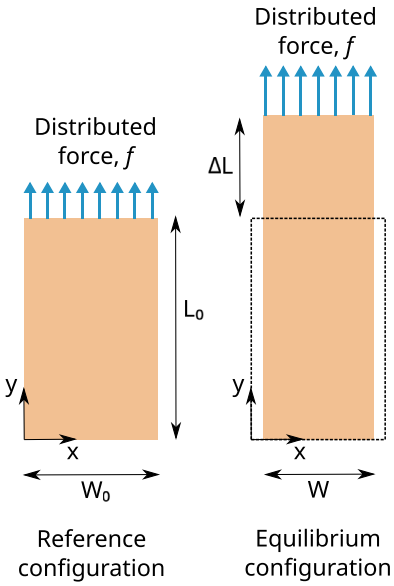

Fig. 1. Sketch of the model considered in the approximate analytical solution.

right y–boundaries, respectively (see Fig. 1). Fifty levels of the external load f, ranging from zero to the maximum prescribed value, were calculated on every computational run. For every particular load level, the resulting displacement at the right y–boundary, ΔL, was recorded. The accuracy and computational performance of the present FE simulations are assessed in Appendix A.

2.3.2. Implementation details

The `Code Aster` FE software features a large number of built–in material behaviors and also allows the user the possibility to incorporate custom–made constitutive models. The `Code Aster` nonlinear solver was set to apply the FE discretization scheme of Simo and Miehe [27], which is well suited for large deformations. Since the resulting set of nonlinear equations was solved by means of the Newton method the contribution of the constitutive model to the global Jacobian has to be provided in the form of the fourth order tangent tensor, $\mathbb{E}$:

$$\mathbb{E} = \mathbb{E}_{vol} + \mathbb{E}_{ich} = (\mathbf{S}_{vol})_{,\mathbf{C}} + (\mathbf{S}_{ich})_{,\mathbf{C}} \tag{27}$$

The contribution of the volumetric part to the Jacobian is given by,

$$\mathbb{E}_{vol} = (\mathbf{S}_{vol})_{,\mathbf{C}} = \frac{1}{2}\left(U''J^2 + U'J\right)\mathbf{C}^{-1}\otimes\mathbf{C}^{-1} - U'J\mathbf{C}^{-1}\odot\mathbf{C}^{-1} \tag{28}$$

where $U'' = \dfrac{d^2U}{dJ^2}$ and $\left(\mathbf{C}^{-1}\odot\mathbf{C}^{-1}\right) = -\mathbf{C}^{-1}{}_{,\mathbf{C}}$ [6]. The contribution of the isochoric part to the Jacobian is more involved:

$$\mathbb{E}_{ich} = \mathbb{P}^T : \overline{\mathbb{E}} : \mathbb{P} - \frac{1}{3}J^{-2/3}\left(\overline{\mathbf{S}}\otimes\mathbf{C}^{-1} + \mathbf{C}^{-1}\otimes\overline{\mathbf{S}}\right) + \frac{1}{3}\left(\overline{\mathbf{S}} : \overline{\mathbf{C}}\right)\left(\mathbf{C}^{-1}\odot\mathbf{C}^{-1} + \frac{1}{3}\mathbf{C}^{-1}\otimes\mathbf{C}^{-1}\right) \tag{29}$$

$$\overline{\mathbb{E}} = \overline{\mathbf{S}}_{,\overline{\mathbf{C}}} \tag{30}$$

Considering Eqs. (19) and (21) then the particular forms of the fourth order tensors $\mathbb{E}_{vol}$ and $\overline{\mathbb{E}}$ for the present TIHM are:

$$\mathbb{E}_{vol} = K\left(J^2\mathbf{C}^{-1}\otimes\mathbf{C}^{-1} - \left(J^2-1\right)\mathbf{C}^{-1}\odot\mathbf{C}^{-1}\right) \tag{31}$$

$$\overline{\mathbb{E}} = \overline{\delta}_1\mathbf{I}\otimes\mathbf{I} + \overline{\delta}_4\mathbf{a}_0\otimes\mathbf{a}_0\otimes\mathbf{a}_0\otimes\mathbf{a}_0 \tag{32}$$

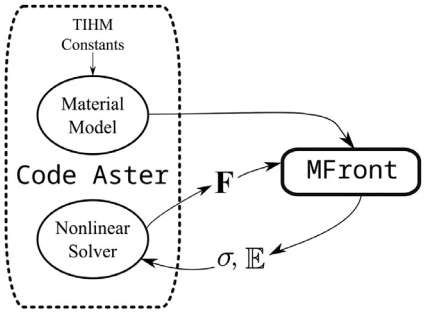

Fig. 2. Sketch of the flow of data between the `Code Aster` and `MFront` programs.

$$\overline{\delta}_1\left(\bar{I}_1\right) = \frac{\partial\overline{\gamma}_1}{\partial\bar{I}_1} = 4C_2 \tag{33}$$

$$\overline{\delta}_4\left(\bar{I}_4\right) = \frac{\partial\overline{\gamma}_4}{\partial\bar{I}_4} = 4C_3 + 24C_4(\bar{I}_4 - 1)^2 \tag{34}$$

As sketched in Fig. 2, in a custom implementation of a constitutive model into `Code Aster` the code supplied by the user will receive the gradient tensor $\mathbf{F}$ as an input argument and will return the calculated values of both $\mathbf{S}$ (or $\boldsymbol{\sigma}$) and $\mathbb{E}$ on exit. In the present study we used the specific interface provided by the `MFront` software [33] to incorporate the present TIHM into `Code Aster`. Besides its straightforward integration with `Code Aster` the most attractive feature of `MFront` is its elegant high–level language, especially suited for tensor algebra [34]. Hence, `MFront` provides a representation for second and fourth order tensors and most of their operations involved in the constitutive model equations. Table 1 shows the `MFront` code that we wrote for the present TIHM. Note that the code includes a call to the non–standard `circledot()` function (instruction # 18), written by ourselves in C++, that performs the tensor operation $\mathbf{C}^{-1}\odot\mathbf{C}^{-1} = -\mathbf{C}^{-1}{}_{,\mathbf{C}}$ based on the following equivalences [6]:

$$\begin{aligned}\mathbf{I} &= \mathbf{C}^{-1}\mathbf{C}\\ \mathbb{O} &= \mathbf{C}^{-1}{}_{,\mathbf{C}}\,\mathbf{C} + \mathbf{C}^{-1}\mathbf{C}_{,\mathbf{C}} = \mathbf{C}^{-1}{}_{,\mathbf{C}}\,\mathbf{C} + \mathbf{C}^{-1}\mathbb{I}^s\\ \mathbf{C}^{-1}{}_{,\mathbf{C}} &= -\mathbf{C}^{-1}\mathbb{I}^s\mathbf{C}^{-1} = -\mathbf{C}^{-1}\odot\mathbf{C}^{-1}\end{aligned} \tag{35}$$

In Eq. (35), $\mathbb{I}^s$ denotes a specialized symmetric version of the fourth order identity tensor [15]. A more computationally efficient, although far more convoluted as well, alternative for the calculation of the $\mathbb{P}^T : \overline{\mathbb{E}} : \mathbb{P}$ term in Eq. (29) is presented in Appendix B.

2.3.3. Approximate analytical solution

An approximate analytical model for the deformation of the tissue sample (see a sketch in Fig. 1) as a function of the applied external load f can be obtained as follows. First we assume that the load is homogeneously applied to the tissue sample lateral surface. Then assuming a small value of the volumetric strain $\Delta V/V$, that is, $J = (LWH)/(L_0W_0H_0) = 1 + \Delta V/V \approx 1$, the deformation gradient tensor can be simplified to

$$\mathbf{F} = \begin{pmatrix}\lambda^{-1/2} & 0 & 0\\ 0 & \lambda & 0\\ 0 & 0 & \lambda^{-1/2}\end{pmatrix} \approx \begin{pmatrix}\xi^{-1/2} & 0 & 0\\ 0 & \xi & 0\\ 0 & 0 & \xi^{-1/2}\end{pmatrix} \tag{36}$$

where we have also assumed $\lambda \approx \xi = 1 + \Delta L/L_0$. Note that Eq. (36) implies the assumptions $L = \xi L_0$, $W = \xi^{-1/2}W_0$ and $H = \xi^{-1/2}H_0$ for the deformation of the sample, that is, isotropy is maintained in the $x-z$ plane.

In order to compare the stresses actually measured with the predicted ones we need to consider, in addition to the second

Table 1
Pseudocode illustrating the `MFront` calculation sequence for the present TIHM. The variables defined in the code are denoted using math symbols for the sake of clarity with the only exception of `F1`, which is the reserved word for **F**. The keyword `Stensor` is a shortcut to the type (C++ class) defined in the `MFront` library for the representation of symmetric second order tensors. The keyword `Stensor4` refers to the `MFront` type that represents the subset of fourth order tensors that can be defined by the tensor product ($\otimes$) of two symmetric second order tensors.

#	Variables	Equations	`MFront` expression
1	`Real` J	$\det(\mathbf{F})$	`det(F1)`
2	`Stensor` $\mathbf{C}$	$\mathbf{F}^T\mathbf{F}$	`computeRightCauchyGreenTensor(F1)`
3	`Stensor` $\mathbf{C}^{-1}$		`invert(C)`
4	`Real` $J^{-2/3}$		`pow(J,-2./3.)`
5	`Stensor` $\overline{\mathbf{C}}$	$J^{-2/3}\mathbf{C}$	$(J^{-2/3})$`*C`
6	`Stensor` $\mathbf{A}_0$	$\mathbf{a}_0\otimes\mathbf{a}_0$	`buildFromVectorDiadicProduct(`$\mathbf{a}_0$`)`
7	`Real` $\overline{I}_1$	(12)	`trace(`$\overline{\mathbf{C}}$`)`
8	`Real` $\overline{I}_4$	(14)	$\overline{\mathbf{C}}\,|\,\mathbf{A}_0$
9	`Real` $\overline{\gamma}_1$	(22)	$2^*C_1+4^*C_2^*(\overline{I}_1-3)$
10	`Real` $\overline{\gamma}_4$	(23)	$4^*C_3^*(\overline{I}_4-1)+8^*C_4^*$`pow(`$\overline{I}_4-1$`,3)`
11	`Real` $\overline{\delta}_1$	(33)	4^*C_2
12	`Real` $\overline{\delta}_4$	(34)	$4^*C_3+24^*C_4^*(\overline{I}_4-1)^*(\overline{I}_4-1)$
13	`Stensor` $\overline{\mathbf{S}}$	(21)	$\overline{\gamma}_1$`*Stensor::Id()+`$\overline{\gamma}_4$`*`$\mathbf{A}_0$
14	`Stensor` $\mathbf{S}_{ich}$	(5)	$(J^{-2/3})^*(\overline{\mathbf{S}}-(\overline{\mathbf{S}}\,|\,\mathbf{C})/3^*\mathbf{C}^{-1})$
15	`Stensor` $\mathbf{S}_{vol}$	(19)	$K^*(J^*J-1)^*\mathbf{C}^{-1}$
16	`Stensor` $\boldsymbol{\sigma}$	(2), (37)	`convertSecondPiolaKirchoffStress toCauchyStress(`$\mathbf{S}_{vol}+\mathbf{S}_{ich}$`,F1)`
17	`Stensor4` $\mathbb{C}^{-1}_{\otimes}$	$\mathbf{C}^{-1}\otimes\mathbf{C}^{-1}$	$\mathbf{C}^{-1}\wedge\mathbf{C}^{-1}$
18	`Stensor4` $\mathbb{C}^{-1}_{\odot}$	(35)	`circledot(`$\mathbf{C}^{-1}$`)`
19	`Stensor4` $\mathbb{E}_{vol}$	(31)	$K^*J^*J^*\mathbb{C}^{-1}_{\otimes}-K^*(J^*J-1)^*\mathbb{C}^{-1}_{\odot}$
20	`Stensor4` $\overline{\mathbb{E}}$	(32)	$\overline{\delta}_1$`*(Stensor::Id()∧Stensor::Id())+`$\overline{\delta}_4$`*(`$\mathbf{A}_0\wedge\mathbf{A}_0$`)`
21	`Stensor4` $\mathbb{P}$	(7)	$(J^{-2/3})^*$`(Stensor4::Id()-(1./3.)*(`$\mathbf{C}\wedge\mathbf{C}^{-1}$`))`
22	`Stensor4` $\mathbb{P}^T$		$(J^{-2/3})^*$`(Stensor4::Id()-(1./3.)*(`$\mathbf{C}^{-1}\wedge\mathbf{C}$`))`
23	`Stensor4` $\mathbb{E}_{ich}$	(29)	$\mathbb{P}^T{}^*\overline{\mathbb{E}}^*\mathbb{P}-$`(1./3.)*`$(J^{-2/3})^*(\overline{\mathbf{S}}\wedge\mathbf{C}^{-1}+\mathbf{C}^{-1}\wedge\overline{\mathbf{S}})+$ `(1./3.)*`$(\overline{\mathbf{S}}\,|\,\overline{\mathbf{C}})^*(\mathbb{C}^{-1}_{\odot}+$`(1./3.)*`$\mathbb{C}^{-1}_{\otimes})$
24	`Stensor4` $\mathbb{E}$	(27)	$\mathbb{E}_{vol}+\mathbb{E}_{ich}$

Piola–Kichoff stress, $\mathbf{S}$, the Cauchy stress tensor, $\boldsymbol{\sigma}$,

$$\boldsymbol{\sigma} = J^{-1}\mathbf{F}\mathbf{S}\mathbf{F}^T \tag{37}$$

and the nominal stress tensor:

$$\boldsymbol{\Pi} = \mathbf{S}\mathbf{F}^T \tag{38}$$

The definition of the nominal stress tensor, $\boldsymbol{\Pi}$, is similar to that of the Cauchy stress except that it is expressed in terms of the area and normal of the surface in the reference configuration. Thus, $f/W_0H_0 = \Pi^{yy}$ is the quantity in our model that is to be compared with the experimental value since the nominal area, W_0H_0, is the one used to determine the measured stress level.

The simplified form (36) of the gradient tensor implies, on account of Eqs. (12) and (14), that $\overline{I}_1 = J^{-2/3}(\xi^2 + 2/\xi)$ and $\overline{I_4} = J^{-2/3}\xi^2$. Therefore, from Eqs. (5), (8), (19), (21) and (38) it follows, after some algebraic manipulation:

$$S^{yy} = S^{yy}_{vol} + S^{yy}_{ich} = \frac{K\left(J^2-1\right)}{\xi^2} + \frac{2}{3}J^{-2/3}\left(\left(1-\frac{1}{\xi^3}\right)g_1(\xi) + g_4(\xi)\right) \tag{39}$$

$$\Pi^{yy} = \xi S^{yy} \tag{40}$$

$$g_1(\xi) = 2C_1 + 4C_2\left(J^{-2/3}\left(\xi^2 + \frac{2}{\xi}\right) - 3\right)$$

$$g_4(\xi) = 4C_3\left(J^{-2/3}\xi^2 - 1\right) + 8C_4\left(J^{-2/3}\xi^2 - 1\right)^3$$

We used Eqs. (39) and (40) in conjunction with the numerical simulations (described above) to determine the set of constants involved in the proposed THIM. Note that Eqs. (39) and (40) can be used to fit experimental data from tensile tests provided that a certain form is assumed for the variation of J with the sample stretch, ξ. Results from the numerical simulations suggested the use of a function of the type $J = 1 + a(\xi - 1)^3$, with $a = 0.10$.

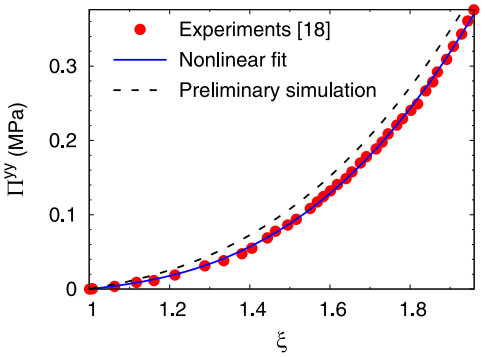

Fig. 3. Example of the nonlinear fit of the present TIHM to previous data by Cardoso [23] for the TR muscle. The results of the preliminary numerical simulation, performed using the constants values given by the fit, are also plotted.

The general approach to determine the constants K, C_1, C_2, C_3, and C_4 was to first obtain preliminary values of these constants by means of a nonlinear fit of the analytical model (39)–(40) to experimental data available in the literature. These preliminary values were subsequently refined by trial and error using the numerical simulations. Fig. 3 illustrates an instance for the deduction of the TIHM constants in the case of the TR muscle. In this figure we see that the analytical model (39)–(40) fits very well experimental data. However, this figure also shows that the preliminary set of constants does not perform so well in the numerical simulation which indicates that a subsequent refinement of the constants is needed.

3. Results and discussion

We determined, for each of the tissues considered, the whole set of constants (K, C_1, C_2, C_3, C_4) involved in the proposed TIHM.

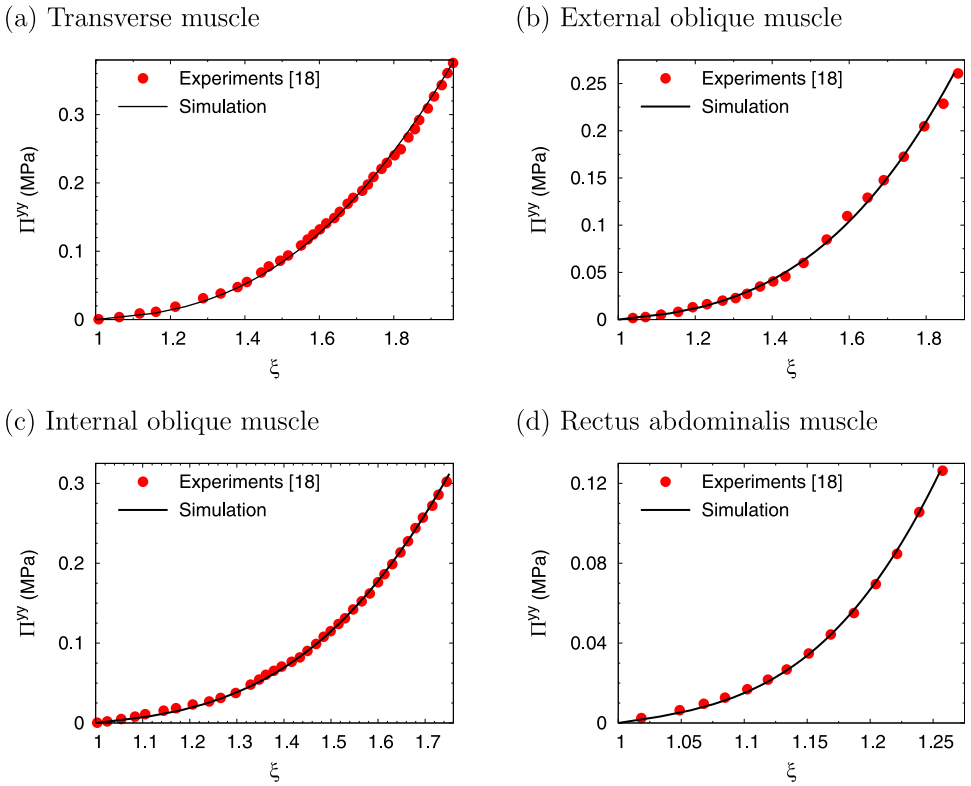

Fig. 4. Results of the present simulations are compared with the measurements reported by Cardoso [23] on tissue samples of (a) TR, (b) EO, (c) IO and (d) RA. In all of the cases the tissue was stretched along the main direction of the fibers. Data from the same specimen in Cardoso's study is used in all of the four plots.

It is worth noting that in the abdominal wall we can distinguish two types of materials, namely those basically composed of collagenous and aponeurotic tissues, such as LA and RS, and those that can be viewed as muscles, such as EO, IO, RA and TR. The former tissues deform much less than the latter ones when subjected to a certain external load. As the value of the bulk modulus, K, showed an enormous sensitivity to changes in the objective function we had to fix suitable values for K. Numerical tests showed that $K = 100$ MPa worked well in the LA and RS simulations but a considerably smaller K value had to be used for the muscles. For the latter tissues we eventually chose $K = 1$ MPa, a value low enough to guarantee numerical stability of the simulations but high enough to maintain low levels of volumetric strain [35].

In the case of the EO, IO, RA and TR muscles we found that the C_1 values generated by the fits were very sensitive to small changes in the objective function. Therefore, we introduced the additional requirement that the final constant values of C_1 and C_3 had to be physically meaningful. Eqs. (39)–(40) predict that the slope of the stress–strain curve at the origin is $E_0 = \lim_{J,\xi\to 1} \partial\Pi^{yy}/\partial\xi = 4C_1 + 16C_3/3$, a result that was also validated by the numerical simulations. Thus, we required that the final values of C_1 and C_3 had to produce values of E_0 that were consistent with values typically reported in the literature for the elastic modulus of muscles at low strain levels [36]. In addition, in the trial and error adjustment we opted for a unique C_1 value for all of the four muscles. As a consequence of these additional restrictions, in the present TIHM the isotropic contribution to the tissue response will be roughly the same for the four muscles when a low external load is applied.

Fig. 4 (a) shows the comparison between experimental data and the results of the final simulations for the EO, IO, RA and TR muscles. For these four muscles we used the experimental data reported by Cardoso [23]. In all of the tensile tests performed by this author the tissue sample was only stretched along the main fiber direction. The final set of TIHM constants for every tissue are presented in Table 2. Note that from the respective C_1 and C_3 values in this table it can be checked that E_0 is within the $24 - 57$ kPa range for the EO, IO, RA and TR, a result that is in agreement with previously reported values [36].

Table 2
Values of the K, C_1, C_2, C_3 and C_4 constants in the present TIHM for every tissue of the abdominal wall.

Tissue	K(MPa)	C_1(MPa)	C_2(MPa)	C_3(MPa)	C_4(MPa)
LA			11	0.1	34
RS	100	0.05	4.7	0.01	0.95
EO			0.012	0.0029	0.00051
IO			0.016	0.0053	0.0015
RA	1	0.0021	0.024	0.0092	0.052
TR			0.019	0.0031	0.00043

For the LA and RS we respectively fitted the experimental data reported by Forstemann et al. [7] and Martins et al. [24]. These authors carried out tensile tests where tissue samples were stretched either longitudinally (along the main fiber direction) and transversely. For these tissues, we first fitted transverse tests data to obtain preliminary values of C_1 and C_2 under the $C_3 = C_4 = 0$ constraint (no fiber contribution). These preliminary C_1 and C_2 values were set as constants in the fit of the corresponding longitudinal test data where preliminary C_3 and C_4 values were obtained. Numerical simulations were subsequently used to simultaneously refine the values of C_1, C_2, C_3 and C_4 for LA and RS. Figs. 5 and 6 respectively compare experimental data and numerical results for the LA and RS tissues. The final values of the TIHM constants for LA and RS are shown in Table 2.

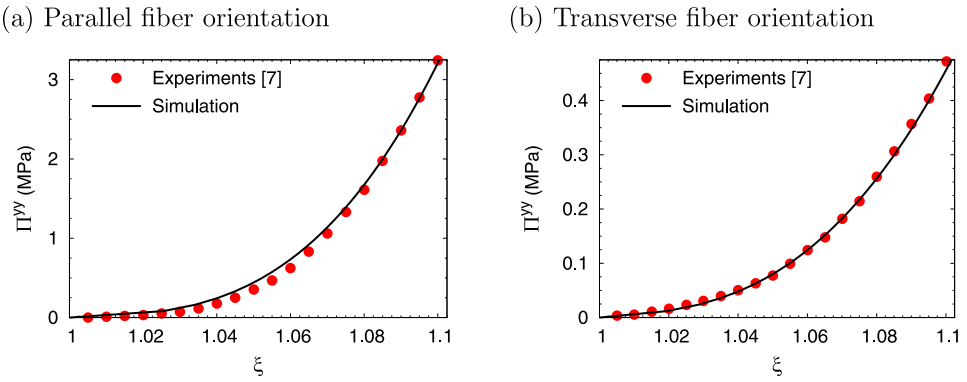

Fig. 5. Results of the present simulations for the LA tissue are compared with the measurements reported by Forstemann et al. [7]. In parts (a) and (b) the main direction of the fiber alignment was respectively assumed to be parallel and normal to the direction along which the tissue sample was stretched.

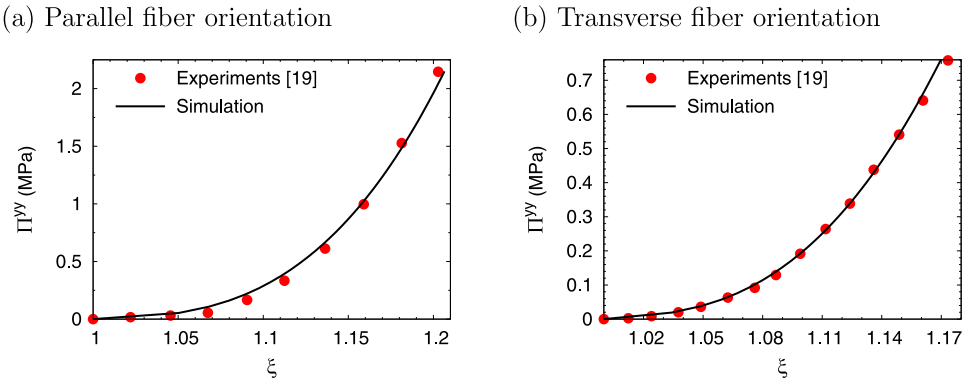

Fig. 6. Results of the present simulations for the RS tissue are compared with the measurements reported by Martins et al. [24]. In parts (a) and (b) the main direction of the fiber alignment was respectively assumed to be parallel and normal to the direction along which the tissue sample was stretched. Data from the same specimen in Martins et al.'s study is used in both plots.

4. Conclusions

In this work we have developed a new constitutive TIHM formulation for tissues of the human abdominal wall. The present TIHM can be safely used to simulate problems in which tissues are being stretched with stress levels up to $\sigma = 0.2$ MPa. This is a wide enough range of application for the intended future use of the model, i.e., FE simulations of the abdominal wall where the maximum loads applied will be about $\sigma = 0.025$ MPa [21]. If higher stress values were to be applied the resulting large deformations ($\lambda > 2$) would render the FE simulation not only physically unreliable but, most probably, numerically unstable as well. In this respect, TIHM formulations using exponential functions of the invariants might be more numerically resilient (as the slope of the stress–strain curve tends to infinity large increases in σ would produce no further deformation of the material) but they might yield unrealistic predictions when used beyond their range of validity.

As was discussed above, under strong compression ($\bar{I}_4 \ll 1$) the present TIHM might produce a failure of the FE calculation. In previous TIHM formulations such a failure would be avoided by imposing the constraint (24) as a workaround. Our point of view is that under conditions where the real fibers would split it is preferable to obtain a breakage of the FE calculation rather than a physically meaningless numerical solution.

In the present study we have exclusively relied on open source software such as `MFront` and `Code Aster`. There are of course alternative methods to incorporate a custom material model into FE solvers but we think that as MFront provides a large number of tensorial operations its usage significantly eases the implementation of complex orthotropic finite strain behaviors. It is worth mentioning that `MFront` provides specific interfaces not only to `Code Aster` but to several other open source and commercial FE solvers as well.

A future application of the present TIHM will be in the analysis of the stress map on the abdominal wall in order to determine the best zone to practice a colostomy. As a preliminary step, we have also tested the present TIHM in the simulation of larger structures of the abdominal wall. As an example, Fig. 7 shows the predicted distribution of the longitudinal deformation (Δz) in the simulations of the right RA muscle under two different levels of vertical load, namely 5 kPa (left plot) and 10 kPa (right plot).

We have hitherto considered the passive response of the abdominal muscles under an external load. A future goal will be the implementation of the current TIHM into a broader formulation able to simulate the action of active muscles (see, e.g., Refs. [37] and [38]). Future variations of the present TIHM might be developed for other tissues beyond the abdominal wall. Such future models might incorporate additional functions of the $\bar{I}_2$ and $\bar{I}_5$ invariants if a comprehensive enough experimental database was available for the tissues involved. The increased mathematical complexity of a new TIHM would imply an additional effort for its efficient implementation into the FE solver. At this point we would benefit of one of the main features of the current methodology as is the use of the `MFront` software, a both flexible and powerful tool.

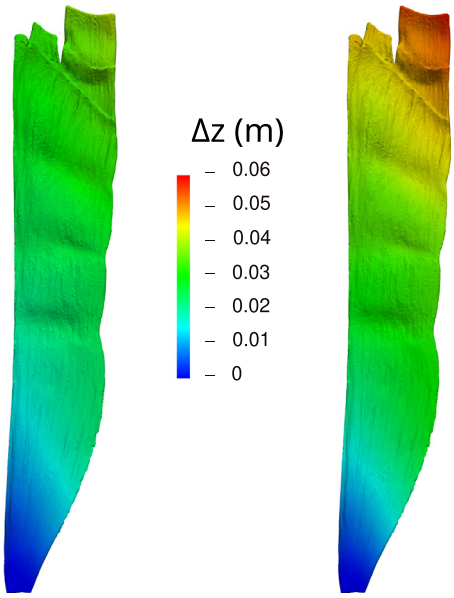

Fig. 7. Vertical (z) component of the predicted deformation on the surface of the right RA muscle. The 3D mesh used in this simulation, consisting of 310 497 tetrahedra, was generated from a surface mesh consisting of 65 188 triangles. The dimensions of the bounding box surrounding the right RA model are 0.0762 m × 0.0727 m in the $x-y$ (horizontal) plane and 0.394 m in the z (vertical) direction. The boundary conditions in these simulations were roughly equivalent to the ones prescribed earlier for the rectangular tissue sample (see Fig. 1); that is, the right RA model was fixed at the bottom edge ($\Delta z = 0$) and a uniform stress load of either (a) 5 kPa (left) or (b) 10 kPa (right) was applied to the upper edge boundaries. The muscle fibers were assumed to be initially aligned with the z–axis.

Conflict of Interests

The authors declare that there is no conflict of interests regarding the publication of this paper.

Acknowledgment

Financial support for the current research was granted by Universitat Rovira i Virgili, project number 2018PFR-URV-B2-29.

Appendix A. Accuracy and performance assessment of the finite element method

Table A.1 shows the dependence of the accuracy and computational efficiency on the mesh size for simulations on two different abdominal tissues, namely LA and TR. In the case of the LA simulations, the calculated deformations are much smaller than they are in the TR runs so that the total number of Newton iterations is, for a given mesh size, significantly lower in the former simulations. The total number of solves (N_{solve}) was actually higher than the number of scheduled load levels (50) as the FE solver implemented an adaptive step strategy that ensured the convergence of the Newton iterations on every particular instance. As expected, the total CPU time (T_{cpu}) required to complete a simulation run increases with increasing mesh size (N_{tet}). The FE solver was allowed to use 2 CPU cores in the simulations but the paralellization efficiency factor was modest, about 70% on the average. The `Code Aster` software used parallel code during the stage of matrix factorization, which in the present problem is relatively fast due to the regularity of the computational mesh. For the same reason, the average CPU time per Newton iteration (T_{cpu}/N_{iter}) is roughly proportional to the mesh size. That is, the matrix representation of the Jacobian tensor is not just sparse but most probably features a well defined structure (bands/blocks), easily amenable to the direct solver factorization algorithms implemented in `Code Aster`.

Table A.1
Accuracy and computational efficiency of FE calculations for the simulations of two different tissue samples (LA and TR) on four different computational meshes. N_{tet} denotes the number of tetrahedra in the computational mesh, $\mathrm{MB}_{\max}$ is the maximum virtual memory (MB) reserved by the `Code Aster` software, $\Delta L_{\max}$ is the calculated (absolute) stretch of the sample at maximum load, N_{iter} is the total number of Newton iterations performed, N_{solve} is the total number of solves during the whole calculation and T_{cpu} and T_{wall} respectively denote the elapsed CPU and wall time. These simulations were performed on a Intel Core i5-6600 CPU (Skylake-S) Quad Core with a maximum clock speed of 3900 MHz.

N_{tet}	662	1 819	4 164	7 789
$\mathrm{MB}_{\max}$	629	645	709	756
		LA (fiber direction)		
$\Delta L_{\max}$(mm)	3.476	3.511	3.537	3.536
N_{iter}	443	487	438	444
N_{solve}	122	122	122	122
T_{cpu}(s)	16.21	35.36	68.53	127.44
T_{wall}(s)	9.42	25.05	51.85	99.07
T_{cpu}(s)/N_{iter}	0.037	0.073	0.156	0.287
		TR		
$\Delta L_{\max}$(mm)	33.324	33.625	33.747	33.756
N_{iter}	777	758	1 020	842
N_{solve}	122	122	122	126
T_{cpu}(s)	27.16	53.31	151.34	231.30
T_{wall}(s)	15.36	37.36	112.54	177.57
T_{cpu}(s)/N_{iter}	0.035	0.070	0.148	0.275

Table A.1 also shows that the calculated maximum deformations ($\Delta L_{\max}$) are almost identical for the two larger computational meshes whereas the relative numerical error at maximum load conditions in the mesh with $N_{tet} = 1\,819$ is 0.71% and 0.39% for the LA and TR runs, respectively. The computational mesh with 1 819 tetrahedra was subsequently adopted in the remainder of the simulations as a compromise between numerical accuracy and computational cost.

Appendix B. An optimized version of the `MFront` code for the present TIHM

The `MFront` code described in Table 1 relies on a rather straightforward implementation of the constitutive equations and can therefore be easily generalized to other variants of the TIHM. Notwithstanding, we found that the bottleneck in computational efficiency was in instruction #23 where two double contractions between fourth–order tensors ($\mathbb{P}^T : \overline{\mathbb{E}} : \mathbb{P}$) were involved. A more

Table B.1
Pseudocode illustrating the changes introduced in the `MFront` original code, presented in Table 1, to obtain the more efficient formulation based on Eq. (B.1). Instructions #1 – 19, not included here, would be the same ones listed in Table 1.

#	Variables	Equations	`MFront` expression

20	`Stensor4` $\mathbb{P}^T{:}\overline{\mathbb{E}}{:}\mathbb{P}$	(B.1)	`(1./9.)*(`$\overline{\delta}_1$`*`$\overline{I}_1$`*`$\overline{I}_1$`+`$\overline{\delta}_4$`*`$\overline{I}_4$`*`$\overline{I}_4$`)*`$\mathbb{C}_{\otimes}^{-1}$`+`
			`(`$\overline{\delta}_1$`*`$J^{-2/3}$`*`$J^{-2/3}$`)*(Stensor:: Id()`
			`∧Stensor::Id())`
			`+(`$\overline{\delta}_4$`*`$J^{-2/3}$`*`$J^{-2/3}$`)*(`$\mathbf{A}_0\wedge\mathbf{A}_0$`)`
			`−(1./3.)*(`$\overline{\delta}_1$`*`$\overline{I}_1$`*`$J^{-2/3}$`)*(Stensor::Id()∧`$\mathbf{C}^{-1}$
			`+`$\mathbf{C}^{-1}$`∧Stensor::Id())`
			`−(1./3.)*(`$\overline{\delta}_4$`*`$\overline{I}_4$`*`$J^{-2/3}$`)*(`$\mathbf{A}_0\wedge\mathbf{C}^{-1}+\mathbf{C}^{-1}\wedge\mathbf{A}_0$`)`

21	`Stensor4` $\mathbb{E}_{ich}$	(29)	$\mathbb{P}^T{:}\overline{\mathbb{E}}{:}\mathbb{P}-$`(1./3.)*(`$J^{-2/3}$`)*(`$\overline{\mathbf{S}}\wedge\mathbf{C}^{-1}+\mathbf{C}^{-1}\wedge\overline{\mathbf{S}}$`)+` `(1./3.)*(`$\overline{\mathbf{S}}|\overline{\mathbf{C}}$`)*(`$\mathbb{C}_{\odot}^{-1}$`+(1./3.)*`$\mathbb{C}_{\otimes}^{-1}$`)`
22	`Stensor4` $\mathbb{E}$	(27)	$\mathbb{E}_{vol} + \mathbb{E}_{ich}$

UNIVERSITAT ROVIRA I VIRGILI
SIMULACIÓ DE L'EFECTE DE LES INCISIONS QUIRÚRGIQUES EN EL COMPORTAMENT DE LA PARET ABDOMINAL
Lluís Tuset Serra

efficient version of the `MFront` code is based on the following expansion, derived from the combination of Eqs. (7) and (32):

$$\begin{aligned}\mathbb{P}^T : \overline{\mathbb{E}} : \mathbb{P} = & \frac{1}{9}\left(\overline{\delta}_1\bar{I}_1^2 + \overline{\delta}_4\bar{I}_4^2\right)\mathbb{C}_{\otimes}^{-1} \\ & + \overline{\delta}_1 J^{-4/3}(\mathbf{I}\otimes\mathbf{I}) + \overline{\delta}_4 J^{-4/3}(\mathbf{a}_0\otimes\mathbf{a}_0\otimes\mathbf{a}_0\otimes\mathbf{a}_0) \\ & - \frac{1}{3}\overline{\delta}_1\bar{I}_1 J^{-2/3}\left(\mathbf{I}\otimes\mathbf{C}^{-1} + \mathbf{C}^{-1}\otimes\mathbf{I}\right) \\ & - \frac{1}{3}\overline{\delta}_4\bar{I}_4 J^{-2/3}\left((\mathbf{a}_0\otimes\mathbf{a}_0)\otimes\mathbf{C}^{-1} + \mathbf{C}^{-1}\otimes(\mathbf{a}_0\otimes\mathbf{a}_0)\right) \end{aligned} \tag{B.1}$$

Table B.1 describes the modifications that were introduced into the original `MFront` code to implement Eq. (B.1).

References

[1] A. Kingsnorth, K. LeBlanc, Hernias: inguinal and incisional, Lancet 362 (9395) (2003) 1561–1571.
[2] F. Köckerling, M. Simons, Current concepts of inguinal hernia repair, Visceral Med. 34 (2) (2018) 145–150.
[3] C. Beadles, A. Meagher, A. Charles, Trends in emergent hernia repair in the united states, JAMA Surg. 150 (3) (2015) 194–200.
[4] S. Gillern, J.I.S. Bleier, Parastomal hernia repair and reinforcement: the role of biologic and synthetic materials, Clin. Colon Rectal Surg. 27 (4) (2014) 162–171.
[5] M. Kirilova, S. Stoytchev, D. Pashkouleva, V. Kavardzhikov, Experimental study of the mechanical properties of human abdominal fascia, Med. Eng. phys. 33 (1) (2011) 1–6.
[6] G.A. Holzapfel, et al., Biomechanics of soft tissue, in: The Handbook of Materials Behavior Models, 3, 2001, pp. 1049–1063.
[7] T. Förstemann, J. Trzewik, J. Holste, B. Batke, M. Konerding, T. Wolloscheck, C. Hartung, Forces and deformations of the abdominal wall—a mechanical and geometrical approach to the linea alba, J. Biomech. 44 (4) (2011) 600–606.
[8] D. Gräßel, A. Prescher, S. Fitzek, D.G.v. Keyserlingk, H. Axer, Anisotropy of human linea alba: a biomechanical study, J. Surg. Res. 124 (1) (2005) 118–125.
[9] A.E. Ehret, M. Itskov, A polyconvex hyperelastic model for fiber-reinforced materials in application to soft tissues, J. Mater. Sci. 42 (21) (2007) 8853–8863.
[10] B. Zhou, F. Xu, C.Q. Chen, T.J. Lu, Strain rate sensitivity of skin tissue under thermomechanical loading, Phil. Trans. R. Soc. A 368 (2010) 679–690, doi:10.1098/rsta.2009.0238.
[11] A. Vogel, L. Rakotomanana, D.P. Pioletti, Viscohyperelastic strain energy function, in: Y. Payan, J. Ohayon (Eds.), Biomechanics of Living Organs. Hyperelastic Constitutive Laws for Finite Element Modeling, Academic Press, 2017, pp. 59–78.
[12] S.G. Kulkarni, X.-L. Gao, S.E. Horner, R.F. Mortlock, J.Q. Zheng, A transversely isotropic visco-hyperelastic constitutive model for soft tissues, Math. Mech. Solids 21 (6) (2016) 747–770.
[13] A.-A.K. Yousefi, M.A. Nazari, P. Perrier, M.S. Panahi, Y. Payan, A visco-hyperelastic constitutive model and its application in bovine tongue tissue, J. Biomech. 71 (2018) 190–198, doi:10.1016/j.jbiomech.2018.02.008.
[14] D. Garcia-Gonzalez, A. Jérusalem, S. Garzon-Hernandez, R. Zaera, A continuum mechanics constitutive framework for transverse isotropic soft tissues, J. Mech. Phys. Solids 112 (2018) 209–224, doi:10.1016/j.jmps.2017.12.001.
[15] M. Itskov, Tensor algebra and tensor analysis for engineers, with applications to continuum mechanics, Mathematical Engineering, 4th, Springer, 2015.
[16] G. Chagnon, M. Rebouah, D. Favier, Hyperelastic energy densities for soft biological tissues: a review, J. Elast. 120 (2) (2015) 129–160.
[17] B. Hernández-Gascón, E. Peña, H. Melero, G. Pascual, M. Doblaré, M. Ginebra, J. Bellón, B. Calvo, Mechanical behaviour of synthetic surgical meshes: finite element simulation of the herniated abdominal wall, Acta Biomater. 7 (11) (2011) 3905–3913.
[18] B. Calvo, M. Sierra, J. Grasa, M. Munoz, E. Peña, Determination of passive viscoelastic response of the abdominal muscle and related constitutive modeling: stress-relaxation behavior, J. Mech. Behav. Biomed. Mater. 36 (2014) 47–58.
[19] A. Natali, P. Pavan, E. Carniel, M. Lucisano, G. Taglialavoro, Anisotropic elasto-damage constitutive model for the biomechanical analysis of tendons, Med. Eng. Phys. 27 (3) (2005) 209–214.
[20] J. Grasa, M. Sierra, N. Lauzeral, M. Munoz, F. Miana-Mena, B. Calvo, Active behavior of abdominal wall muscles: experimental results and numerical model formulation, J. Mech. Behav. Biomed. Mater. 61 (2016) 444–454.
[21] P. Pachera, P. Pavan, S. Todros, C. Cavinato, C. Fontanella, A. Natali, A numerical investigation of the healthy abdominal wall structures, J. Biomech. 49 (9) (2016) 1818–1823.
[22] G.A. Holzapfel, T.C. Gasser, R.W. Ogden, Comparison of a multi-layer structural model for arterial walls with a fung-type model, and issues of material stability, J. Biomech. Eng. 126 (2004) 264–275.
[23] M.H.S. Cardoso, Experimental study of the human anterolateral abdominal wall. Biomechanical properties of Fascia and muscles, Faculdade de Engenharia, Universidade do Porto, 2012 Ph.D. thesis.
[24] P. Martins, E. Peña, R.N. Jorge, A. Santos, L. Santos, T. Mascarenhas, B. Calvo, Mechanical characterization and constitutive modelling of the damage process in rectus sheath, J. Mech. Behav. Biomed. Mater. 8 (2012) 111–122.
[25] M.L. Raghavan, D.A. Vorp, Toward a biomechanical tool to evaluate rupture potential of abdominal aortic aneurysm: identification of a finite strain constitutive model and evaluation of its applicability, J. Biomech. 33 (2000) 475–482.
[26] X.Q. Peng, Z.Y. Guo, M. B., An anisotropic hyperelastic constitutive model with fiber–matrix shear interaction for the human annulus fibrosus, J. Appl. Mech. 73 (2006) 815–824.
[27] J. Simo, C. Miehe, Associative coupled thermoplasticity at finite strains: formulation, numerical analysis and implementation, Comput. Methods Appl. Mech. Eng. 98 (1) (1992) 41–104.
[28] R.W. Ogden, Large deformation isotropic elasticity–on the correlation of theory and experiment for incompressible rubberlike solids, Proc. R. Soc. Lond. A 326 (1567) (1972) 565–584.
[29] S. Doll, K. Schweizerhof, On the development of volumetric strain energy functions, J. Appl. Mech. 67 (2000) 17–21.
[30] T. Belytschko, W.K. Liu, B. Moran, K.I. Elkhodary, Nonlinear finite elements for continua and structures, 2nd, Wiley, 2014.
[31] J. Merodio, R.W. Ogden, Instabilities and loss of ellipticity in fiber–reinforced compressible non–linearly elastic solids under plane deformation, Int. J. Solids Struct. 40 (2003) 4707–4727.
[32] code Aster, Structures and thermomechanics analysis for studies and research, 2019, https://www.code-aster.org/spip.php?rubrique2. Accessed 26-Feb-2019.
[33] MFront, A code generation tool dedicated to material knowledge, 2019, http://tfel.sourceforge.net/. Accessed 26-Feb-2019.
[34] T. Helfer, B. Michel, J.-M. Proix, M. Salvo, J. Sercombe, M. Casella, Introducing the open-source mfront code generator: application to mechanical behaviours and material knowledge management within the pleiades fuel element modelling platform, Comput. Math. Appl. 70 (5) (2015) 994–1023.
[35] S. Aritan, S.O. Oyadiji, R.M. Bartlett, The *in vivo* mechanical properties of muscular bulk tissue, in: 31st Annual International Conference of the IEEE EMBS, 2009, pp. 5259–5262.
[36] K.M.M. Lima, J.F.S. Costa Júnior, W.C.A. Pereira, L.F. de Oliveira, Assessment of the mechanical properties of the muscle–tendon unit by supersonic shear wave imaging elastography: a review, Ultrasonography 37 (1) (2018) 3–15.
[37] A.E. Ehret, M. Böl, M. Itskov, A continuum constitutive model for the active behaviour of skeletal muscle, J. Mech. Phys. Solids 59 (3) (2011) 625–636.
[38] P.G. Pavan, S. Todros, P. Pachera, S. Pianigiani, A.N. Natali, The effects of the muscular contraction on the abdominal biomechanics: a numerical investigation, Comput. Methods Biomech. Biomed. Eng. 22 (2) (2019) 139–148.

2.2 Estudi 2 - Simulació virtual de l'efecte dels estomes

Virtual simulation of the biomechanics of the abdominal wall with different stoma locations

Lluís Tuset, Manuel López-Cano, Gerard Fortuny, Josep M. López, Joan Herrero i Dolors Puigjaner. *Scientific reports, 12(1), 3545, 2022.*
DOI: 10.1038/s41598-022-07555-z

www.nature.com/scientificreports

scientific reports

Check for updates

OPEN

Virtual simulation of the biomechanics of the abdominal wall with different stoma locations

Lluís Tuset[1], Manuel López-Cano[2], Gerard Fortuny[1]✉, Josep M. López[1], Joan Herrero[3] & Dolors Puigjaner[1]

An ostomy is a surgical procedure by which an artificial opening in the abdominal wall, known as a stoma, is created. We assess the effects of stoma location on the abdominal wall mechanics. We perform three-dimensional finite element simulations on an anatomy model which was generated on the basis of medical images. Our simulation methodology is entirely based on open source software. We consider seventeen different locations for the stoma incision (trephine) and we simulate the mechanical response of the abdominal wall when an intraabdominal pressure as high as 20 kPa is applied. We focus on factors related to the risk of parastomal hernia development such as the deformation experienced by the abdominal wall, the stress levels supported by its tissues and the corresponding level of trephine enlargement. No significant dependence was found between stoma location and the levels of abdominal wall deformations or stress supported by tissues, except for the case with a stoma located on the linea alba. Trephine perimeter and area respectively increased by as much as 44% and 85%. The level of trephine deformation depends on stoma location with considerably higher trephine enlargements found in stomas laterally located with respect to the rectus abdominis muscle.

An ostomy is the creation of an artificial opening into the abdominal wall (AW) through which bodily waste is rerouted outside of the body. This procedure is used to treat certain diseases related to the digestive or urinary tract. The opening created is called stoma and it is placed on the abdominal wall. One of the most common complications of ostomies is the appearance of a parastomal hernia (PH) after the construction of the stoma. Even though PH is a very frequent problem (with reported incidences as high as 78%[1] or 86%[2] when identified by computed tomography) it is difficult to treat and has a huge impact on the quality of life of patients who suffer from it[3–6]. In recent years, there has been a striking interest in the prevention of PH with prosthetic meshes[7–13]. However, advantages of a prosthetic mesh remain a matter of debate[14,15].

Preventive surgical practices of PH other than the placement of a mesh have been described. The use of a stoma incision (trephine) of a diameter not larger than 25 mm was suggested under the assumption that PH were unlikely to develop for a small trephine provided that its size did not increase with time[16]. However, a more recent study showed that enlargement of the trephine, regardless of its original size, took place in almost every surveyed ostomy patient and that most patients developed PH even though the median trephine diameter of the patient cohort was below 25 mm[2]. Other surgical practices, such as an extraperitoneal exteriorization of the stoma (extraperitoneal tunneling of the stoma between the peritoneum and the AW) have been suggested for the prevention of PH. Although these practices were supported by some promising results most of the data came from observational studies, making extraperitoneal exteriorization of the stoma a controversial option[17].

In a recent systematic review, no robust clinical data have been found to indicate which location of the stoma into the AW is optimal for PH prevention[18]. Three-dimensional (3D) modelization of the AW could be of great help to appreciate dynamically and objectively the influence of anatomic variations on the functioning of the AW[19,20]. Numerical simulations can complement clinical studies and can provide data that help abdominal surgeons in their decisions. In the present study, we applied the finite element (FE) computational setup previously

[1]Departament d'Enginyeria Informàtica i Matemàtiques, Universitat Rovira i Virgili, Av Països Catalans 26, Tarragona, Catalunya, Spain. [2]Abdominal Wall Surgery Unit, Department of General Surgery, Hospital Universitari Vall d'Hebron, Universitat Autònoma de Barcelona, Barcelona, Spain. [3]Departament d'Enginyeria Química, Universitat Rovira i Virgili, Av Països Catalans 26, Tarragona, Catalunya, Spain. ✉email: gerard.fortuny@urv.cat

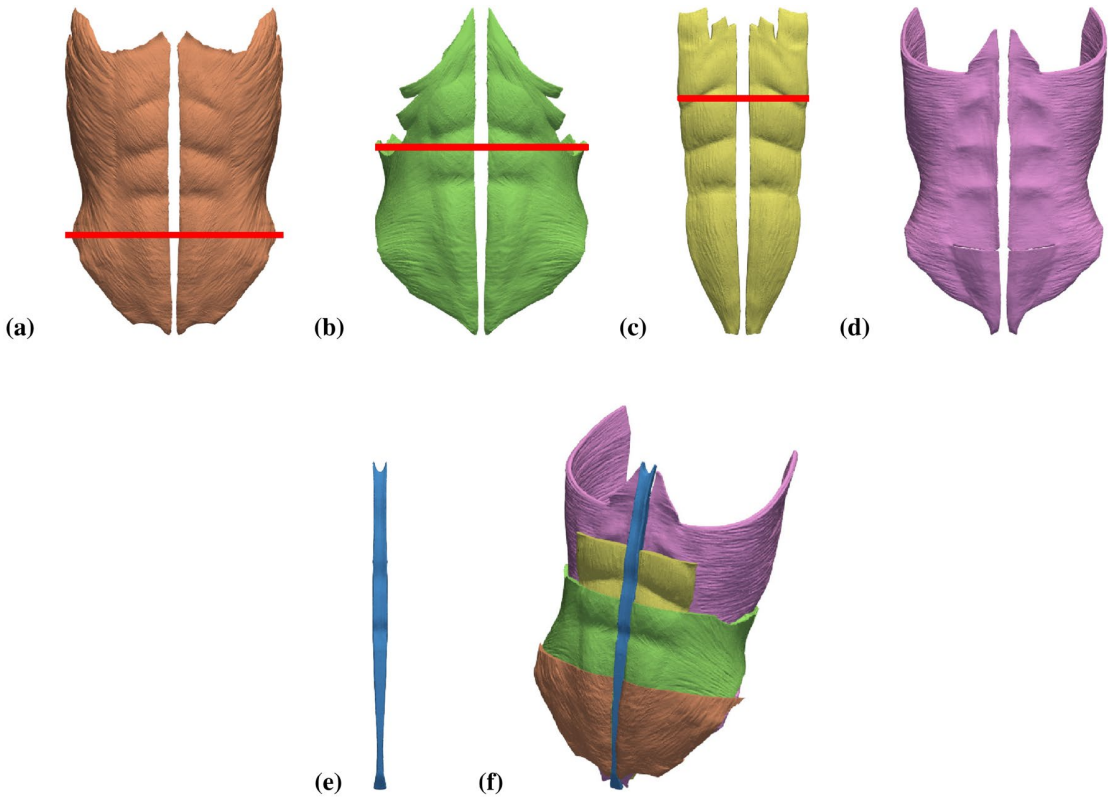

Figure 1. Geometry model of the abdominal wall. The elements included in the model are: (**a**) right and left external oblique muscles (EO), (**b**) right and left internal oblique muscles (IO), (**c**) right and left rectus abdominis muscles (RA), (**d**) right and left transverse abdominis muscles (TR), and (**e**) linea alba (LA). (**f**) View of the whole model; note that muscle regions above the red lines in parts (**a**)–(**c**) were removed from the plot and that since the muscles are superimposed the surfaces of the remaining (non-removed) muscle regions are only partially visible in the composed image.

developed by Tuset et al.[21] to investigate the effect of different transperitoneal stoma locations on the biomechanical behavior of the AW. We considered seventeen different locations for stoma incisions and we focused our analysis in two aspects. First, we assessed whether the response of the AW to a certain level of intraabdominal pressure (IAP), measured in terms of both the deformation and stress levels experienced by the tissues, is affected by the presence of a stoma. In addition, we analyzed the corresponding enlargements and deformations experienced by the trephine. Enlargement of the stoma incision is generally considered a risk factor for PH, even though statistical analyses of patient data on the subject might be inconclusive[2].

Methods

Geometry model. Figure 1 illustrates the geometry model of the AW used in the current study. The model comprises four pairs of superimposed muscles: the two external oblique muscles (EO, Fig. 1a), the two internal oblique muscles (IO, Fig. 1b), the two rectus abdominis muscles (RA, Fig. 1c), the two transverse abdominis muscles (TR, Fig. 1d) and the linea alba (LA, Fig. 1e). Figure 1f shows how the four sets of involved muscles are superimposed in the geometry model.

Our geometry model was based on computerized tomography (CT) images available in the BodyParts3D database for anatomy[22]. Three-dimensional triangular surface meshes for each of the individual elements in the model were downloaded from this database and were subsequently refined. The refined meshes were then merged and undesirable intersections between contiguous elements were removed in order to obtain physically consistent surface meshes. These surface meshes, with a total of 892, 283 triangles, were then uploaded into the Gmsh open source software[23] where the corresponding 3D volume meshes were built. Finally, the individual volume meshes were compounded into a global computational mesh consisting of 3, 495, 765 tetrahedra.

In the present study, the stoma incision was modeled as a circular cylindrical orifice of diameter 2 cm. We considered 17 different locations for the stoma distributed over the AW, as shown in Fig. 2. Except for one stoma located on the LA, stomas are distributed along three vertical lines on the left side of the AW. The stoma located on the LA is denoted as s_0 and the rest of stomas are labelled as $s_{i,j}$, where the i index denotes the particular vertical line (with i growing with increasing horizontal distance to the vertical midline) and j denotes the vertical position of the stoma in the ith vertical line (with j increasing with height).

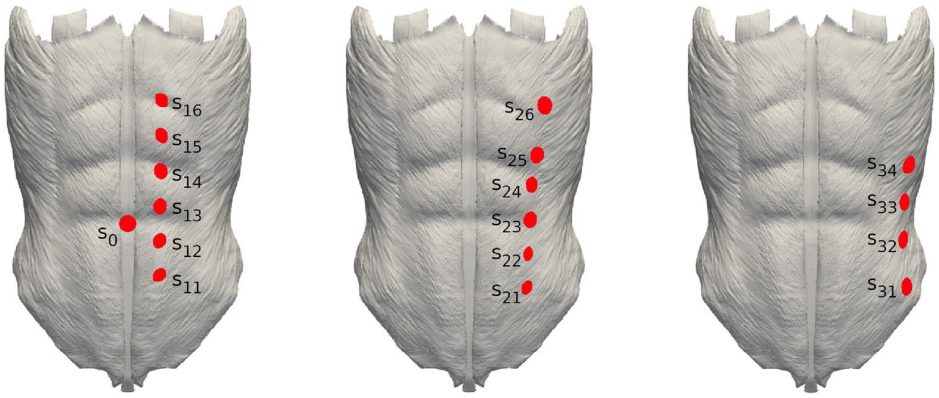

Figure 2. Trephine locations (colored in red) on the outermost AW surface and their labels.

Tissue	E (MPa)	References
EO	1	Cardoso[24]
IO	0.65	Cardoso[24]
RA	0.52	Cardoso[24]
TR	1.03	Cardoso[24]
LA	72	Cooney et al.[25]

Table 1. Values of Young's modulus (E) assumed in the present study for the different tissues in our AW model.

Material properties. We assumed a linear elastic behavior of the AW tissues,

$$\boldsymbol{\sigma} = E\boldsymbol{\epsilon}, \tag{1}$$

where the stress tensor ($\boldsymbol{\sigma}$), characterizing the force per unit surface area experienced by a material volume, is proportional to the strain tensor ($\boldsymbol{\epsilon}$), whose components represent the relative deformations in the material volume along each spatial direction. To describe the mechanical behavior of a linear elastic material two parameters are required, the Young's modulus E, which provides the stiffness of the material (as can be seen in Eq. (1), for a given $\boldsymbol{\sigma}$ level the larger the E value the smaller the relative deformation, $\boldsymbol{\epsilon}$) and the Poisson's ratio (η), which measures the relative volume change as a result of the deformation.

In the present study, the values of E for the EO, IO, RA and TR muscles were prescribed following the experimental uniaxial tensor tests performed by Cardoso[24]. The specific E values for each tissue are listed in Table 1. For the LA, which is essentially a tendinous tissue and thus the stiffest one in the AW, we used the $E = 72$ MPa value reported by Cooney et al.[25]. Note that the present model does not include soft tissues such as skin or subcutaneous abdominal fat. The underlying hypothesis is that as the stiffness of soft tissues is at least one order of magnitude smaller (lower E) than the stiffness of the AW muscles[26] then muscles are the tissues actually determining the biomechanical response of the AW. All the involved tissues were characterized with a Poisson ratio of $\eta = 0.3$.

Numerical simulation. All of the present FE simulations were carried out using the Code Aster open source software[27]. A given uniformly distributed IAP value was set for the computational domain regions corresponding to the inner AW surface. In addition, a fixed zero deformation boundary condition was set for the regions on the AW edges, where the real muscular tissue would be attached to bone tissue. For each particular geometry, we considered five levels of IAP up to $P = 20$ kPa (150 mmHg), a maximum value which would be typically achieved when coughing or jumping[28]. In each simulation, the distributions of stress ($\boldsymbol{\sigma}$) and deformations along the AW were calculated. As $\boldsymbol{\sigma}$ is a tensor quantity, often its physical interpretation is not straightforward. The so-called von Mises stress, σ_v, was therefore calculated and analyzed. The von Mises stress is a scalar quantity devised to characterize the risk of rupture of a solid material when subjected to stresses[29].

As mentioned earlier, trephine enlargement seems to be a key risk factor for the development of PH. Consequently, in every simulation the resulting trephine dimensions (perimeter and area) in the deformed geometry were also measured and the relative change with respect to the reference (non-deformed) geometry was calculated.

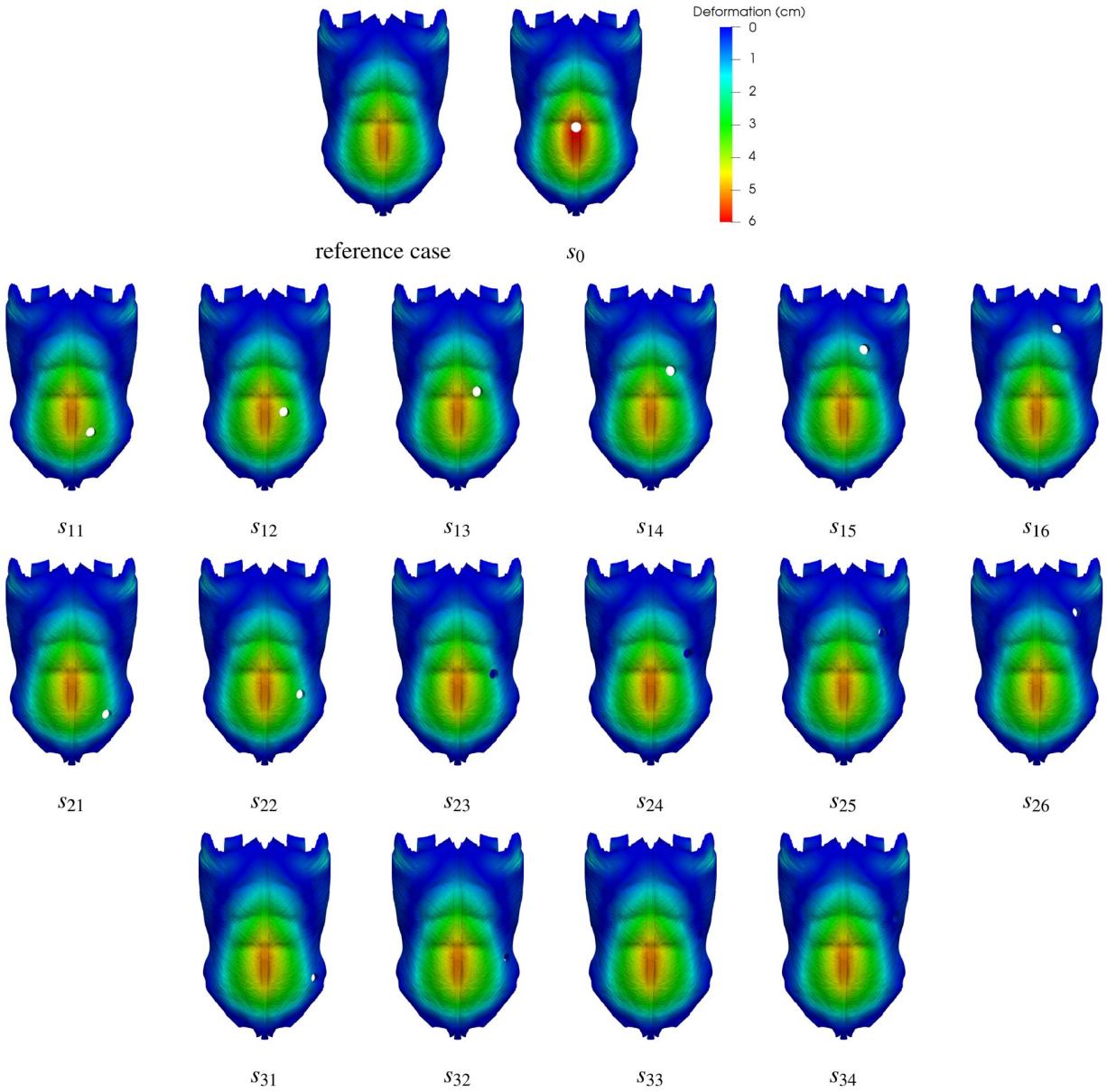

Figure 3. The predicted deformation distributions are plotted on the base (undeformed) geometry of the abdominal wall for all the cases investigated, that is, the reference case (no stoma) and the seventeen stoma locations. In all cases, the results correspond to the simulations with the maximum value of the applied intraabdominal pressure, $P = 20$ kPa.

Results

We performed FE simulations with the reference geometry model (no stoma) and with each of the 17 geometry models having a stoma in the locations shown in Fig. 2. In what follows, we analyze the effects of IAP on the overall AW mechanics and, in particular, the corresponding levels of trephine enlargement. For the sake of compactness, only results from simulations with the largest IAP value, $P = 20$ kPa, are presented here.

Deformation and stress distribution on the abdominal wall. Figure 3 shows the deformation distribution on the outer AW surface as predicted by our numerical simulations for all the cases investigated. Note that since in this figure deformations are plotted on the undeformed geometry trephines preserve their original size (trephine enlargement will be the subject of the next subsection). As expected, the result of applying any positive IAP level is always a forwards protrusion of the AW, with a maximum deformation of 52.09 mm in the reference case. In the 16 cases with the stoma located away from the LA, predicted maximum deformations ranged between 51.09 and 53.25 mm, which indicates that differences with respect to the reference case are not significant. Moreover, as it can be observed in Fig. 3, all deformations for geometries other than s_0 strongly

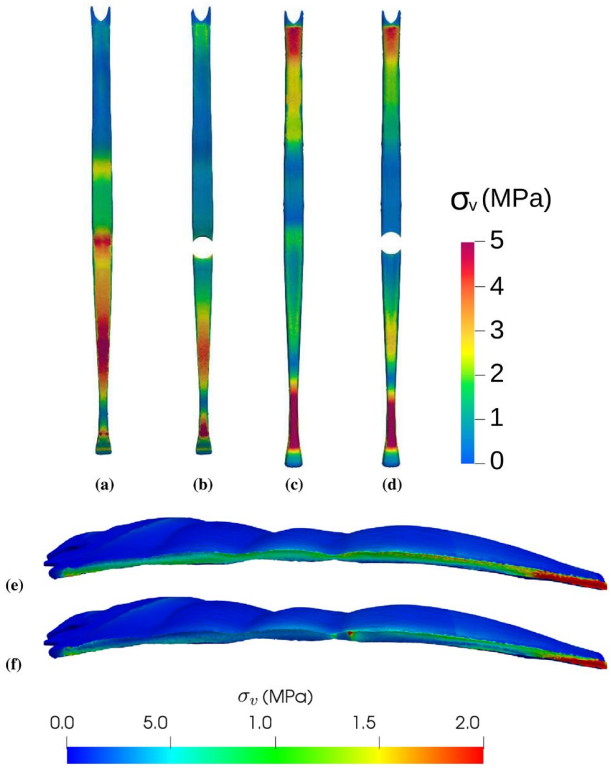

Figure 4. Distribution of Von Mises tension (σ_v) on the anterior (**a**,**b**) and posterior (**c**,**d**) surfaces of the linea alba and (**e**,**f**) on the inner lateral region of the left rectus abdominis muscle (the surface that is in contact with the LA). (**a**,**c**,**e**) Reference case (model without incisions). (**b**,**d**,**f**) Case with a stoma located on the linea alba (s_0). Note that in parts (**e**) and (**f**) the axes are rotated so that the leftmost region of the RA here corresponds to the uppermost RA region in Fig. 1c.

resemble the distribution for the reference case. Similarly, small differences were found between all cases other than s_0 in terms of the von Mises stress distributions, with maximal values (σ_v^{max}) in the 11.19–11.36 MPa range (with $\sigma_v^{max} = 11.29$ MPa in the reference case).

The s_0 case was devised as an *acid test* for the current methodology. That is, the classical recommendation that a stoma should not be constructed through a midline laparotomy incision[1] ought to be also supported from a mechanical standpoint. As illustrated in the first row of Fig. 3, the maximum AW deformation is about a 18% larger in the s_0 case (61.23 mm) than it is in the reference case (52.09 mm). The corresponding σ_v^{max} increase is more modest, about a 3% ($\sigma_v^{max} = 11.65$ MPa for s_0). The LA plays a key role in AW mechanics as it pulls together the muscles from the left and right sides (see Fig. 1f). Consequently, as shown in Fig. 4a,c, in the current IAP-promoted AW expansion scenario LA is the element experiencing the highest stress levels, with the largest σ_v values found near its lower edge (closer to the pubic region). From a mechanical point of view, the main drawback with the s_0 stoma location is that the trephine severs the LA into two independent sections (see Fig. 4b,d). Despite the larger AW deformation for s_0 in Fig. 3, comparison of Fig. 4d with Fig. 4b shows that the two independent LA sections keep performing their main function, i.e., they remain attached to the muscles from both sides of the AW.

As the two rectus abdominis are the muscles in closer contact with the LA through their inner lateral surfaces, one would expect AW expansion to produce relatively high stress levels within the RA tissue. Figures 4e,f show the σ_v distribution on the inner lateral region of the left RA muscle for the reference case and the s_0 case. In the reference case (Fig. 4e), the largest σ_v values are concentrated at the lower part of the muscle (rightmost section of the plot), consistently with the stress distribution on the LA itself (see Fig. 4c). In contrast, in the s_0 case (Fig. 4f) a second region of high σ_v (i.e., a red spot) appears around the axial location of the trephine.

Trephine enlargement. The trephine original size was significantly increased as a result of the AW deformation in all the cases investigated, as illustrated in Fig. 5 where the deformed geometry of the left TR muscle is displayed. The elliptic forms adopted by stoma incisions in the deformed geometries are clearly visible in these plots. In agreement with the radiological measurements reported by Ho et al.[2], our simulations predict that the trephine sagittal diameter grows more than its axial diameter does. Table 2 summarizes the deformations experienced by stomas in terms of trephine perimeter and area, as well as the corresponding percent increase of these two quantities with respect to the original geometry. Note that when the largest IAP of 20 kPa is applied trephine enlargements as high as 44% in terms of perimeter and 85% in terms of area (for the s_{32} stoma) are obtained. A

Stoma	Area of the deformed stoma (cm^2)	% increase in area	Perimeter of the deformed stoma (cm)	% increase in perimeter
s_0	3.76	20	6.93	10
s_{11}	3.59	14	6.88	9
s_{12}	3.64	16	6.96	11
s_{13}	4.18	33	7.56	20
s_{14}	4.18	33	7.46	19
s_{15}	4.25	35	7.45	19
s_{16}	4.07	30	7.30	16
s_{21}	4.75	51	7.76	23
s_{22}	4.82	53	8.05	28
s_{23}	5.37	71	8.70	38
s_{24}	5.58	78	9.00	43
s_{25}	4.34	38	7.56	20
s_{26}	3.93	25	7.14	14
s_{31}	4.28	36	7.50	19
s_{32}	5.82	85	9.05	44
s_{33}	4.34	38	7.59	21
s_{34}	4.91	56	8.09	29

Table 2. Area and perimeter of stomas in the deformed geometry when an intraabdominal pressure of $P = 20$ kPa is applied. The percentage of increase with respect to the undeformed geometry is also included. Note that in the undeformed geometry the diameter of the stoma is 2 cm, the area is therefore 3.14 cm^2 and the perimeter is 6.28 cm. In all cases, the dimensions of the deformed trephines were measured at the innermost surface of the abodminal wall.

topic which is the subject of some controversy in the literature is whether trephine enlargment levels depend on stoma location. More particularly, the question is whether or not stomas located lateral to the left RA muscle tend to experience largest trephine enlargements than do stomas crossing the RA. For the latter type of stomas, we can see in Table 2 (the ones labeled as $s_{1,j}$, $1 \leq j \leq 6$; see also Fig. 2) that the average incrase in trephine area is 28% whereas for the stomas lateral to the RA muscle the corresponding increases are 53% ($s_{2,j}$) and 54% ($s_{3,j}$). Thus, the present simulations predict trephine enlargements that, on the average, are more pronounced for stomas located lateral to the RA muscle. This result is in apparent contradiction with the findings by Ho et al.[2], who found no statistically significant relation between the rate of trephine size progression and stoma position. Notwithstanding, these authors acknowledged as a limitation of their data analysis the fact that only 11.7% of patients had a stoma created lateral to the RA muscle.

Discussion

Our study shows that the creation of a stoma, unless its location is poorly chosen, does not compromise the mechanical consistency of the AW when subjected to IAP levels as high as 20 kPa. More precisely, except for the case with a stoma located on the LA (s_0), the amount of deformation of the AW (visualized as a forward protrusion of the patient's belly) and the stress levels that it supports show a very weak dependence on stoma location.

On the other hand, an augment of the trephine size was observed in all of the simulations. Such a trephine enlargement was measured in terms of the increase in both trephine perimeter and cross-area. Our simulations therefore indicate that trephine enlargement is inherent to the AW deformation that results when a certain IAP level is applied. It seems plausible to suggest that as trephine enlargement is related to PH development[2] then parastomal hernia would be a long run complication inherent to the ostomy procedure. Notwithstanding, it is important to place the present results in the proper scope. Our model predicts short-time trephine enlargements that would be completely reversible. That is, the whole AW and thus the trephines would recover their original shape once the IAP is released. What is seen and measured in the patients' CT scans[2] is trephine defect, i.e., the level of permanent (irreversible) enlargement of trephines. We can think of trephine defect in terms of either material fatigue, micro-lesions or, more generically, a progressive adaption of biological tissues to the surrounding constraints. In an ideal world permanent trephine enlargement should not occur but reality (clinical findings) is that trephine defect increases with time after stoma creation. We cannot presently predict, for example, whether trephine defect would develop faster in a (hypothetical) patient with a quiescent life style, who might however experience occasional large AW deformations (e.g., a sudden high peak in IAP level), or in a second patient undergoing mild but frequent exercising.

The present simulations also show that stomas placed lateral to the RA muscle experience higher trephine enlargements as a result of an IAP, a fact suggesting that creation of laterally placed stomas ought to be avoided. However, this result has to be interpreted with caution because of the aforementioned difference between the ideal (reversible) trephine enlargement, predicted in our simulations, and the real (irreversible) trephine defect experienced by ostomy patients. Future research, which will hopefully include radiological measurements and data analyses in large ostomy patients' cohorts[30], will no doubt shed more light on the subject. Moreover, our

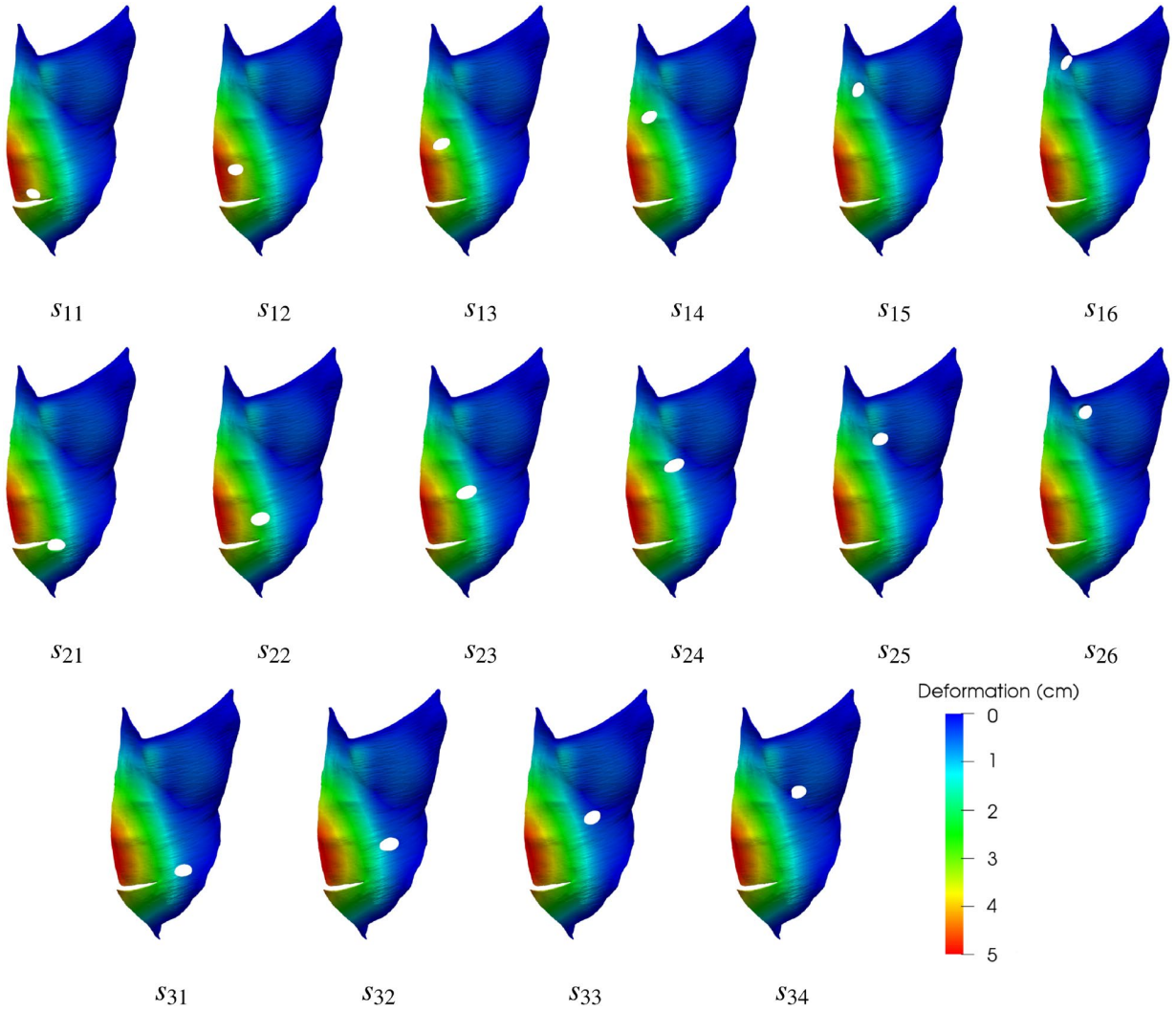

Figure 5. Deformed geometries in the cases where the enlargement of the stomas was apparent at first sight when an IAP of $P = 20$ kPa was applied. For the sake of clarity, only the left TR muscle is shown in each case. The deformation distribution on the TR surface is represented by color levels, as specified in the accompanying color box.

methodology could be used in the future to assess the risks associated to trephine enlargement in a patient-specific basis. For this purpose, simulations would be carried out in geometries built from the patient's CT scans.

Received: 16 September 2021; Accepted: 10 February 2022
Published online: 03 March 2022

References

1. Whitehead, A. & Cataldo, P. Technical considerations in stoma creation. *Colon Rectal Surg.* **30**, 162–171. https://doi.org/10.1055/s-0037-1598156 (2017).
2. Ho, K., Economou, T., Smart, N. & Daniels, I. Radiological progression of end colostomy trephine diameter and area. *BJS Open* **3**, 112–118. https://doi.org/10.1002/bjs5.50109 (2019).
3. Kald, A., Juul, K. N., Hjortsvang, H. & Sjödal, R. I. Quality of life is impaired in patients with peristomal bulging of a sigmoid colostomy. *Scand. J. Gastroenterol.* **43**, 627–633. https://doi.org/10.1080/00365520701858470 (2008).
4. Ripoche, J., Basurko, C., Fabbro-Perray, P. & Prudhomme, M. Parastomal hernia. A study of the French federation of ostomy patients. *J. Visc. Surg.* **148**, e435–e441. https://doi.org/10.1016/j.jviscsurg.2011.10.006 (2011).
5. van Dijk, S. M. *et al.* Parastomal hernia: Impact on quality of life?. *World J. Surg.* **39**, 2595–2601. https://doi.org/10.1007/s00268-015-3107-4 (2015).
6. Hubbard, G. *et al.* Research priorities about stoma-related quality of life from the perspective of people with a stoma: A pilot survey. *Health Expect.* **20**, 1421–1427. https://doi.org/10.1111/hex.12585 (2017).
7. Serra-Aracil, X. *et al.* Randomized, controlled, prospective trial of the use of a mesh to prevent parastomal hernia. *Ann. Surg.* **249**, 583–587 (2009).
8. López-Cano, M. *et al.* Use of a prosthetic mesh to prevent parastomal hernia during laparoscopic abdominoperineal resection: A randomized controlled trial. *Hernia* **16**, 661–667. https://doi.org/10.1007/s10029-012-0952-z (2012).

9. Vierimaa, M. *et al.* Prospective, randomized study on the use of a prosthetic mesh for prevention of parastomal hernia of permanent colostomy. *Dis. Colon Rectum* **58**, 943–949. https://doi.org/10.1097/DCR.0000000000000443 (2015).
10. López-Cano, M. *et al.* Preventing parastomal hernia using a modified sugarbaker technique with composite mesh during laparoscopic abdominoperineal resection. *Ann. Surg.* **264**, 923–928. https://doi.org/10.1097/SLA.0000000000001684 (2016).
11. Brandsma, H.-T. *et al.* Prophylactic mesh placement during formation of an end-colostomy reduces the rate of parastomal hernia short-term results of the dutch prevent-trial. *Ann. Surg.* **265**, 663–669. https://doi.org/10.1097/SLA.0000000000001903 (2017).
12. Odensten, C. *et al.* Use of prophylactic mesh when creating a colostomy does not prevent parastomal hernia. *Ann. Surg.* **269**, 427–431. https://doi.org/10.1097/SLA.0000000000002542 (2019).
13. Prudhomme, M. *et al.* End colostomy with or without mesh to prevent a parastomal hernia (greccar 7). A prospective, randomized, double blinded, multicentre trial. *Ann. Surg.* **274**, 928–934. https://doi.org/10.1097/SLA.0000000000004371 (2021).
14. López-Cano, M., Pereira, J. & García-Alamino, J. Comment on: Meta-analysis and systematic review of the use of a prosthetic mesh for prevention of parastomal hernia. *Ann. Surg.*https://doi.org/10.1097/SLA.0000000000004949 *(2021).*
15. Prudhomme, M., Fabbro-Peray, P., Rullier, E., Occean, B. V. & Bertrand, M. M. Meta-analysis and systematic review of the use of a prosthetic mesh for prevention of parastomal hernia. *Ann. Surg.* **274**, 20–28. https://doi.org/10.1097/SLA.0000000000004944 (2021).
16. Hotouras, A., Murphy, J., Power, N., Williams, N. & Chan, C. Radiological incidence of parastomal herniation in cancer patients with permanent colostomy: what is the ideal size of the surgical aperture?. *Int. J. Surg.* **11**, 425–427 (2013).
17. Kroese, L., de Smet, G., Jeekel, J., Kleinrensink, G. & Lange, J. Systematic review and meta-analysis of extraperitoneal versus transperitoneal colostomy for preventing parastomal hernia. *Dis. Colon Rectum* **59**, 688–695. https://doi.org/10.1097/DCR.0000000000000605 (2016).
18. Hardt, J. *et al.* Lateral pararectal versus transrectal stoma placement for prevention of parastomal herniation. *Cochrane Database Syst. Rev.*https://doi.org/10.1002/14651858.CD009487.pub2 *(2019).*
19. López-Cano, M., Rodríguez-Navarro, J., Rodríguez-Baeza, A., Armengol-Carrasco, M. & Susín, A. A real-time dynamic 3d model of the human inguinal region for surgical education. *Comput. Biol. Med.* **37**, 1321–1326. https://doi.org/10.1016/j.compbiomed.2006.12.006 (2007).
20. Fortuny, G., López-Cano, M., Susín, A. & Herrera, B. Simulation and study of the geometric parameters in the inguinal area and the genesis of inguinal hernias. *Comput. Methods Biomech. Biomed. Eng.* **15**, 195–201. https://doi.org/10.1080/10255842.2010.522182 (2012).
21. Tuset, L., Fortuny, G., Herrero, J., Puigjaner, D. & López, J. M. Implementation of a new constitutive model for abdominal muscles. *Comput. Methods Progr. Biomed.*https://doi.org/10.1016/j.cmpb.2019.104988 *(2019).*
22. Mitsuhashi, N. *et al.* Bodyparts3d: 3d structure database for anatomical concepts. *Nucleic Acids Res.* **37**, 782–785. https://doi.org/10.1093/nar/gkn613 (2009).
23. Geuzaine, C. & Remacle, J.-F. Gmsh. A three-dimensional finite element mesh generator with built-in pre- and post-processing facilities. (2020) http://gmsh.info/. (accessed 10 May 2020).
24. Cardoso, M. *Experimental Study of the Human Anterolateral Abdominal Wall: Biomechanical Properties of Fascia and Muscles*. Master's thesis, Faculdade de Engenharia, Universidade do Porto (2012).
25. Cooney, G. M. *et al.* Uniaxial and biaxial tensile stress-stretch response of human linea alba. *J. Mech. Behav. Biomed. Mater.* **63**, 134–140. https://doi.org/10.1016/j.jmbbm.2016.06.015 (2016).
26. Guimarães, C., Gasperini, L., Marques, A. & Reis, R. The stiffness of living tissues and its implications for tissue engineering. *Nat. Rev. Mater.* **5**, 351–370. https://doi.org/10.1038/s41578-019-0169-1 (2020).
27. code Aster. Structures and thermomechanics analysis for studies and research. https://www.code-aster.org/spip.php?rubrique2 (2020). https://www.code-aster.org/spip.php?rubrique2. (accessed 26 May 2020).
28. Cobb, W. S. *et al.* Normal intraabdominal pressure in healthy adults. *J. Surg. Res.* **129**, 231–235. https://doi.org/10.1016/j.jss.2005.06.015 (2005).
29. Malvern, L. E. Introduction to the mechanics of a continuous medium. In *Engineering of the Physical Sciences* (Prentice-Hall, 1969).
30. Tabusa, H. *et al.* Protocol for the UK cohort study to investigate the prevention of parastomal hernia (the CIPHER study). *Colorectal Dis.* **23**, 1900–1908. https://doi.org/10.1111/codi.15621 (2021).

Acknowledgements
Financial support for the current research was granted by Universitat Rovira i Virgili, project number 2018PFR-URV-B2-29.

Author contributions
Conception: M.L.-C. and G.F. Simulation design and setup: L.T., G.F., J.M.L., J.H. and D.P. Performing the simulations: L.T. Post-processing: L.T., G.F., J.M.L., J.H. and D.P. All authors analyzed and discussed the results of the simulations. All authors contributed to the writing of the manuscript. All authors have read and agreed to the submitted version of the manuscript.

Competing interests
The authors declare no competing interests.

Additional information
Correspondence and requests for materials should be addressed to G.F.

Reprints and permissions information is available at www.nature.com/reprints.

Publisher's note Springer Nature remains neutral with regard to jurisdictional claims in published maps and institutional affiliations.

Open Access This article is licensed under a Creative Commons Attribution 4.0 International License, which permits use, sharing, adaptation, distribution and reproduction in any medium or format, as long as you give appropriate credit to the original author(s) and the source, provide a link to the Creative Commons licence, and indicate if changes were made. The images or other third party material in this article are included in the article's Creative Commons licence, unless indicated otherwise in a credit line to the material. If material is not included in the article's Creative Commons licence and your intended use is not permitted by statutory regulation or exceeds the permitted use, you will need to obtain permission directly from the copyright holder. To view a copy of this licence, visit http://creativecommons.org/licenses/by/4.0/.

© The Author(s) 2022

2.3 Estudi 3 - Simulació virtual de l'efecte de les incisions laparoscòpiques

---

A virtual simulation approach to assess the effect of trocar-site placement and scar characteristics on the abdominal wall biomechanics

Lluís Tuset, Manuel López-Cano, Gerard Fortuny, Josep M. López, Joan Herrero i Dolors Puigjaner. *Scientific reports, 14, 3583, 2024.*
DOI: 10.1038/s41598-024-54119-4

www.nature.com/scientificreports

scientific reports

Check for updates

OPEN

A virtual simulation approach to assess the effect of trocar-site placement and scar characteristics on the abdominal wall biomechanics

Lluís Tuset[1], Manuel López-Cano[2], Gerard Fortuny[1], Josep M. López[1], Joan Herrero[3] & Dolors Puigjaner[1]✉

Analyses of registries and medical imaging suggest that laparoscopic surgery may be penalized with a high incidence of trocar-site hernias (TSH). In addition to trocar diameter, the location of the surgical wound (SW) may affect TSH incidence. The intra-abdominal pressure (IAP) exerted on the abdominal wall (AW) might also influence the appearance of TSH. In the present study, we used finite element (FE) simulations to predict the influence of trocar location and SW characteristics (stiffness) on the mechanical behavior of the AW subject to an IAP. Two models of laparoscopy patterns on the AW, with trocars in the 5–12 mm range, were generated. FE simulations for IAP values within the 4 kPa–20 kPa range were carried out using the Code Aster open-source software. Different stiffness levels of the SW tissue were considered. We found that midline-located surgical wounds barely deformed, even though they moved outwards along with the regular LA tissue. Laterally located SWs hardly changed their location but they experienced significant variations in their volume and shape. The amount of deformation of lateral SWs was found to strongly depend on their stiffness. Trocar incisions placed in a LA with non-diastatic dimensions do not compromise its mechanical integrity. The more lateral the trocars are placed, the greater is their deformation, regardless of their size. Thus, to prevent TSH it might be advisable to close lateral trocars with a suture, or even use a prosthetic reinforcement depending on the patient's risk factors (e.g., obesity).

The prevalence of trocar-site hernias (TSH) is not clear[1]. Analysis of registries suggests a high incidence of TSH[2] and that, depending on their location, reparation of these hernias can be complex[3]. Moreover, the recently updated guidelines for closure of abdominal wall incisions[4] provide no support to the notion that the fascial closure at the trocar site can benefit TSH prevention. These guidelines also mention that there is no evidence supporting the best trocar location and they recommend suturing the fascial defect for trocar sites of 10 mm or larger, and for trocars located at the umbilical site[4].

Finite element (FE) simulations may strengthen our understanding of how surgical wounds (SWs) alter the mechanical behavior of the abdominal wall (AW)[5,6]. Our key assumption is that the response of the AW to intra-abdominal pressure (IAP) sometime after surgery will depend on the mechanical properties of the tissue regrown at the surgical sites, that is, the tissue conforming the SWs, and the laparoscopy pattern used in the surgery. The resilience of the AW to an applied IAP value, P_a, is mostly due to the stiffness of its tissues, which are of muscular or tendinous nature. Both types of tissue are characterized by the presence of fibers in their architecture[7]. The new SW tissue might be weak and, from a mechanical point of view, softer than expected[8]. On the other hand, the regrown tissue in the SW might become scarred[9,10] and exceedingly stiff[11].

In silico analysis could help to virtually simulate the influence of trocar location or trocar scar characteristics on the mechanical behavior of the AW. However, to the best of our knowledge, there is no study on how the SW

[1]Departament d'Enginyeria Informàtica i Matemàtiques, Universitat Rovira i Virgili, Av. Països Catalans 26, Tarragona, Catalunya, Spain. [2]Abdominal Wall Surgery Unit, Department of General Surgery, Hospital Universitari Vall d'Hebron, Universitat Autònoma de Barcelona, Barcelona, Spain. [3]Departament d'Enginyeria Química, Universitat Rovira i Virgili, Av. Països Catalans 26, Tarragona, Catalunya, Spain. ✉email: dolors.puigjaner@urv.cat

characteristics, or its location alter the mechanical response of the AW. The aim of this work is to use FE simulations to predict AW deformation as a function of the stiffness and location of the SWs (mimicking trocar-site placement), and the level of IAP applied.

Models and methods

Geometry model

The present geometry model, illustrated in Fig. 1, is similar to the one used in our previous work[5]. It consists of external oblique (EO), internal oblique (IO), rectus abdominis (RA) and transverse abdominis (TR) muscles, as well as the linea alba (LA), which was considered with standard dimensions of 2 cm (i.e., without rectus diastasis)[12]. Notwithstanding, a novelty in the present geometry model is that the aponeurosis of the TR, EO and IO muscles is considered as a distinct tissue, having mechanical properties different from those of the regular muscle (see Fig. 1).

We investigated two laparoscopy patterns, denoted as models A and B (see Fig. 2a,b). We considered surgical wounds after surgery, i.e., assuming all trocar-sites closed. SWs were modeled as elliptic cylinders orthogonal to the outer AW surface (see Fig. 2c) with the ellipse major axis representing the trocar diameter, and the minor axis set to 2 mm in all cases. We will henceforth refer to the length and width of a laparoscopy SW instead of to the ellipse axes.

Length, surface area and volume of each SW geometry are summarized in Table 1. Model A (Fig. 2a) comprises six surgical wounds. Two 12-mm long incisions are located on the LA (A1, A4), two 5-mm long incisions are located on the left lateral region (A2, A3), and two more SWs, respectively 5- and 12-mm long, are on the right lateral region (A5, A6). Model B (Fig. 2b) consists of five surgical wounds. Two incisions, a 10-mm long supraumbilically placed (B1) and a 5-mm long infraumbilically placed (B4), are embedded in the LA. Two 5-mm long incisions are located on the left lateral region (B2, B3) and a 12-mm long SW is placed on the right lateral region (B5).

Material properties

Following our previous work[5] we assumed a linear elastic behavior of the AW tissues,

$$\sigma = E\varepsilon \tag{1}$$

where $\boldsymbol{\sigma}$ is the stress tensor, $\boldsymbol{\varepsilon}$ is the strain tensor, accounting for the relative deformation of tissues, and E is the elastic modulus. The specific E values for each tissue, together with the bibliographic source, are listed in Table 2. A value of $\nu = 0.49$ was assumed for the Poisson's ratio of muscular tissues. The aponeurosis of the TR, EO and

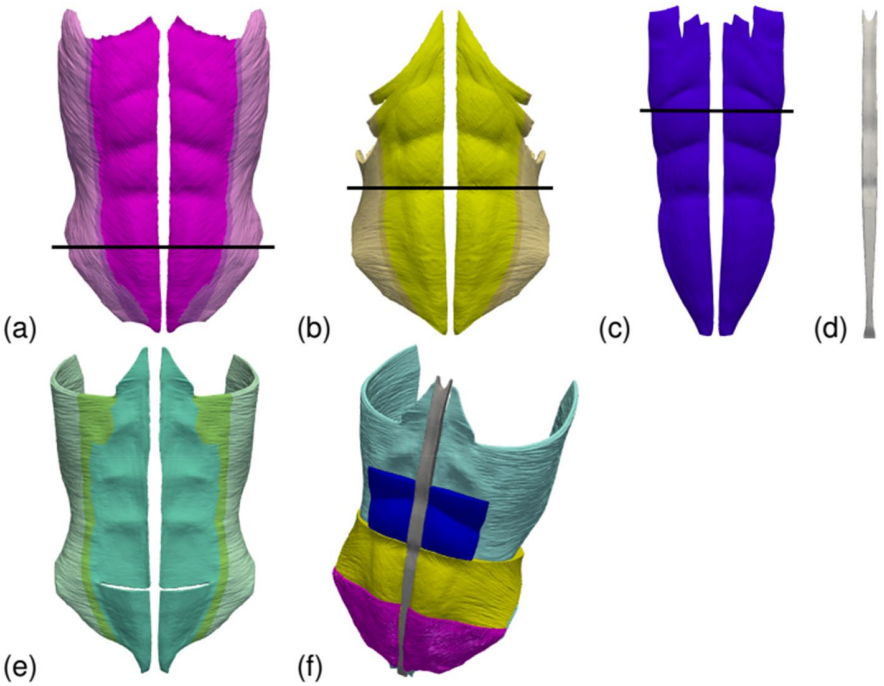

Figure 1. Geometry model of the abdominal wall. The elements involved in the model are: (**a**) right and left external oblique muscles (EO), (**b**) right and left internal oblique muscles (IO), (**c**) right and left rectus abdominis muscles (RA), (**d**) linea alba (LA) and (**e**) right and left transverse abdominis muscles (TR). (**f**) View of the whole model. Note that as the involved muscles are superimposed only those muscle regions below black lines in parts (**a**–**c**) are displayed. In parts (**a**,**b**,**e**) the different regions (regular, intermediate, and aponeurotic muscle tissue) are denoted with increasingly saturated color tones.

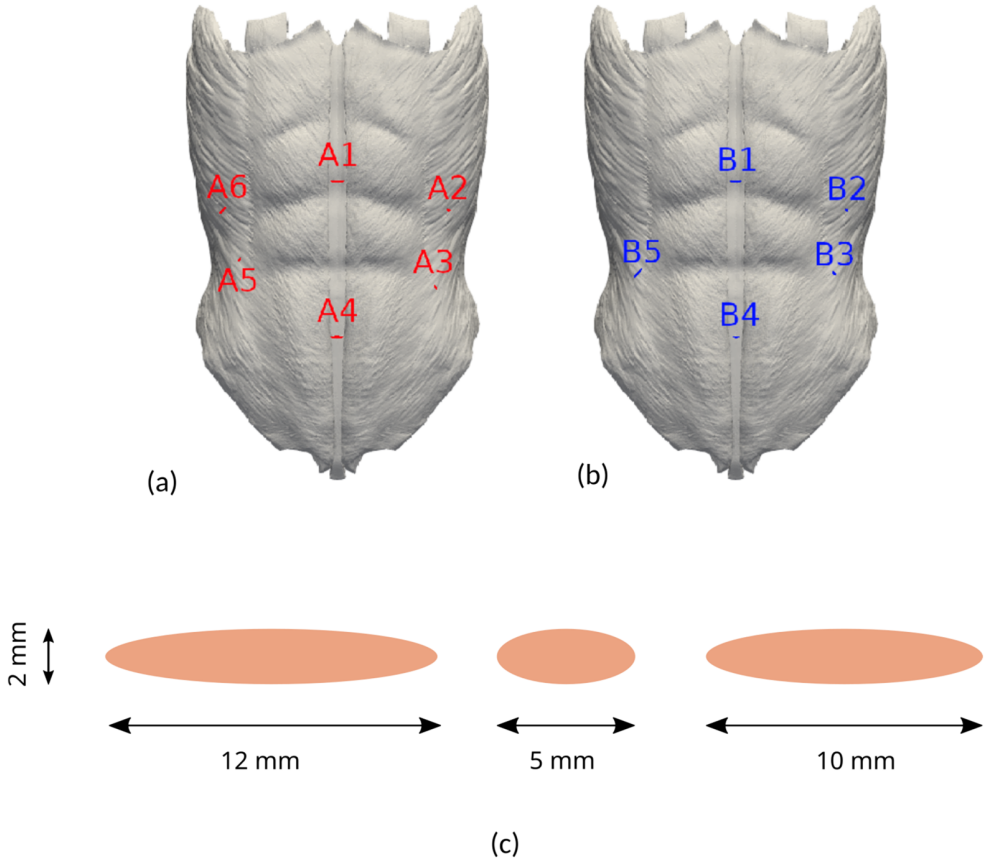

Figure 2. Distribution of the incisions on the AW for the two laparoscopy patterns studied in this work. (**a**) Laparoscopy model A, with three 5-mm long and three 12-mm long incisions. (**b**) Laparoscopy model B, with one 10-mm long, one 12-mm long and three 5-mm long surgical wounds (see Table 1 for details on the length, surface area and volume of each laparoscopic SW). (**c**) Sketch of the elliptic profile for the three geometry models of laparoscopy surgical wounds assumed in the present study.

	length (mm)	surface area (cm^2)	volume (cm^3)		length (mm)	surface area (cm^2)	volume (cm^3)
A1	12	3.31	0.217	B1	10	2.78	0.179
A2	5	3.00	0.190	B2	5	3.00	0.190
A3	5	2.27	0.142	B3	5	2.18	0.135
A4	12	3.48	0.231	B4	5	1.67	0.100
A5	5	2.16	0.134	B5	12	4.80	0.332
A6	12	6.78	0.477				

Table 1. Dimensions of every SW in the present laparoscopy trocar models.

IO muscles forms the so-called rectus sheath[13,14]. The tissue in the rectus sheath is more fibrous (higher E) than regular muscular tissue. Figure 3 illustrates the definition of the three regions (regular muscle, rectus sheath, and a thin intermediate transition region). In the transition region, we assumed an E value halfway the values for rectus sheath and regular muscle.

A wide variability in the mechanical properties of wounds can be found in the literature. For example, Ibrahim et al.[15] reported E values of a few kPa for uninjured human skin, whereas Samartsev et al.[16] obtained elastic moduli of a few GPa in their experiments with sutured samples. In the current study, we performed simulations within a wide range of E values for the SWs, namely 0.1 MPa $\leq E_w \leq$ 10,000 MPa. The Poisson ratio for SW tissue was set to $\nu_w = 0.40$[16].

Tissue		*E* (MPa)	References
RA		0.52	Cardoso[28]
LA		72	Cooney et al.[29]
EO	Regular muscle	1	Cardoso[28]
	Transition region	3.3	
	Rectus sheath	5.6	Ben Abdelounis et al.[30]
IO	Regular muscle	0.65	Cardoso[28]
	Transition region	3.1	
	Rectus sheath	5.6	Ben Abdelounis et al.[30]
TR	Regular muscle	1.03	Cardoso[28]
	Transition region	3.3	
	Rectus sheath	5.6	Ben Abdelounis et al.[30]

Table 2. Elastic modulus (*E*) assumed for the different tissues in our AW model. *RA* Rectus Abdominis, *LA* Linea Alba, *EO* Internal Oblique, *IO* Internal Oblique, *TR* Transverse Abdominis.

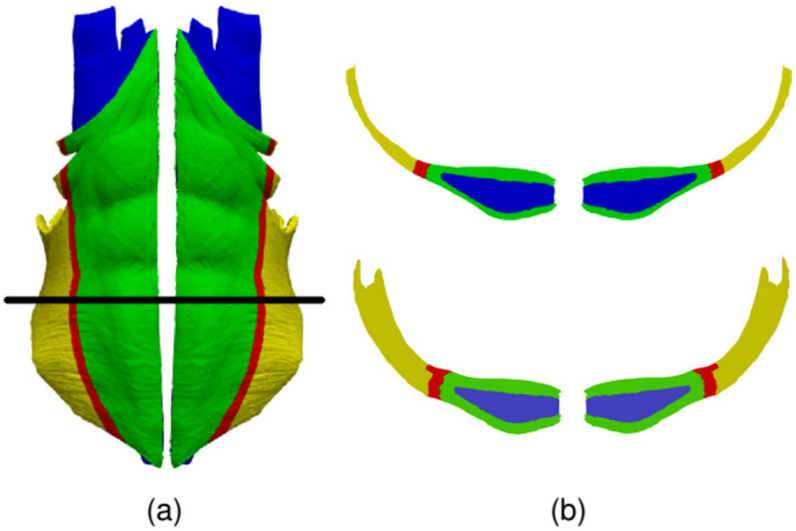

Figure 3. Illustration of the transition between the regular muscle tissue (yellow), intermediate tissue (red) and aponeurotic tissue (green). (**a**) Frontal view of the left and right IO muscles that surround most of the RA muscles (blue). (**b**) Axial slices taken at the height denoted by the horizontal black line in part (**a**); the upper plot shows only the IO and RA tissues whereas the lower plot shows also the EO and TR muscle tissues for the sake of completeness.

Numerical simulation

The current simulations were performed using the Code Aster open-source FE software[17]. As illustrated in Fig. 4, fixed (zero deformation) boundary conditions were prescribed at the edge of the abdominal wall, where the muscles would attach to the bones. The IAP was uniformly applied to the AW inner surface. For each geometry, we performed simulations for five uniformly distributed values pf P_a between 4 and 20 kPa, a normal IAP range during typical activities of daily living[18]. In each simulation, the resulting deformations of the geometry were computed and analyzed.

The geometry model was generated by refinement of the raw model available in the BodyParts3D database for anatomy, which in turn was generated from CT images of an adult man[19]. In this refinement process, internally consistent, high quality triangular surface meshes were generated for each of the AW components in our model. Subsequently, the corresponding volume meshes, consisting of linear tetrahedra, were constructed. Table 3 shows the dimensions of the three computational meshes used in the present study, i.e., the mesh for the base case (no-trocar) and the respective meshes for the trocar patterns A and B. Special care was taken to ensure the homogeneity of the computational meshes. That is, the values of the (mesh wide) mean triangle surface area and mean tetrahedron volume, listed in Table 3, are characteristic of most of the mesh elements. A exception to this rule is found in the particularly refined meshes that were generated for the trocar elements (see Table 3). These trocar meshes replaced the corresponding portions of the base mesh at the trocar sites and the mesh elements in the surrounding regions were correspondingly adapted to ensure continuity and smoothness of the resulting computational mesh. As an example, Fig. 5a shows a section of the surface mesh of the RA muscles and LA

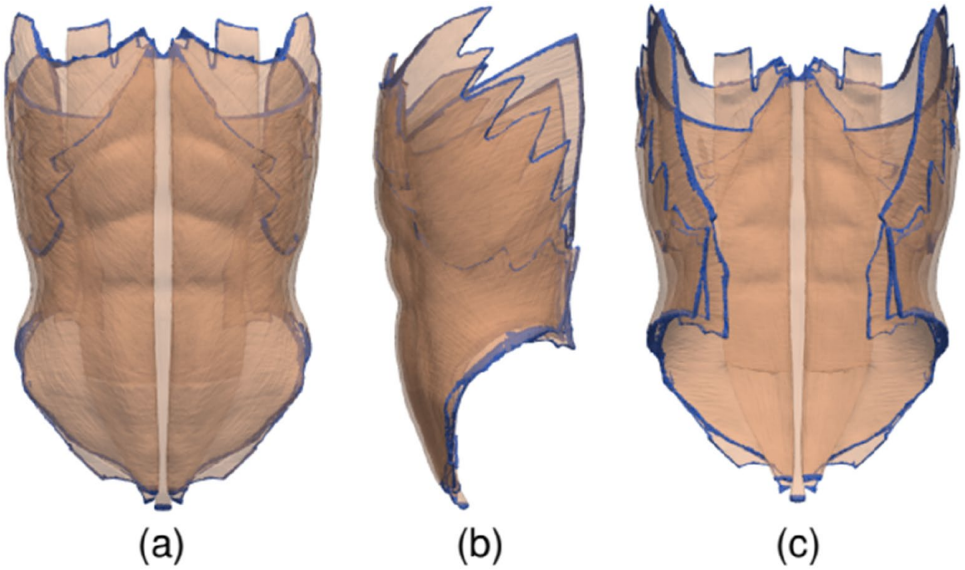

Figure 4. Views of the AW geometry with a dark blue color denoting areas where the fixed boundary condition is applied. (**a**) Front view. (**b**) Side view. (**c**) Rear view. Note that the surfaces of the different geometry elements (muscles) have been made translucent to enhance the visibility of fixed-boundary areas.

	Base case (no trocars)	Model A	Model B
Nodes	714 816	748 607	746 629
Surface mesh triangles	486 620	486 998	486 858
Tetrahedrons	3 495 765	3 712 302	3 701 001
Average triangle area (mm^2)	0.811	0.811	0.811
Average tetrahedron volume (mm^3)	0.698	0.658	0.660
Trocar average triangle area (mm^2)	–	0.235	0.234
Trocar average tetrahedron volume (mm^3)	–	0.086	0.082

Table 3. Main features of the computational meshes used in the present FE simulations. In the three models, the internal total volume is 2441 cm^3 and the external surface area (volume external boundaries) is 0.3947 m^2. The number of triangles and their properties refer only to the external surfaces, i.e., those that define the exterior boundary of a volume.

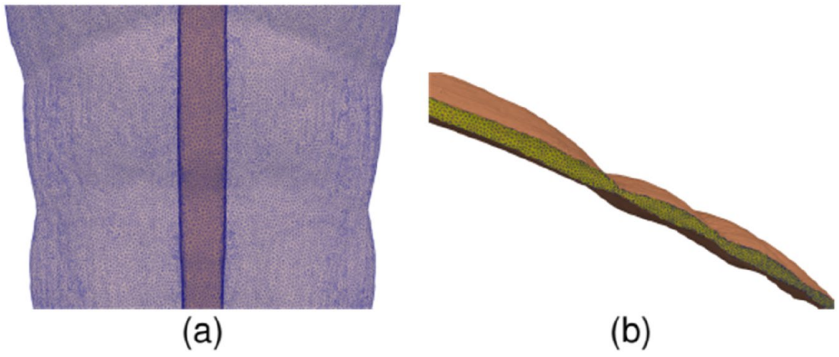

Figure 5. (**a**) Detail of the computational mesh on a sector of the RA muscles (pink) and LA (brown) frontal surfaces; the edges of the surface-mesh triangles are denoted with blue lines. (**b**) Side view of a cross-section of the left RA mesh showing the lateral surface (yellow, with blue triangle edges) that is shared with the LA mesh.

whereas Fig. 5b provides a detailed view of the mesh on the internal surface separating, and common to, the left RA and LA volumes.

Characterization of the deformation patterns of incisions

For each laparoscopy pattern (A and B), we first performed a reference case simulation in which E_w values for every SW were set to the average E of the muscles surrounding it (that is, SWs were considered to be healed). Then we performed a set of simulations in which one SW at a time was softened to $E_w = 0.1$ MPa. Since the predicted displacements of each computational node are available in the FE simulation output, we computed the corresponding changes in surface area and volume of the deformed SWs by means of numerical integration along the mesh surface elements (triangles) and volume elements (tetrahedra), respectively.

There are two main effects in the deformation of a SW: (i) an undulation of its outer surface, and (ii) a reduction in its length (depth) in the direction normal to the AW surface.

Even though the concept of surface undulation arises intuitively from the visualization of the SW deformed geometry—obtained from the FE simulation output—its quantification is by no means straightforward. In what follows we explain in some detail the methodology that we developed to quantify this concept. Specifically, our main goal is to associate a map of the predicted SW surface changes to a quantity that estimates the SW degree of surface undulation. In the non-deformed geometry, each SW is an elliptic cylinder with two end lids, respectively located on the AW inner and outer surfaces. For every computational node ("i") along the rim of a lid, we determined the nearest node ("j") in the rim of the opposite lid, and we measured the Euclidean distance ($d_{i,j}$) and the minimum geodesic distance ($D_{i,j}$) between these two nodes. A geodesic distance between two points on a surface is the length of a path between the two points along the surface. The full set of distances between rim node pairs was used to compute averaged Euclidean (d) and minimum geodesic (D) distances for every SW. In the original geometry (Fig. 6a), the SW surface is hardly undulated, and we initially have $D_0 \approx d_0$. After a FE simulation was completed, the final Euclidean (d_f) and geodesic (D_f) distances were computed for the deformed SW (see Fig. 6b). The SW undulation was characterized using the averaged tortuosity,

$$\overline{\tau} = \frac{\overline{D}}{\overline{d}} \tag{2}$$

as well as its variation,

$$\Delta\tau = 100\left(\frac{\overline{\tau}_f - \overline{\tau}_0}{\overline{\tau}_0}\right) \tag{3}$$

To characterize the compression of the SW due to a decrease in its depth, we defined the averaged geodesic deformation as:

$$\overline{G}_d = \frac{\overline{D}_f}{\overline{D}_0} \tag{4}$$

Results

Table 4 shows predicted G_d and $\Delta\overline{\tau}$ values for the simulations with $P_a = 20$ kPa. Surgical wounds within the LA (A1, A4, B1 and B4) hardly experience any deformation ($G_d \approx 1$ and $\Delta\overline{\tau} \approx 0$) but they travel a significant distance outward, together with the rest of the LA tissue. Figure 6 shows the predicted deformations for the simulations with $P_a = 20$ kPa and either a soft A4 or B2 SW. The deformation behavior of a SW in the LA is illustrated in Fig. 6c for a soft A4 ($E_w = 0.1$ MPa). Laterally located surgical wounds (A2, A3, A5, A6, B2, B3 and B5) hardly change their location instead but their shape is significantly modified (see Table 4). This second behavior is illustrated in Fig. 6d for a soft B2. The depth of laterally placed surgical wounds is reduced, with G_d values in the 0.96–0.97 range. Also, lateral surgical wounds located in the upper lumbar region (A2, A6 and B2) experience significant surface undulations, as characterized by higher $\Delta\overline{\tau}$ values in Table 4.

To further investigate the mechanical response of the SWs as a function of their toughness (E_w), we selected one SW from each pattern, namely A6 and B2, which featured the largest surface undulation in terms of G_d and $\Delta\overline{\tau}$ (see Table 4). Figure 7a–d illustrates the relative change of surface area and volume of A6 and B2 as a function of P_a. Figure 7a,c shows that for a very tough SW ($E_w = 2000$ MPa) the surface area of both A6 and B2 is preserved. The surface area of these wounds decreases with increasing IAP, up to about 1% at $P_a = 20$ kPa, when their stiffness is comparable to that in the surrounding muscles ($E_w = 1$–2 MPa), and it slightly decreases (for $P_a < 15$ kPa) or increases (for $P_a \geq 15$ kPa) when the wounds are soft ($E_w = 0.1$–0.2 MPa). Figure 7b,d shows that the volume of A6 and B2 increases steadily with increasing IAP and with decreasing E_w, with a maximum expansion of 5.3% for A6 with $E_w = 0.1$ MPa. Figure 7e,f shows that for a fixed IAP level of 20 kPa changes in E_w lead to modest changes in SW volume and surface area, with some increase in surface area only observed for the softest SWs ($E_w = 0.1$ MPa). In the 0.2 MPa $\leq E_w \leq$ 10 MPa range SW surface area decreases instead for both A6 and B2, with a minimum of about $E_w = 1$ MPa.

Discussion

Even though laparoscopic surgery can be associated with benefits in different procedures when compared with open surgery[20,21] it might be penalized with an unclear incidence of TSH[1]. TSH incidence turns out to be high when we analyze data from the real-world evidence (i.e., registries)[2] or we examine medical imaging such as

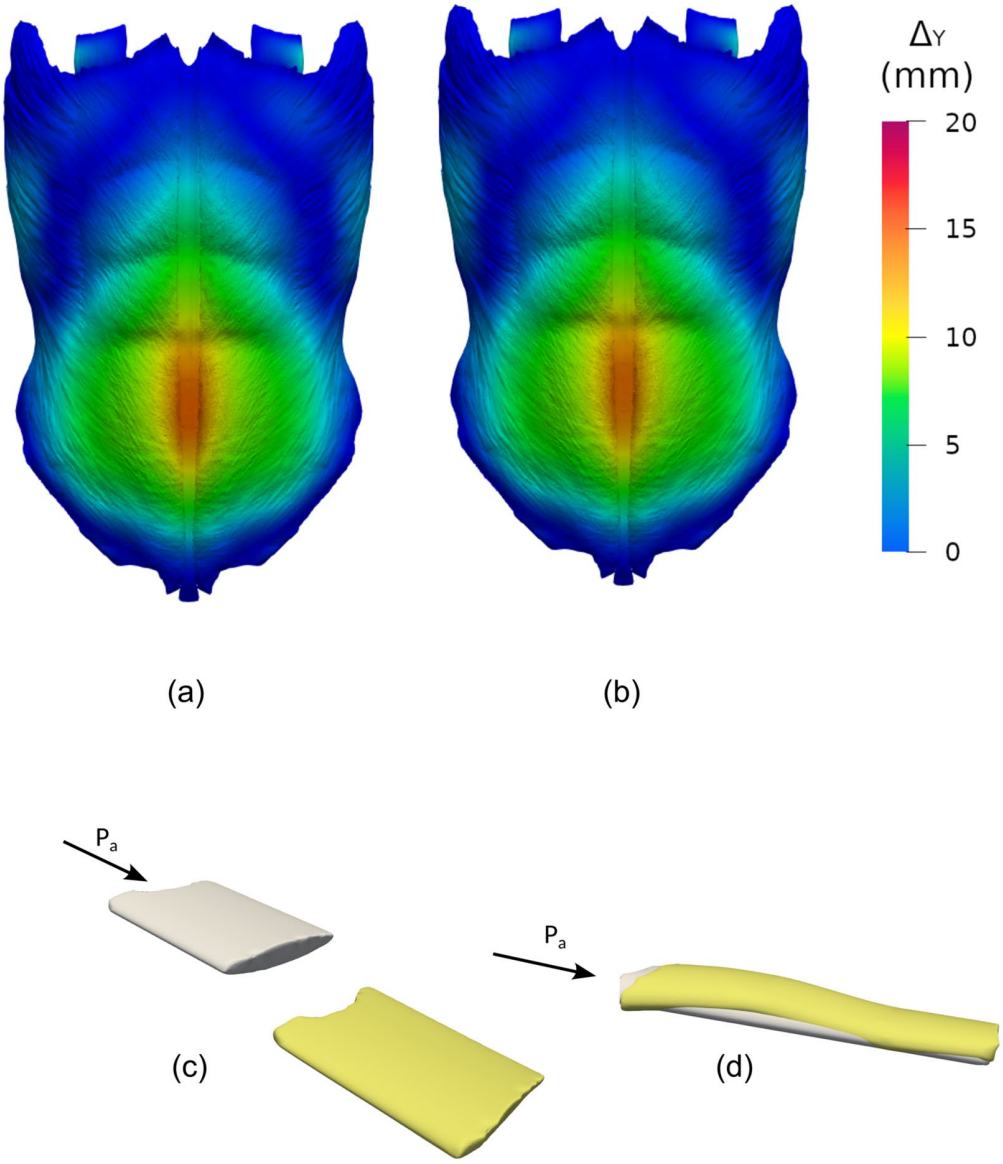

Figure 6. Results from the simulations with $P_a = 20$ kPa for soft ($E_w = 0.1$ MPa) A4 (**a**,**c**) and B2 (**b**,**d**) laparoscopy surgical wounds. (**a**,**b**) Deformation of the entire AW external surface is plotted for the simulations with a soft A4 (**a**) and B2 (**b**) surgical wound. (**c**,**d**) Comparison of the original and deformed geometries of A4 (**c**) and B2 (**d**) surgical wounds.

ultrasound and CT scans, which help to diagnose a considerable amount of TSH that would be otherwise clinically undetectable[1].

Evidence supporting the benefits of trocar-site closure after completing the surgical procedure is very limited. This data uncertainty might be the reason why some authors believe it is not necessary to close the trocar-site wound to prevent a TSH[22]. Nevertheless, the most recent clinical guidelines recommend the closure of trocars with large diameters (10 mm or larger)[4]. In addition to trocar diameter[4], the location of the trocar-site may affect TSH incidence[22]. Literature reviews suggest higher TSH incidence rates for trocars in the LA, compared to the off midline locations[22]. Moreover, the umbilical trocar site along with the use of larger trocars and obesity have been reported as risk factors for developing TSH[23]. The IAP exerted on the abdominal wall, and consequently on the trocar-site wounds, might also influence the appearance of TSH. Correlation between central obesity and increase in IAP has been described in several works[24–26].

In the present study, we performed virtual simulations of the mechanical behavior of the AW for different properties of the SW tissues and different IAP levels. Our results indicate that laparoscopic SWs embedded in the LA barely deform as a result of the AW expansion. These wounds, having a diameter smaller than the standard LA width (2 cm), are surrounded by the stiffer LA tissue and thus have very little room for deformation, even when they are very soft ($E_w = 0.1$ MPa). On the contrary, laterally placed laparoscopic SWs significantly deform

Incision	$E_w = 0.1$ MPa[a]		Reference case[b]	
	$\overline{G}_d$	$\Delta\overline{\tau}$ (%)	$\overline{G}_d$	$\Delta\overline{\tau}$ (%)
A1	1.00	0.00	1.00	0.00
A2	0.97	0.35	0.97	0.30
A3	0.97	0.06	0.97	0.03
A4	1.00	0.01	1.00	0.00
A5	0.97	0.08	0.97	0.05
A6	0.96	0.59	0.97	0.52
B1	1.00	0.00	1.00	0.00
B2	0.97	0.37	0.97	0.30
B3	0.96	0.04	0.97	0.01
B4	1.00	0.02	1.00	0.00
B5	0.96	0.06	0.97	0.01

Table 4. Quantification of SW shape change in simulations with $P_a = 20$ kPa. [a]Just one SW at a time was softened. [b]In the Reference Case simulation, each incision had the same elastic modulus as the muscles around it.

when the AW is expanded. The volume growth of laterally placed SWs increases with decreasing E_w, up to a maximum of 5% for $E_w = 0.1$ MPa. A soft SW opposes less resistance to the motion of the muscular tissue (TR and EO) around it and the SW tissue just follows the muscles and adjusts to fill the new space generated. The increase in SW volume is accompanied by either an increase or a decrease in its surface area, depending on the E_w value. When a pressure push is applied on the inner AW surface, the innermost muscular layer (TR and EO) is slightly compressed, that is, its depth is slightly reduced. Consequently, the depth of laterally placed SWs is similarly reduced. However, even though SW depth is reduced the increase in SW volume entails an increase in both its length and width. As the total SW surface area is proportional to its depth, length and width, an increase of the two latter quantities can partly compensate, or even outreach, the decrease in the former.

Study limitations

As a rule, virtual simulations ought to be validated by comparison with experimental results. To the best of our knowledge, no available experimental data exists on the present subject, a fact resulting from the difficulties that are inherent to experimentation with living persons. Nonetheless, the absence of verification constitutes a limitation of the present study.

The present geometrical and mathematical models have several limitations. Only one linea alba geometry, 2 cm wide, has been considered and the present model does not account for the placement of sutures or prostheses at trocar sites. Simulations of surgical wounds located on the LA at the umbilical site level were dismissed. Moreover, a linear isotropic elastic behavior was assumed for all abdominal wall tissues to constrict the computational costs. Even though it is well established that the AW tissues are fibrous and thus anisotropic[27], our simulations predict modest strain levels even at the highest IAP values considered. That is, proximity to the stress–strain (zero) origin would partly justify the use of the linear constitutive model.

Another limitation of the present study is that only one geometry model, obtained from a specific subject, is considered. This raises a crucial question on the applicability of the present results to the broader population. The substantial inter-subject variability in both morphology and the mechanical properties of the different AW tissues introduces a significant challenge. Therefore, a generalization of the present results would be meaningful at a qualitative level, and even so, it should be approached with caution.

Despite these limitations, we think that the present methodology establishes the basis for future advancements. Specifically, virtual simulations may serve as the basis for a more refined, patient-specific assessment on how trocar placement influences the mechanics of the abdominal wall. Future work should therefore aim to the automation of the geometry building process from individual CT scans, thus offering a more personalized and clinically relevant perspective.

Conclusion

In conclusion, trocar incisions placed in a LA with non-diastatic dimensions (up to 2 cm) do not seem to compromise the LA mechanical integrity. However, we previously found that trocar holes exceeding the dimensions of a non-diastatic LA can cause an alteration in its mechanical integrity, especially trocars placed in the lowermost area of the LA (hypogastric)[5]. This can be especially important when a surgeon must decide whether to close a trocar placed in the LA, mainly if we consider the "pivot point" or "fulcrum" clinical concept[1] that affects the part of the trocar held by the abdominal wall muscles around which the trocar performs its movement. Depending on the characteristics of the intervention, the trocar will pivot around a distinct set point, potentially causing shearing injury to the abdominal wall, enlarging the defect in the abdominal wall musculature. Maybe robotic trocars, which move with more precision, would maintain the integrity of the LA without exceeding its dimensions because they are pivoting in the same set point all time, regardless of the characteristics of the intervention. Laterally placed trocar incisions (beyond the rectus abdominis muscles) experience greater deformation with IAP than those placed on LA. The more lateral the trocars are placed the greater is their deformation, regardless

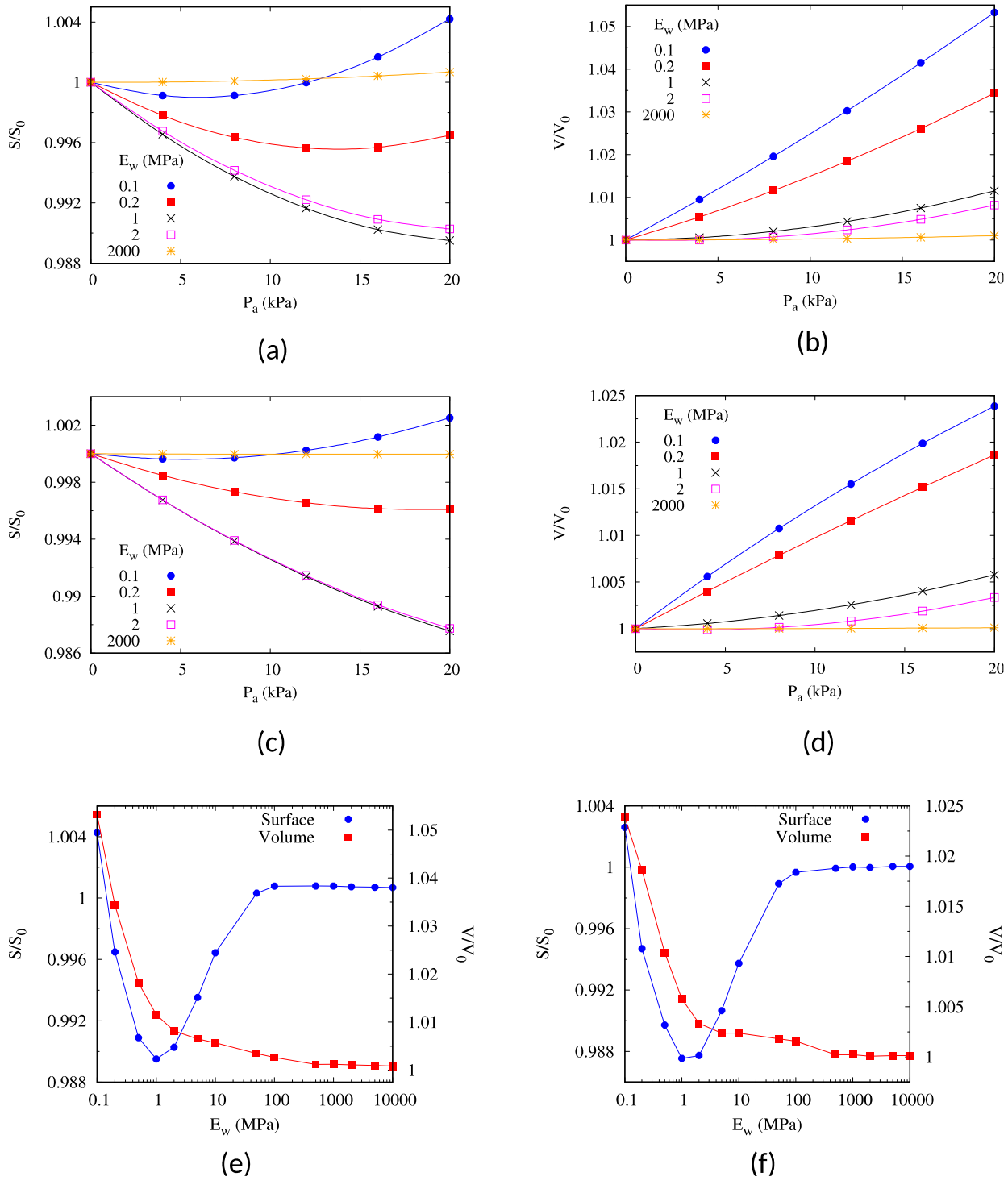

Figure 7. Relative change in surface area (**a**,**c**,**e**) and volume (**b**,**d**,**f**) of the A6 and B2 laparoscopy surgical wounds. In parts (**a–d**), changes in SW geometry are plotted against the level of applied IAP for several values of E_w whereas in parts (**e**,**f**) the predicted changes in surface area and volume are plotted against E_w for the simulations with $P_a = 20$ kPa. Calculated values are marked with a symbol whereas the solid line segments are intended just as a visual aid.

of their size. It could be speculated that the mechanical behavior of lateral trocars may be compromised if left only at the expense of scar resistance, with potential risk of finally developing TSH. It might be, therefore, advisable to close lateral trocars with a suture or even use a prosthetic reinforcement depending on the patient's risk factors (e.g., obesity) and regardless of the size of the trocar.

Data availability

The datasets used and/or analyzed during the current study are available from the corresponding author on reasonable request.

Received: 15 May 2023; Accepted: 8 February 2024
Published online: 13 February 2024

References

1. de Beaux, A. C. & East, B. Thoughts on trocar site hernia prevention. A narrative review. *J. Abdom. Wall Surg.* **1**, 11034 (2022).
2. Pereira, J. A., López-Cano, M., Hernández-Granados, P., Feliu, X. & del grupo EVEREG, en representación. Initial results of the national registry of incisional hernia [Resultados iniciales del registro español de hernia incisional]. *Cirugía Española* **94**, 595–602 (2016).
3. Ciscar Belles, A. *et al.* Umbilical incisional hernias (M3): Are trocar-site hernias different? Comparative analysis of the EVEREG Registry. *Cirugía Española* **100**, 336–344 (2022).
4. Deerenberg, E. B. *et al.* Updated guideline for closure of abdominal wall incisions from the European and American Hernia Societies. *Br. J. Surg.* **109**, 1239–1250 (2022).
5. Tuset, L. *et al.* Virtual simulation of the biomechanics of the abdominal wall with different stoma locations. *Sci. Rep.* **12**, 3545 (2022).
6. Karrech, A., Ahmad, H. & Hamdorf, J. M. Biomechanical stability of hernia-damaged abdominal walls. *Sci. Rep.* **13**(1), 4936 (2023).
7. Abat González, F., Turmo Garuz, A., Campos Moraes, J. & Capurro Soler, B. Physiology and mechanobiology of tendon and muscle tissue. *Rev. Esp. Artroscopia Cirugía Articular* **29**, 3–12 (2022).
8. Garg, S., Dahiya, N. & Gupta, S. Surgical scar revision: An overview. *J. Cutan. Aesthet. Surg.* **7**(1), 3–13 (2014).
9. Mann, C. J. *et al.* Aberrant repair and fibrosis development in skeletal muscle. *Skelet. Muscle* **1**, 21 (2011).
10. Laumonier, T. & Menetrey, J. Muscle injuries and strategies for improving their repair. *J. Exp. Orthop.* **3**, 15 (2016).
11. Corr, D. T. & Hart, D. A. Biomechanics of scar tissue and uninjured skin. *Adv. Wound Care* **2**, 37–43 (2013).
12. Hernández-Granados, P. *et al.* European Hernia Society guidelines on management of rectus diastasis. *Br. J. Surg.* **108**, 1189–1191 (2021).
13. Martins, P. *et al.* Mechanical characterization and constitutive modelling of the damage process in rectus sheath. *J. Mech. Behav. Biomed. Mater.* **8**, 111–122 (2012).
14. Deeken, C. R. & Lake, S. P. Mechanical properties of the abdominal wall and biomaterials utilized for hernia repair. *J. Mech. Behav. Biomed. Mater.* **74**, 411–427 (2017).
15. Ibrahim, M. M. *et al.* A novel immune competent murine hypertrophic scar contracture model: A tool to elucidate disease mechanism and develop new therapies. *Wound Repair Regener.* **22**, 755–764 (2014).
16. Samartsev, V. A., Kuchumov, A. G. & Gavrilov, V. A. Sutures in abdominal surgery: biomechanical study and clinical application. *Cent. Eur. J. Med.* **9**, 849–859 (2014).
17. Electricité de France. *code_aster. Structures and Thermomechanics Analysis for Studies and Research* (2023).
18. Cobb, W. S. *et al.* Normal intraabdominal pressure in healthy adults. *J. Surg. Res.* **129**, 231–235 (2005).
19. Mitsuhashi, N. *et al.* BodyParts3D: 3D structure database for anatomical concepts. *Nucleic Acids Res.* **37**, D782–D785 (2009).
20. Ozair, A. *et al.* Minimally invasive versus open hepatectomy for the resection of colorectal liver metastases: a systematic review and meta-analysis. *Surg. Endosc.* **36**, 7915–7937 (2022).
21. Luo, W., Wu, M. & Chen, Y. Laparoscopic versus open surgery for elderly patients with colorectal cancer: a systematic review and meta-analysis of matched studies. *ANZ J. Surg.* **92**, 2003–2017 (2022).
22. Gutierrez, M., Stuparich, M., Behbehani, S. & Nahas, S. Does closure of fascia, type, and location of trocar influence occurrence of port site hernias? A literature review. *Surg. Endosc.* **34**, 5250–5258 (2020).
23. Ahlqvist, S. *et al.* Trocar site hernia after gastric sleeve. *Surg. Endosc.* **36**, 4386–4391 (2022).
24. Smit, M. *et al.* How central obesity influences intra-abdominal pressure: A prospective, observational study in cardiothoracic surgical patients. *Ann. Intensive Care* **6**, 1–10 (2016).
25. Lambert, D. M., Marceau, S. & Forse, R. A. Intra-abdominal pressure in the morbidly obese. *Obes. Surg.* **15**, 1225–1232 (2005).
26. Wilson, A., Longhi, J., Goldman, C. & McNatt, S. Intra-abdominal pressure and the morbidly obese patients: The effect of body mass index. *J. Trauma Injury Infect. Crit. Care* **69**, 78–83 (2010).
27. Tuset, L., Fortuny, G., Herrero, J., Puigjaner, D. & López, J. M. Implementation of a new constitutive model for abdominal muscles. *Comput. Methods Progr. Biomed.* **179**, 104988 (2019).
28. Cardoso, M. *Experimental Study of the Human Anterolateral Abdominal Wall: Biomechanical Properties of Fascia and Muscles* 7–16, 52 (Faculdade de Engenharia, Universidade do Porto, 2012).
29. Cooney, G. M. *et al.* Uniaxial and biaxial tensile stress-stretch response of human linea alba. *J. Mech. Behav. Biomed. Mater.* **63**, 134–140 (2016).
30. Ben Abdelounis, H., Nicolle, S., Otténio, M., Beillas, P. & Mitton, D. Effect of two loading rates on the elasticity of the human anterior rectus sheath. *J. Mechan. Behav. Biomed. Mater.* **20**, 1–5 (2013).

Acknowledgements

This project has been partially founded by AGAUR research group 2021SGR-00111: "ASCLEPIUS: Smart Technology for Smart Healthcare".

Author contributions

Conception and design: all authors; Methodology: L.T., G.F., J.M.L., J.H., D.P.; Numerical simulations: L.T.; Analysis and interpretation of data: all authors; Study supervision: J.H. and D.P.; Writing Original Draft: all authors; Writing Review and Editing: all authors. All authors have read and approved the final manuscript.

Competing interests

The authors declare no competing interests.

Additional information

Correspondence and requests for materials should be addressed to D.P.

Reprints and permissions information is available at www.nature.com/reprints.

Publisher's note Springer Nature remains neutral with regard to jurisdictional claims in published maps and institutional affiliations.

Open Access This article is licensed under a Creative Commons Attribution 4.0 International License, which permits use, sharing, adaptation, distribution and reproduction in any medium or format, as long as you give appropriate credit to the original author(s) and the source, provide a link to the Creative Commons licence, and indicate if changes were made. The images or other third party material in this article are included in the article's Creative Commons licence, unless indicated otherwise in a credit line to the material. If material is not included in the article's Creative Commons licence and your intended use is not permitted by statutory regulation or exceeds the permitted use, you will need to obtain permission directly from the copyright holder. To view a copy of this licence, visit http://creativecommons.org/licenses/by/4.0/.

© The Author(s) 2024

3. Conclusions i treball futur

3.1 Nou model constitutiu

S'ha aconseguit crear un nou model constitutiu, basat en el model hiperelàstic transversalment isotròpic, que només utilitza funcions polinòmiques de manera que aquest és robust i computacionalment eficient. Els resultats tensió-deformació d'aquest nou model (simulació) s'han comparat amb els obtinguts experimentalment per diversos autors i autores i s'ha comprovat que l'ajust entre ambdós valors és molt alt de manera que **aquest model descriu bé el comportament de la paret abdominal**.

El model dissenyat es pot utilitzar amb seguretat per a simular situacions en què **els teixits s'estiren fins a un nivell de tensió de $\boldsymbol{\sigma = 0.2}$ MPa** la qual cosa suposa un ventall d'aplicacions prou ampli. Cal destacar, però, que si la compressió és molt forta aquest model pot patir errors de càlcul la qual cosa significaria un possible trencament del teixit real. Es creu que és millor que el model tingui un error de càlcul que no pas doni una solució numèrica que no tingui sentit físic.

3.2 Simulacions virtuals

L'estudi sobre la localització dels estomes revela que la seva ubicació, excepte si se situa sobre la línia alba, no compromet la consistència mecànica de la paret abdominal quan se sotmet a nivells de pressió intraabdominal de fins a 20 kPa. De manera específica, la deformació de la paret anterior de l'abdomen així com el nivell de tensió suportat mostra poca correlació respecte la localització de l'estoma quan aquest no es troba sobre la línia alba.

Pel que fa a la mida de la incisió, s'observa que aquesta augmenta en tots els casos en aplicar-se la pressió intraabdominal tant en termes de perímetre com de superfície. Aleshores, ja que quan augmenta la mida de la incisió, com a conseqüència augmenta el risc d'aparició d'una hèrnia paraestomal [39], es pot concloure que l'aparició d'hèrnies paraestomals està directament relacionada amb el fet de crear un estoma sigui quina sigui la seva localització. Tot i això, sembla coherent preveure que si l'augment percentual de l'àrea o del perímetre és superior, serà superior el risc de que aparegui una hèrnia

(vegeu Taula 2 de l'estudi 2, secció 2.2) i, per tant, segons els resultats obtinguts en les simulacions, **cal evitar la creació d'estomes al lateral dels músculs rectes abdominals**.

De totes maneres, cal destacar que tant la deformació de la paret abdominal com de l'estoma serà reversible i, per tant, es recuperaria la forma original tot i que els teixits poden patir conseqüències en forma de fatiga o de petites lesions. A més, segons diversos estudis clínics [39], [40] aquest defecte de la incisió augmenta amb el temps després de la creació de l'estoma.

Cal interpretar amb cautela els resultats anteriors a causa d'una diferència entre l'augment de la mida de la incisió (reversible) que preveuen les nostres simulacions numèriques i els defectes reals (irreversibles) que pateixen els pacients a llarg termini segons estudis clínics reals [41]–[43]. De totes maneres es pot concloure que **cal evitar crear els estomes sobre la línia alba** o al lateral extern dels músculs rectes, essent les localitzacions òptimes la s_{11} i la s_{12}. Aquestes dues posicions se situen a la part inferior esquerra de la paret abdominal i a poca distància horitzontal de la línia alba.

Pel que fa a les incisions laparoscòpiques, els resultats mostren que si aquestes mesuren fins a 2 cm i se situen sobre la línia alba pateixen molt poca deformació, ja que tenen una mida inferior a l'amplada d'aquest múscul el qual té un teixit molt rígid amb la qual cosa tenen molt poc espai de deformació, fins i tot quan les cicatrius són molt toves. Per contra, si les incisions se situen lateralment, aquestes es deformen significativament i aquesta deformació augmenta en disminuir el mòdul elàstic de la cicatriu. És a dir, com més tova sigui la cicatriu, oposa menys resistència al moviment dels músculs del seu entorn de manera que la cicatriu s'ajusta a l'espai lliure generat augmentant el seu volum.

Tal com també passa amb els estomes, si les incisions laparoscòpiques se situen al lateral extern dels músculs rectes experimenten una deformació més elevada que si se situen sobre la línia alba. De fet, com més laterals se situïn, més gran serà la seva deformació independentment de la mida.

Tenint en compte aquests resultats, es pot deduir que si la incisió se situa molt lateralment, la seva resistència mecànica es pot veure compromesa si no es tanca i es deixa que la cicatriu suporti tot l'esforç mecànic amb el risc de provocar una hèrnia incisional. Per aquest motiu, **podria ser recomanable tancar les incisions laterals amb les tècniques habituals de sutura o amb un reforç protètic** [44] per tal de millorar-ne la resistència.

3.3 Conclusions generals

Tenint en compte els 3 estudis anteriors, es pot afirmar que aquesta investigació ha assolit l'objectiu principal de modelitzar adequadament el comportament biomecànic de la paret abdominal ja que els resultats obtinguts són coherents amb els resultats clínics publicats en la literatura. A diferència de l'experimentació amb teixits reals, humans o animals, aquest model virtual permet fer múltiples simulacions tenint en compte un gran ventall de paràmetres i característiques concretes.

Pel que fa al nou model constitutiu, ha modelitzat adequadament el comportament dels músculs de la paret abdominal en un ampli ventall de situacions combinant **simplicitat i eficiència**.

Per altra banda, es pensa que **la simulació numèrica és un gran pas endavant en la investigació de les hèrnies incisionals** i, en general, en l'estudi del comportament mecànic de la paret abdominal ja que és un estudi no invasiu, permet una anàlisi detallada de les interaccions entre els teixits, pot ajudar a desenvolupar nous tractaments i permet predir resultats clínics considerant situacions que d'altra manera no seria possible. A més, és un mètode que els professionals de la cirurgia poden aprofitar per tal d'**optimitzar les tècniques quirúrgiques ja que permet construir un coneixement complert del comportament de la paret abdominal**.

Finalment, es considera que la modelització dels dos tipus d'incisions ha estat adequada i el fet d'haver considerat vàries localitzacions ha proporcionat informació rellevant pel que fa a la distribució de tensions i deformacions que permet predir possibles complicacions. A més, s'ha pogut estudiar degudament quin és l'efecte de la geometria de la incisió en la resposta biomecànica de la paret abdominal. De nou, aquest coneixement pot ajudar a optimitzar les tècniques quirúrgiques actuals comparant diferents tipus de talls o la seva ubicació.

3.4 Treball futur

La metodologia que es detalla en aquesta tesi es podria aplicar en altres tipus d'incisions que es practiquen sobre la paret abdominal. Una d'elles, de la qual ja es disposa de resultats preliminars és l'efecte de la laparotomia. La laparotomia és un procediment quirúrgic en el qual es realitza una incisió oberta a la paret abdominal per accedir a la cavitat peritoneal. Tot i que aquesta tècnica és més invasiva que la cirurgia laparoscòpica, típicament ha estat considerat el tractament estàndard [45] i s'acostuma a utilitzar en casos complexos o bé quan es requereix una exploració més extensa de l'interior de la cavitat [46].

En aquest cas la incisió s'ha modelitzat de cinc maneres diferents per tal de comparar-ne els resultats segons la seva mida i localització:

- Laparotomia mitjana: incisió vertical de 12 cm sobre la línia alba. Aquest és el procediment més habitual en les laparotomies [47].
- Laparotomia transrectal: incisió vertical de 12 cm al costat esquerre de la paret abdominal a través del múscul recte.
- Laparotomia pararectal lateral: incisió vertical de 12 cm al costat esquerre de la paret abdominal a través de la vora lateral externa del múscul recte [48]. Aquesta incisió està més allunyada de la línia alba que la laparotomia transrectal.
- Laparotomia transversa supraumbilical: incisió horitzontal de 6 cm al costat dret sobre el múscul recte.
- Laparotomia obliqua subcostal: incisió horitzontal amb certa inclinació de 9 cm de llarg i situada al costat dret, més avall que l'anterior.

Les primeres simulacions que s'han fet revelen que la superfície i el volum de la cicatriu de la laparotomia augmenta poc després de l'operació, quan la cicatriu encara és tova. Mentre que si es considera la sutura curada, la deformació de la cicatriu disminueix.

Pel que fa al camp de tensions, s'ha observat que augmenta si la cicatriu és molt tova o també si s'endureix. Aquest resultat és degut a la combinació de dos efectes que apareixen quan diversos músculs amb diferents elasticitats estan en contacte. Per una banda, el teixit més elàstic és deformarà més i les zones amb deformacions elevades estaran associades amb zones d'altes tensions i, per tant, hi haurà un risc més elevat de ruptura dels teixits. Per altra banda, per continuïtat de la matèria, prop de la frontera entre els dos, el teixit amb una elasticitat més baixa seguirà el teixit més elàstic de manera que hi haurà deformacions elevades i, com a conseqüència, es generaran regions amb tensions elevades entorn de la frontera. Aleshores, aquest resultat permetria determinar un interval de valors de l'elasticitat de la cicatriu pels quals seria possible una ruptura dels teixits.

Per altra banda, un altre treball de futur seria incorporar el nou model hiperelàstic transversalment isotròpic en els estudis de les incisions. D'aquesta manera, es podrien comparar els resultats obtinguts en aquesta investigació amb el model elàstic lineal amb els del nou model hiperelàstic la qual cosa permetria obtenir una visió més àmplia de la matèria.

Bibliografia

[1] B. Pandya, T. Huda, D. Gupta, B. Mehra, and R. Narang, "Abdominal wall hernias: An epidemiological profile and surgical experience from a rural medical college in central india," *The Surgery Journal*, vol. 7, no. 01, e41–e46, 2021.

[2] K LeBlanc and A Kingsnorth, "Hernias: Inguinal and incisional," *Lancet*, vol. 362, no. 9395, pp. 1561–71, 2003.

[3] M. Lindmark, T. Löwenmark, K. Strigård, and U. Gunnarsson, "Major complications and mortality after ventral hernia repair: An eleven-year swedish nationwide cohort study," *BMC surgery*, vol. 22, no. 1, p. 426, 2022.

[4] P Pachera, P. Pavan, S Todros, C Cavinato, C. Fontanella, and A. Natali, "A numerical investigation of the healthy abdominal wall structures," *Journal of biomechanics*, vol. 49, no. 9, pp. 1818–1823, 2016.

[5] B Hernández-Gascón, E Peña, H Melero, *et al.*, "Mechanical behaviour of synthetic surgical meshes: Finite element simulation of the herniated abdominal wall," *Acta biomaterialia*, vol. 7, no. 11, pp. 3905–3913, 2011.

[6] P. C. Ambe, N. R. Kurz, C. Nitschke, S. F. Odeh, G. Möslein, and H. Zirngibl, "Intestinal ostomy: Classification, indications, ostomy care and complication management," *Deutsches Ärzteblatt International*, vol. 115, no. 11, p. 182, 2018.

[7] J Shabbir and D. Britton, "Stoma complications: A literature overview," *Colorectal disease*, vol. 12, no. 10, pp. 958–964, 2010.

[8] I Robertson, E Leung, D Hughes, *et al.*, "Prospective analysis of stoma-related complications," *Colorectal Disease*, vol. 7, no. 3, pp. 279–285, 2005.

[9] Y. J. Sohn, S. M. Moon, U. S. Shin, and S. H. Jee, "Incidence and risk factors of parastomal hernia," *Journal of the Korean Society of Coloproctology*, vol. 28, no. 5, p. 241, 2012.

[10] P. Carne, G. Robertson, and F. Frizelle, "Parastomal hernia," *Journal of British Surgery*, vol. 90, no. 7, pp. 784–793, 2003.

[11] S. M. van Dijk, L. Timmermans, E. B. Deerenberg, *et al.*, "Parastomal hernia: Impact on quality of life?" *World journal of surgery*, vol. 39, pp. 2595–2601, 2015.

[12] S. Y. Hong, S. Y. Oh, J. H. Lee, K. W. Suh, *et al.*, "Risk factors for parastomal hernia: Based on radiological definition," *Journal of the Korean Surgical Society*, vol. 84, no. 1, pp. 43–47, 2013.

[13] M. López-Cano, J. Rodríguez-Navarro, A. Rodríguez-Baeza, M. Armengol-Carrasco, and A. Susín, "A real-time dynamic 3d model of the human inguinal region for surgical education," *Computers in biology and medicine*, vol. 37, no. 9, pp. 1321–1326, 2007.

[14] L. Liang, M. Liu, C. Martin, and W. Sun, "A deep learning approach to estimate stress distribution: A fast and accurate surrogate of finite-element analysis," *Journal of The Royal Society Interface*, vol. 15, no. 138, p. 20 170 844, 2018.

[15] R Simón-Allué, A Ortillés, and B Calvo, "Mechanical behavior of surgical meshes for abdominal wall repair: In vivo versus biaxial characterization," *Journal of the mechanical behavior of biomedical materials*, vol. 82, pp. 102–111, 2018.

[16] D. C. Bosanquet, J. Ansell, T. Abdelrahman, *et al.*, "Systematic review and meta-regression of factors affecting midline incisional hernia rates: Analysis of 14 618 patients," *PLoS One*, vol. 10, no. 9, e0138745, 2015.

[17] X.-F. Yang and J.-L. Liu, "Laparoscopic repair of abdominal incisional hernia," *Annals of Translational Medicine*, vol. 4, no. 18, 2016.

[18] M. J. Worley Jr, B. M. Slomovitz, and P. T. Ramirez, "Complications of laparoscopy in benign and oncologic gynecological surgery," *Reviews in Obstetrics and Gynecology*, vol. 2, no. 3, p. 169, 2009.

[19] J. J. Tiedeken and A. J. LaPorta, "Chapter 80 - laparoscopic surgery," in *GI/Liver Secrets (Fourth Edition)*, P. R. McNally, Ed., Fourth Edition, Philadelphia: Mosby, 2010, pp. 589–594.

[20] Z. Khan and K. Ma, "Complications of laparoscopic surgery," *Obstetrics, Gynaecology & Reproductive Medicine*, vol. 30, no. 11, pp. 342–346, 2020.

[21] A. Coda, M. Bossotti, F. Ferri, *et al.*, "Incisional hernia and facial defect following laparoscopic surgery," *Surgical Laparoscopy Endoscopy & Percutaneous Techniques*, vol. 9, no. 5, pp. 348–352, 1999.

[22] A. Ciscar, J. M. Badia, F. Novell, S. Bolívar, and E. Mans, "Incidence and risk factors for trocar-site incisional hernia detected by clinical and ultrasound examination: A prospective observational study," *BMC surgery*, vol. 20, no. 1, pp. 1–7, 2020.

[23] E. B. Deerenberg, N. A. Henriksen, G. A. Antoniou, *et al.*, "Updated guideline for closure of abdominal wall incisions from the european and american hernia societies," *British Journal of Surgery*, vol. 109, no. 12, pp. 1239–1250, 2022.

[24] A. E. Ehret and M. Itskov, "A polyconvex hyperelastic model for fiber-reinforced materials in application to soft tissues," *Journal of Materials Science*, vol. 42, pp. 8853–8863, 2007.

[25] G. A. Holzapfel *et al.*, "Biomechanics of soft tissue," *The handbook of materials behavior models*, vol. 3, no. 1, pp. 1049–1063, 2001.

[26] P. Martins, R. Natal Jorge, and A. Ferreira, "A comparative study of several material models for prediction of hyperelastic properties: Application to silicone-rubber and soft tissues," *Strain*, vol. 42, no. 3, pp. 135–147, 2006.

[27] N. Mitsuhashi, K. Fujieda, T. Tamura, S. Kawamoto, T. Takagi, and K. Okubo, "Bodyparts3d: 3d structure database for anatomical concepts," *Nucleic acids research*, vol. 37, pp. D782–D785, 2009.

[28] P Martins, E Peña, R. N. Jorge, *et al.*, "Mechanical characterization and constitutive modelling of the damage process in rectus sheath," *Journal of the mechanical behavior of biomedical materials*, vol. 8, pp. 111–122, 2012.

[29] C. R. Deeken and S. P. Lake, "Mechanical properties of the abdominal wall and biomaterials utilized for hernia repair," *Journal of the mechanical behavior of biomedical materials*, vol. 74, pp. 411–427, 2017.

[30] M. Kirilova, S. Stoytchev, D. Pashkouleva, and V. Kavardzhikov, "Experimental study of the mechanical properties of human abdominal fascia," *Medical engineering & physics*, vol. 33, no. 1, pp. 1–6, 2011.

[31] E. Hearn, "Chapter 11 - strain energy," in *Mechanics of Materials 1 (Third Edition)*, E. Hearn, Ed., Third Edition, Oxford: Butterworth-Heinemann, 1997, pp. 254–296.

[32] A. Granados, F. Perez-Garcia, M. Schweiger, *et al.*, "A generative model of hyperelastic strain energy density functions for multiple tissue brain deformation," *International Journal of Computer Assisted Radiology and Surgery*, vol. 16, pp. 141–150, 2021.

[33] R. M. Hackett, "Strain-energy functions," in *Hyperelasticity Primer*. Cham: Springer International Publishing, 2016, pp. 19–25.

[34] D. Gräβel, A. Prescher, S. Fitzek, D. G. v. Keyserlingk, and H. Axer, "Anisotropy of human linea alba: A biomechanical study," *Journal of Surgical Research*, vol. 124, no. 1, pp. 118–125, 2005.

[35] X. Yue, L., and R. Wang, "Tissue modeling and analyzing with finite element method: A review for cranium brain imaging," *International journal of biomedical imaging*, vol. 2013, 2013.

[36] C. Geuzaine and J.-F. Remacle, "Gmsh: A 3-d finite element mesh generator with built-in pre-and post-processing facilities," *International journal for numerical methods in engineering*, vol. 79, no. 11, pp. 1309–1331, 2009.

[37] code_aster, *Analyse des structures et thermo-mécanique pour des études et des recherches*, https://code-aster.org/spip.php?rubrique1, Accessed 09-May-2023.

[38] T. Helfer, B. Michel, J.-M. Proix, M. Salvo, J. Sercombe, and M. Casella, "Introducing the open-source mfront code generator: Application to mechanical behaviours and material knowledge management within the pleiades fuel element modelling platform," *Computers & Mathematics with Applications*, vol. 70, no. 5, pp. 994–1023, 2015.

[39] K. Ho, T Economou, N. Smart, and I. Daniels, "Radiological progression of end colostomy trephine diameter and area," *BJS open*, vol. 3, no. 1, pp. 112–118, 2019.

[40] A. Hu and E. M. Pauli, "Management of parastomal hernias," *Seminars in Colon and Rectal Surgery*, vol. 34, no. 2, p. 100 956, 2023, Intestinal Stomas and Their Complications.

[41] D. Kokotovic, T. Bisgaard, and F. Helgstrand, "Long-term recurrence and complications associated with elective incisional hernia repair," *Jama*, vol. 316, no. 15, pp. 1575–1582, 2016.

[42] M. Mureşan, S. Mureşan, T. Bara, R. Neagoe, D. Sala, and B. Suciu, "Seguimiento remoto de la recaída de hernia después de procesos abiertos de plastia de la pared abdominal–estudio prospectivo que incluye 142 pacientes," *Cirugía y Cirujanos*, vol. 84, no. 5, pp. 376–383, 2016.

[43] P. Rogmark, S. Smedberg, and A. Montgomery, "Long-term follow-up of retromuscular incisional hernia repairs: Recurrence and quality of life," *World Journal of Surgery*, vol. 42, pp. 974–980, 2018.

[44] P. K. Chowbey, A. Sharma, M. Mehrotra, R. Khullar, V. Soni, and M. Baijal, "Laparoscopic repair of ventral/incisional hernias," *Journal of Minimal Access Surgery*, vol. 2, no. 3, p. 192, 2006.

[45] J. Wang, L. Cheng, J. Liu, *et al.*, "Laparoscopy vs. laparotomy for the management of abdominal trauma: A systematic review and meta-analysis," *Frontiers in Surgery*, vol. 9, 2022.

[46] A. Pooria, A. Pourya, and A. Gheini, "A descriptive study on the usage of exploratory laparotomy for trauma patients," *Open Access Emergency Medicine*, pp. 255–260, 2020.

[47] D. Joshi, N. Varandani, and M. Vaidya, "Study of different methods of midline laparotomy incision closure and their outcomes," *MVP Journal of Medical Sciences*, pp. 249–252, 2022.

[48] S. M. Conde, F. B. Morandeira, P. H. Granados, and X. F. Palá, *Cirugía de la pared abdominal*. Arán Ediciones, 2013.

UNIVERSITAT ROVIRA I VIRGILI
SIMULACIÓ DE L'EFECTE DE LES INCISIONS QUIRÚRGIQUES EN EL COMPORTAMENT DE LA PARET ABDOMINAL
Lluís Tuset Serra

UNIVERSITAT ROVIRA I VIRGILI
SIMULACIÓ DE L'EFECTE DE LES INCISIONS QUIRÚRGIQUES EN EL COMPORTAMENT DE LA PARET ABDOMINAL
Lluís Tuset Serra